

University of Naples FEDERICO II

DEPARTMENT OF AEROSPACE ENGINEERING

Ph.D. in Aerospace Engineering

**EXPERIMENTAL AND NUMERICAL
ESTIMATION OF DAMPING IN COMPOSITE
PLATES WITH EMBEDDED VISCOELASTIC
TREATMENTS**

Candidate:

Eng. Angelo De Fenza

Research Supervisor:

Prof. Leonardo Lecce

The Chairman of the Ph.D. School:

Prof. Antonio Moccia

Thesis submitted in November 2011

Acknowledgments

First of all I would like to express my sincere gratitude to Prof. Leonardo Lecce, Full Professor of the Department of Aerospace Engineering, University of Naples Federico II, who has been my supervisor since the beginning of my study. He provided me with many helpful suggestions, important advice and constant encouragement. During the course of this work he was an essential guide for me, and I will remember forever that to work with him was a privilege for me.

I also wish to express my appreciation to Eng. Ernesto Monaco and Eng. Francesco Amoroso for the valuable suggestions and constructive advices they gave me.

I would like to thank my friend Eng. Diego Della Porta for his valuable suggestions and the time he spent to the revision of my thesis.

Special thanks also goes to Alenia Aeronautica S.p.A. for giving me the possibility to perform the experimental tests in its laboratories and to IMAST S.c.a.r.l. for providing me the properties of viscoelastic materials.

My special appreciation goes to my dear parents, my sisters and my friends Lorenzo, Elia, Rino and Giuseppe who always encouraged and supported me on my study. Finally, I would like to express very special thanks to my loving and my wife Fiorenza. She helped me to concentrate on completing this dissertation and supported mentally during the course of this work. Without her help and encouragement, this study and all my life would not have been the same.

Contents

Acknowledgments	i
List of Figures	vii
List of Tables	ix
Introduction	1
1 Damping treatments:	
State of the Art	3
1.1 Noise and Vibration Control	3
1.2 Types of Damping Treatments	4
1.3 Analytical models	6
1.3.1 Ross, Kerwin and Ungar model	7
1.4 Numerical models	9
1.4.1 Modal Strain Energy	9
1.4.2 Complex Eigenvalues Method	10
2 Composite materials	13
2.1 Micromechanical behaviour of a Lamina	14
2.2 Macromechanical behaviour of a Lamina	19
2.3 Macromechanical behaviour of a Laminate	21
3 Viscoelastic materials	27
3.1 Linear response of materials	27
3.1.1 Elasticity	28
3.1.2 Viscosity	30
3.1.3 Viscoelasticity	33
3.2 Constitutive models of linear viscoelasticity	36
3.2.1 Maxwell model	36
3.2.2 Kelvin-Voigt model	39

3.2.3	SLS (Standard Linear Solid) or Zener model	40
3.3	The dynamic behavior	43
3.3.1	The DMA (Dynamic Mechanical Analysis)	43
3.3.2	Loss Modulus, Storage Modulus, Complex Modulus and Loss Factor	44
3.3.3	Other consideration about Loss Factor	46
3.3.4	Temperature effects on viscoelastic behavior	47
3.3.5	Frequency effects on viscoelastic behavior	49
3.3.6	Cyclic Strain Amplitude Effects on Complex Modulus	50
3.3.7	Environmental effects on complex modulus	51
4	Experimental Approach	53
4.1	Impulse Response Decay Method (IRDM)	54
4.1.1	Excitation type	55
4.1.2	Hilbert Transform	56
4.1.3	Decay Rate evaluation	58
4.2	Experimental set-up	59
4.2.1	Excitation system	60
4.2.2	Climatic room	61
4.2.3	Acquisition system	61
4.3	Structure lay-up	62
4.4	Results	63
4.4.1	Position effect	70
4.4.2	Temperature effect	71
4.4.3	Statistical analysis	73
5	Numerical approach	77
5.1	Finite Element modelling	77
5.2	Explicit non linear analysis	82
5.2.1	Results	85
5.3	Direct Frequency Response Analysis	86
5.3.1	Results	89
	Conclusions	90
	Bibliography	96

List of Figures

1.1	Airborne and Structure-borne noise	4
1.2	Damping treatments: free-layer (a) and constrained-layer (b)	5
1.3	Embedded viscoelastic damping treatment	6
1.4	Three layer beam, with viscoelastic treatments	7
2.1	Basic question of micromechanics	14
2.2	Representative volume element loaded in the 1-Direction	15
2.3	Representative volume element loaded in the 2-Direction	16
2.4	Representative volume element loaded in the 1-Direction	17
2.5	Representative volume element loaded in Shear	18
2.6	Unidirectionally reinforced lamina	19
2.7	Positive Rotation of Principal Material Axes from x-y Axes	20
2.8	Laminate	22
2.9	Geometry of Deformation in the x-z Plane	23
2.10	Geometry of an N-Layered Laminate	25
2.11	In-Plane Force on a Flat Laminate	25
2.12	Moments on a Flat Laminate	26
3.1	Network of entangled polymers [21]	27
3.2	Stress-Strain curve	29
3.3	Example of viscous flow	30
3.4	Laminar shear of fluid between two plates	31
3.5	Fluid thin layers	31
3.6	Shear rate	32
3.7	Shear rate for newtonian and non-newtonian fluids	32
3.8	Shear strain vs time	34
3.9	Elastic, Viscous and Viscoelastic behaviour to an applied stress	34
3.10	Responses of different materials during creep recovery tests	35
3.11	Viscoelastic and Elastic behavior to a stress relaxation test	35

3.12	Element in a Maxwell model	37
3.13	Deformed element in a Maxwell model	37
3.14	Relaxation in a Maxwell model	38
3.15	Creep in a Maxwell model	39
3.16	Creep in a Kelvin-Voigt model	41
3.17	Elements in a Zener model	41
3.18	Creep (a) and Relaxation (b) tests for Maxwell, Kelvin-Voigt and Zener models	43
3.19	Hysteresis loop in a viscoelastic materials	43
3.20	DMA of Elastic, Viscous and Viscoelastic materials	44
3.21	Storage modulus and loss modulus	46
3.22	Temperature effects on Storage Modulus and Loss Factor	48
3.23	Temperature effects on different materials: plastic (a), elastomer (b)	48
3.24	Optimum regions for the Loss Factor	49
3.25	Frequency effects on Storage Modulus and Loss Factor	50
3.26	Both Temperature and Frequency effects	51
4.1	Excitation	55
4.2	The use of Hilbert transform to determine a signal envelope	56
4.3	Example of MDOF system	57
4.4	IRF for a SDOF system	57
4.5	Filtered time-history and its Hilbert envelope, $F_c=508\text{Hz}$	58
4.6	Regression line, $F_c=508\text{Hz}$	59
4.7	Excitation system (a) and some of its components (b)	60
4.8	Excitation signal	60
4.9	Climatic room of Alenia Aeronautica laboratories	61
4.10	Acquisition system	61
4.11	Panels lay-up: (a) treated, (b) no-treated	62
4.12	Test Panel	62
4.13	Acceleration time histories for treated and no-treated panels	63
4.14	No-treated (a) vs treated (b) time histories, $F_c=254\text{Hz}$	64
4.15	No-treated (a) vs treated (b) time histories, $F_c=508\text{Hz}$	65
4.16	No-treated (a) vs treated (b) time histories, $F_c=806\text{Hz}$	66
4.17	No-treated (a) vs treated (b) time histories, $F_c=1016\text{Hz}$	67
4.18	No-treated (a) vs treated (b) time histories, $F_c=2032\text{Hz}$	68
4.19	No-treated (a) vs treated (b) time histories, $F_c=3225\text{Hz}$	69
4.20	Loss factor for each accelerometers in a no-treated panels at $T=-35^\circ\text{C}$	70
4.21	Loss factor for each accelerometers in a treated panels at $T=-35^\circ\text{C}$	71
4.22	Loss factor for both test panels (treated and no-treated) at $T=-35^\circ\text{C}$	72

4.23	Treated panel: loss factor vs frequency at different temperature conditions	72
4.24	Standard deviation for each temperature condition	73
4.25	Confidence interval for no-treated panel, T=-35°C	74
4.26	Confidence interval for treated panel, T=-35°C	74
5.1	Finite element models for composite structures with viscoelastic core	78
5.2	Shear locking: real (a) and approximate (b) linear representations of bending deflections	78
5.3	Test panel: real (a) and FE model(b)	79
5.4	Reference system for composite lay-up	80
5.5	Loss Factor for HPLT viscoelastic material	80
5.6	Complex Modulus for HPLT viscoelastic material	81
5.7	G' and G'' for HPLT viscoelastic material	81
5.8	Application of interconversion methods to HPLT viscoelastic material	84
5.9	Loss Factor vs. frequency result for test 1	85
5.10	Loss Factor vs. frequency results for all explicit non linear simulations	86
5.11	Frequency Response Function (FRF) for two temperature conditions	89
5.12	FRF (a) and accelerations (b), for both temperature conditions . .	89
5.13	Loss Factor vs. frequency results for all direct frequency response simulations	90

List of Tables

- 3.1 List of some polymer types 28

- 4.1 Position of the accelerometers 70

- 5.1 Number of Nodes and Elements of the FE model 79
- 5.2 Properties of the Composite plies 80
- 5.3 Parameters used in a first numerical simulation 85
- 5.4 Parameters used in simulations from 1 to 4 85

Introduction

This thesis summarizes the work done by the author in the frame of the Ph.D. Program in Aerospace, Naval and Quality Engineering at the University of Naples Federico II, following the research projects ARCA and COMFORT, which were aimed to develop innovating solutions for the noise and vibration control in the aeronautical field. In the last years, a constant pursuit in performance improvement has been demanded to the aeronautical products, mainly in reducing weight and fuel consumption, hence in reducing the emissivity of polluting agents (Nox). The employment of composite materials in bigger parts of the structures is one of the solutions found to reduce weight, culminating in the design of Boeing 787, the first airplane with a massive part of carbon fiber also in the main frames of the fuselage structure. However, like any other engineering solution, using composite materials has its own drawbacks; while they allow considerable weight reductions, they show high noise permeability thus negatively influencing the comfort level, when employed in the structural elements of an airplane fuselage. To contrast this behavior and comply with comfort requirements in the cabin, it was suggested the use of soundproof or damping materials. Adding one or more viscoelastic material layers within the laminate allows to increase the damping properties of the structure, hence limiting the noise, whether it is structure-borne or air-borne. This approach is called *passive control of noise*. Inserting a viscoelastic material between composite plies increases the total weight of the panel, contrasting the weight gained by using composite materials. On the other hand, this technique only reduces the noise by increasing the structural damping of the system panel-viscoelastic layer. Damping is very important for noise and vibration control and for structural stability as well; however, the experimental characterization of the damping level of a structure and its numerical modeling are very hard to realize, especially when viscoelastic materials are employed. At the present day, few references can be found in literature on the subject of damping measurements on composite structures with embedded damping treatment, depending on temperature. From the numerical point of view, things get even more complicated, since even fewer results are found in literature, given the lack of adequate modeling criteria and analysis procedures. This thesis was motivated by the need of further development in both the modeling and the prediction of viscoelastic damping materials properties, for the practical use in aeronautical applications. The aim of this work is to identify, define and validate a procedure for experimental-numerical analyses capable to characterize the behavior of structures with embedded viscoelastic damping treatments, as a function of temperature, in a range of values similar to that of flight conditions. The present research activity can thus be split up in two parts: the first one related to ex-

perimental tests and the second related to the numerical simulations. About the experimental part, the objectives have been primarily the identification and validation of a procedure capable to extract the loss factor with a low dispersion of the data in different temperature conditions and, subsequently, the characterization of the performance of two test panels in different environmental conditions like flight temperature conditions. About the numerical part, the objective has been the identification of a numerical procedure able to give as output the same result of the experimental tests, in terms of loss factor. In this direction, two ways have been undertaken by two different numerical approaches: explicit in time domain and direct in frequency domain.

For the numerical part of the study, a FEM solver was used, NASTRAN. As it will be shown in the following, the damping extraction procedures were realized with dedicated routines written in Matlab. This thesis is organized as follows: in chapter 1, the state of the art about damping treatments is exposed, together with analytical and numerical models that allow to study it. In chapter 2, composite materials are described, as they are characterized as laminates starting from fiber and matrix characteristics. In chapter 3 viscoelastic materials are introduced, first describing viscous and elastic properties separately, then introducing the constitutive models already present in literature to describe such materials. Then these properties were described as functions of several external factors, such as temperature, frequency, etc. In chapter 4, the approach adopted for the experimental part is presented. A detailed description of the loss factor extraction procedure is proposed (IRDM) with the hypotheses to take into account to consider this procedure applicable to highly damped structures as well. The test bed set-up and the lay-up of analyzed panels are described. In the end, the results in terms of position effect (due to the accelerometers position) and temperature effect are shown. Then, in order to validate a procedure of experimental analysis on over 700 acquisitions, a statistical analysis is proposed. In chapter 5, the FEM modeling criterion is shown, in terms of element types, boundary conditions and constraints. Then, two possible approaches are confronted, a time-domain explicit approach and a frequency-domain direct approach. Thereafter, a numerical-experimental comparison is performed to define which procedure is the most suitable to the analysis at the subject of this thesis.

Chapter 1

Damping treatments: State of the Art

Viscoelastic materials are rubber-like polymers possessing stiffness and damping characteristics which vary strongly with temperature and frequency. In most case, practical structures and machines requiring vibration or structure-borne noise control cannot be made of these materials, because they are usually far too weak. Instead, the materials must be added strategically to the structure or machine in a way which may vary according to the system involved. It may be noted, however, that many parts of modern machines and structures are frequently made of stiff plastic materials.

The goal of an effective damping treatments is to add the viscoelastic material in such a way and in such location as to ensure that the greatest possible cyclic deformation of the damping materials will occur as the structure vibrates in the modes of interest, to dissipate as much vibrational energy during each cycle as possible. This requires an understanding of the dynamic behaviour of the structure or machine and an understanding of the deformation of the viscoelastic material which occurs during vibration of the structure, and by no means least, an understanding of the complex modulus properties of the candidate damping materials in order that a proper treatment can be developed. Many other engineering factors must also be considered, some of which may be far more difficult to overcome than the damping treatments design itself. In this reaserch work, only the effects of temperature and frequency on the viscoelastic material properties have been considered and so the effects on the overall structure were evaluated.

1.1 Noise and Vibration Control

The internal noise has an important role in the design of aircraft, if it is too high reduces comfort in the fuselage and could cause interferences with aircraft systems. The noise inside the cabin can be generated by various sources and, depending on its propagations, can be classified into two types:

- *airborne noise*: external noise generated, for example, by turbofans propellers and turbulent boundary layer and transmitted through the air;

- *structure-borne noise*: noise generated by vibrations of the structure and transmitted through the same.

The noise transmitted by air is critical to high frequencies because it is characterized by high sound pressure level, instead the sound transmission through the structures is particularly critical to lower frequencies. In this way the worst condition is when there are both (fig.1.1). The noise control and its reduction

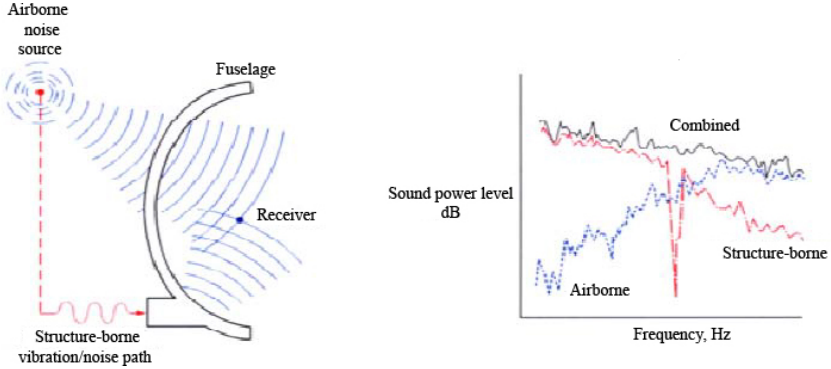


Figure 1.1: Airborne and Structure-borne noise

can be achieved in two ways:

- acting directly on the primary source of noise (*active control*);
- increasing the attenuation and dissipation along the path of waves' propagation (*passive control*)

In aeronautical field, generally, the passive control systems are preferred to the active ones due to their lower complexity and costs. A vibrating structure, has a mechanical energy distributed between: kinetic energy associated to mass; deformation energy associated to stiffness and dissipated energy, usually in form of heat, associated to damping. Thereafter the reduction of vibration level can be performed by increasing the structural damping. The main effects of this are: the attenuation of structure-borne noise, the reducing of vibration amplitude in resonance conditions, the reduction of the structural fatigue phenomena and the transmission loss increase near the critical frequencies. A possible way to increase the damping in composite structures is using viscoelastic materials embedded between the plies giving benefits both for airborne and structural-born trasmission ways. Others damping treatments will be shown in the next paragraphs.

1.2 Types of Damping Treatments

Viscoelastic damping materials can be applied in many ways, some of which are showed in a figure 1.2a-b. The extensional treatment or free-layer treatment (fig.1.2a) can be applied in parallel with member which are deformed in extension during vibration. This case is relatively simple, since stiffness are then directly added as [1]:

$$k^* = k_s + k_v(1 + i\eta_v) \quad (1.1)$$

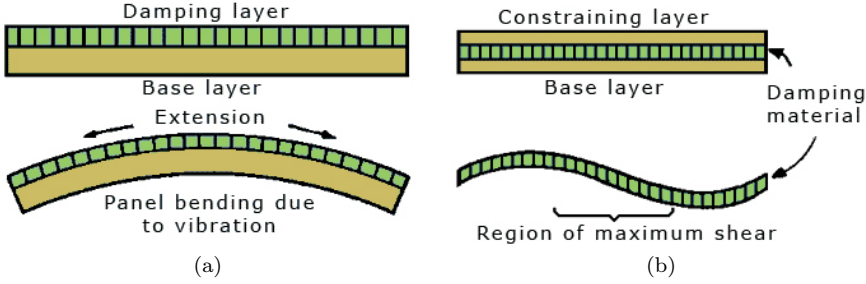


Figure 1.2: Damping treatments: free-layer (a) and constrained-layer (b)

where $k^* = k(1 + i\eta)$ is the complex stiffness of the combination, k_s is the initial stiffness of the member and $k_v(1 + i\eta_v)$ is the complex stiffness of the parallel viscoelastic element. The effective stiffness and loss factor of the combined system is, therefore:

$$k = k_s + k_v \quad (1.2)$$

$$\eta = \frac{\eta_v}{1 + k_v/k_s} \quad (1.3)$$

so that the maximum loss factor of the damped member depends upon the value of both η_v and the ratio k_v/k_s .

The simplest flexural damping treatment (free-layer) consists simply of a viscoelastic coating applied to a beam or plate surface in a sufficient thickness to materially increase the damping of the coated member. The change of flexural rigidity of the plate or beam is readily calculated from the dimensions and modulus of the plate or beam material, and the thickness and complex modulus values of the viscoelastic coating by means of an equation first introduced by Oberst [3]. Invariably, for this type of treatment, high thicknesses and high modulus and loss factor value are required, so the treatments are somewhat inefficient from a weight point of view. However, costs of materials and application processes are often lowest for this type of treatment. The simplest form of Oberst's equations are written in the form:

$$\frac{(EI)^*}{E_s I_s} = 1 + \frac{E_v^*}{E_s} \left(\frac{h_v}{h_s} \right)^3 + 3 \left(1 + \frac{h_v}{h_s} \right)^2 \frac{(E_v^*/E_s)(h_v/h_s)}{1 + (E_v^*/E_s)(h_v/h_s)} \quad (1.4)$$

where h_s is the thickness and E_s is the Young's modulus of the structural member and h_v is the thickness of the damping layer, and $I_s = h_s^3/12$. E_v^* is the complex Young's modulus of the viscoelastic layer. The real and imaginary parts of this equation may readily be calculated, and the effective flexural rigidity and loss factor of the damped member determined. Oberst's equation is approximate, and applies only to members which deform in flexure. These members may, of course, be part of a large system.

A more complicated flexural damping treatment is the so-called shear or constrained layer damping treatment (fig.1.2b). In this case, the viscoelastic layer is capped by another elastic layer, such as a metal sheet or plate. In fact, multiple layers can be applied when needed. In this case, the effective flexural modulus of the damped configuration is much more difficult to calculate, since it depends upon the boundary conditions and the mode shape, as well as the various dimensions and damping material complex modulus. Approximate equations of various

types are known, such as the Ross-Kerwin-Ungar equation [4], which applies accurately only to beam-like members with pinned-pinned boundary conditions, but is often applied to cases having other simple boundary conditions, such as cantilever beams and clamped-clamped beams. More complicated configurations with this type of treatment, such as stiffened panel, can be properly addressed only by means of finite element analysis.

One application of this last treatment is the so-called embedded viscoelastic damping treatment (fig.1.3). In this configuration the host structure and the

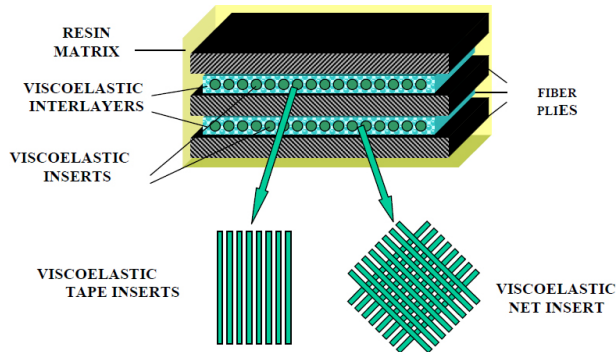


Figure 1.3: Embedded viscoelastic damping treatment

constraining layer are laminates made up with the same composite material, while the damping layer is made up of viscoelastic material embedded between them. The traditional analytical models, such as Ross-Kerwin-Ungar model, do not allow the calculation of the damping for these complex structures. The only way forward is one that uses finite element approach, as we shall see later.

1.3 Analytical models

There have been several analytical methods developed since the late 1950's to predict response of damped systems. Some of the more popular methods include those developed by Ross, Kerwin, and Ungar [4], Mead and Markus [5], DiTaranto [6], Yan and Dowell [7], and Rao and Nakra [8]. However, the development of finite element software has increased the accuracy and precision of estimations of the dynamic responses of damped structures. For fairly simple structures, analytical methods can be used as a substitution for finite element predictions. Furthermore, finite element packages are often computationally expensive, something that might not be needed for damping predictions of simpler systems. In this case, a simple code or program can be written implementing an analytical method to derive a simple, sufficiently accurate damping model. As the complexity of the system increases, however, finite element formulations should be strongly considered as the boundary conditions and system parameters may prove too difficult to define using a simple analytical based formulation.

1.3.1 Ross, Kerwin and Ungar model

Ross, Kerwin, and Ungar developed one of the earliest damping models for threelayered sandwich beams based on damping of flexural waves by a constrained viscoelastic layer. They employed several major assumptions, including [10]:

- For the entire composite structure cross section, there is a neutral axis whose location varies with frequency;
- There is no slipping between the elastic and viscoelastic layers at their interfaces;
- The major part of the damping is due to the shearing of the viscoelastic material, whose shear modulus is represented by complex quantities in terms of real shear moduli and loss factors;
- The elastic layers displaced laterally the same amount;
- The beam is simply supported and vibrating at a natural frequency, or the beam is infinitely long so that the end effects may be neglected.

These assumptions apply to any constrained layer damping treatment applied to a rectangular beam. Figure 1.4 shows an example system which the Ross, Kerwin, and Ungar (RKU) equations could be applied to.

Comparison between experimental data and this theory have shown that results

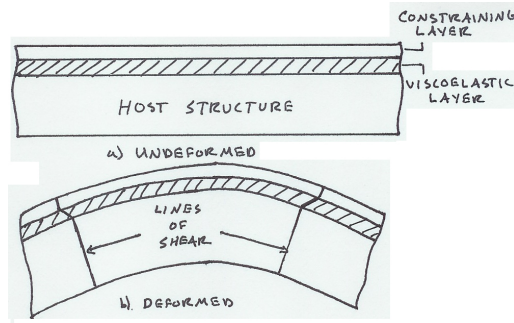


Figure 1.4: Three layer beam, with viscoelastic treatments

from theory correlate well to experiment [4]. The model is represented by a complex flexural rigidity, $(EI)^*$, where the * denotes a complex quantity, given by:

$$\begin{aligned}
 (EI)^* = & \frac{E_s h_s^3}{12} + \frac{E_v^* h_v^3}{12} + \frac{E_c h_c^3}{12} - \frac{E_v^* h_v^2 (d - D)}{12(1 + g_v^*)} + \\
 & + E_s h_s D^2 + E_v^* h_v (h_{vs} - D)^2 + E_c h_c (d - D)^2 + \\
 & - \left[\frac{E_v^* h_v (h_{vs} - D)}{2} + E_c h_c (d - D) \right] \left[\frac{(d - D)}{(1 + g_v^*)} \right]
 \end{aligned} \tag{1.5}$$

where D is the distance from the neutral axis of the three layer system to the neutral axis of the host beam,

$$\begin{aligned}
 D &= \frac{E_v^* h_v (h_{vs} - \frac{d}{2}) + g_v^* (E_v^* h_v h_{vs} + E_c h_c d)}{E_s h_s + \frac{E_v^* h_v}{2} + g_v^* (E_s h_s + E_v^* h_v + E_c h_c)} \\
 h_{vs} &= \frac{h_s + h_v}{2} \\
 g_v^* &= \frac{G_v^*}{E_c h_c h_v p_1} \\
 d &= h_v + \frac{h_s + h_c}{2}
 \end{aligned} \tag{1.6}$$

In these equations E_s, E_v^*, E_c and h_s, h_v, h_c are the elastic moduli and thickness of the host structure, viscoelastic layer and constraining layer, respectively. The term g_v^* is known as the *shear parameter* which varies from very low when G_v^* is small to a large number when G_v^* is large. The term p within the shear parameter is the wave number, namely the n^{th} eigenvalue divided by the beam length. The shear parameter can also be expressed in terms of modal frequencies by

$$\begin{aligned}
 g_v^* &= \frac{G_v^* L^2}{E_c h_v h_c \xi_n^2 \sqrt{C_n}} \\
 \xi_n^4 &= \frac{\rho_s b h_s \omega_n^2 L^4}{E_s I_s}
 \end{aligned} \tag{1.7}$$

where ω_n is the n^{th} modal frequency and C_n are correction factors determined by Rao [8].

The equation 1.5, imposing $h_c = 0$ (extensional layer) and $g_v^* \rightarrow \infty$, become:

$$\frac{(EI)^*}{E_s I_s} = \frac{1 + 4 \frac{E_v^*}{E_s} \frac{h_v}{h_s} + 6 \frac{E_v^*}{E_s} \left(\frac{h_v}{h_s}\right)^2 + 4 \frac{E_v^*}{E_s} \left(\frac{h_v}{h_s}\right)^3 + \left(\frac{E_v^*}{E_s}\right)^3 \left(\frac{h_v}{h_s}\right)^4}{1 + \frac{E_v^*}{E_s} \frac{h_v}{h_s}} \tag{1.8}$$

remembering that $E^* = E(1 + i\eta)$ and $E_v^* = E_v(1 + i\eta_v)$ where η is the loss factor of the entire structure and η_v is the loss factor of the viscoelastic layer, we can write:

$$\eta_v = \frac{\frac{E_v}{E_s} \frac{h_v}{h_s} \left[3 + 6 \frac{h_v}{h_s} + 4 \left(\frac{h_v}{h_s}\right)^2 + 2 \frac{E_v}{E_s} \left(\frac{h_v}{h_s}\right)^3 + \left(\frac{E_v}{E_s}\right)^2 \left(\frac{h_v}{h_s}\right)^4 \right]}{\left(1 + \frac{E_v}{E_s} \frac{h_v}{h_s}\right) \left[1 + 4 \frac{E_v}{E_s} \frac{h_v}{h_s} + 6 \left(\frac{h_v}{h_s}\right)^2 + 4 \left(\frac{h_v}{h_s}\right)^3 + \left(\frac{E_v}{E_s}\right)^2 \left(\frac{h_v}{h_s}\right)^4 \right]} \tag{1.9}$$

By this approach, known thickness and loss factor of the viscoelastic material, the equation 1.9 gives the loss factor of the structure treated with the free layer

treatment.

Similarly one can derive the equation of the loss factor in the case of the treated structure with Extensional layer treatments. The equation 1.9 can be written as:

$$\frac{\eta}{\eta_v} = \frac{g_v^* Y}{1 + (2 + Y)g_v^* + (1 + Y)(1 + \eta_v^2)(g_v^*)^2} \quad (1.10)$$

where g_v^* is the shear parameter and Y is called *geometric parameter* if both host structure and constraining layer are of the same material ($E_s/E_c = 1$) and it is equal to:

$$Y = \frac{12 \left(\frac{d}{h_s} \right)^3}{\left[1 + \frac{E_c}{E_s} \left(\frac{h_c}{h_s} \right)^3 \right]} \left[\frac{\frac{E_c}{E_s} \left(\frac{h_c}{h_s} \right)}{\frac{E_c}{E_s} \left(\frac{h_c}{h_s} \right) + 1} \right] \quad (1.11)$$

from equation 1.10 is known as the loss factor η varies with the geometrical parameter (Y) and η_v . In addition, fixed Y and η_v , there is an optimum value for the shear parameter given by:

$$(g_v^*)_{opt} = \frac{1}{\sqrt{(1 + Y)(1 + \eta_v^2)}} \quad (1.12)$$

A significant effect on performance of the damping treatments is due to temperature. At low temperatures, where the viscoelastic material is in the glassy region with a very high shear modulus, the host structure and constraining layer are rigidly connected and so are therefore coupled; the shear contribution in the viscoelastic layer is negligible. At high temperatures, however, when the material is in the rubbery region, the host structure and constraining layer are uncoupled: in this case, the shear deformation is very high but the shear modulus is low then the dissipated energy is low to. Between these two cases the maximum loss factor is found.

Ultimately for the loss factor calculation of a treated panel with a constrained layer treatment, the relationship between the wavelength and frequency of the flexural modes of the treated panel must be known so the problem can be solved iteratively [9].

1.4 Numerical models

The analytical methods are applicable only on relatively simple structures, while the need to analyze complex structures turn our attention to the methods based on finite element analysis. For the application of all the numerical models presented in the following, the NASTRAN software was used.

1.4.1 Modal Strain Energy

The assumptions of the Modal Strain Energy (MSE) model consists in representing the modal behavior of the damped structure as a real eigenvalues problem, ie neglecting the effects of damping on the modal frequencies and modal shapes. This narrows the applicability of the MSE method to slightly damped structures.

In fact, in the reality, if the damping is not small its effect can be seen on both modal frequencies and modal shapes [12]. Mathematically, it is a real eigenvalues problem that initially requires to calculate the natural frequencies for the undamped system. The modal loss factors are calculated using the real modal deformation and assigning the loss factor for each material. This approach was suggested by Ungar and Kerwin in 1962 [13] and the next implementation in a Finite Element Model (FEM) was developed by Rogers in 1980 [14].

The MSE principle states that the ratio of composite system loss factor to the viscoelastic material loss factor for a given mode of vibration can be estimated from the ratio of elastic strain energy in the viscoelastic elements to the total strain energy in the model for a given mode. This is shown mathematically in the following equation:

$$\eta^n = \eta_v \frac{U_v^n}{U_{Tot}^n} \quad (1.13)$$

where:

η^n is the loss factor of the structure treated for the n^{th} mode of vibration;

η_v is the viscoelastic damping for the appropriate frequency and temperature;

U_v^n is the elastic strain energy stored in the viscoelastic core for the n^{th} mode;

U_{Tot}^n is the total elastic strain energy for n^{th} mode shape.

Typically, the MSE approach is used in conjunction with an undamped, normal modes analysis to compute the strain energy ratio. The strain energies are determined from the relative mode shapes. It is assumed that the viscoelastic properties are linear in terms of the dynamic strain rate.

Despite the strong assumptions of low damping, this method is widely used because in many finite element software some procedure to calculate the strain energy have been developed.

1.4.2 Complex Eigenvalues Method

The complex eigenvalue analysis problem in general is a quadratic eigenvalue problem in the form:

$$M\ddot{u} + B\dot{u} + Ku = 0 \quad (1.14)$$

where u is the displacement vector; \ddot{u} is the acceleration of the grid points, i.e., the second time derivative of u ; \dot{u} refers to the velocity or first time derivative; M, B, K are the mass, damping and stiffness matrixes respectively. The B matrix may be purged and the M and K matrixes may be real or complex, symmetric or unsymmetric.

The solution of this homogeneous system (the free, but damped vibrations) is of the form

$$u = e^{\lambda^* t} \Phi \quad (1.15)$$

where Φ is a vector of complex numbers and λ^* the eigenvalue is also complex. By substituting equation 1.15 into equation 1.14, we get:

$$(M(\lambda^*)^2 + K) \Phi = 0 \quad (1.16)$$

In order to solve the quadratic eigenvalue problem, first a linearization transformation is executed. This transformation converts the original quadratic problem to a linear problem of twice the size.

It is obtained by simply rewriting last equation as a 2x2 block matrix equation:

$$\lambda^* \begin{bmatrix} M & 0 \\ 0 & I \end{bmatrix} \begin{bmatrix} \dot{\Phi} \\ \Phi \end{bmatrix} + \begin{bmatrix} 0 & K \\ -I & 0 \end{bmatrix} \begin{bmatrix} \dot{\Phi} \\ \Phi \end{bmatrix} = 0 \quad (1.17)$$

where:

$$\dot{\Phi} = \lambda^* \Phi \quad (1.18)$$

The complex eigenvalue can be expressed by *real* and *imaginary* contribution as:

$$\lambda^* = \lambda + i\lambda' \quad (1.19)$$

By this approach, for each n^{th} mode, and so for each n^{th} eigenvalue, the loss factor can be obtained as relationship between *real* and *imaginary* parts of the eigenvalue as:

$$\eta^n = \frac{\lambda'^n}{\lambda^n} \quad (1.20)$$

Unlike the MSE, this method allows to characterize the loss factor of very damped structures but with a computational cost about three times higher than the MSE. Moreover, in many FEM software its use is limited by the material models. Many of these software, in fact, does not allow to use the viscoelastic material models with the complex eigenvalues analysis. Thus this method can not be used in the present case [15].

Other numerical approaches can be used. In these methods the loss factor must be calculated using the same approach used in experimental tests (IRDM) contrarily to what occurs in the previous models in which the damping is directly provided by the software. Two of these approaches (in time and frequency domains) are discussed in chapter 5 where, as we shall see, the real behavior of the structure as done in the experimental tests, in the same load and boundary's conditions, has been simulated. Two different models of viscoelastic material, Herman and Peterson and Hysteretic formulation respectively, have been used.

Chapter 2

Composite materials

In all space and aeronautical applications the fundamental constructions' requirement is the lightness, associated with the strength and stiffness. In this direction, composite materials perfectly meet these specifications.

The word *composite* in the term *composite material* signifies that two or more materials are combined on a macroscopic scale to form a useful third material. Different materials can be combined on a macroscopic scale, such as in alloying of metals, but the resulting material is, for all practical purposes, macroscopically homogeneous, i.e. the components cannot be distinguished by the naked eye and essentially act together. The advantage of composite materials is that, if well designed, they usually exhibit the best qualities of their components or constituents and offer some qualities that neither constituent possesses. Some of the properties that can be improved by forming a composite material are:

- strength
- stiffness
- corrosion resistance
- wear resistance
- weight
- fatigue life
- temperature-dependent behavior
- thermal insulation
- thermal conductivity
- acoustical insulation

Naturally, not all of these properties are improved at the same time nor is there usually any requirement to do so. In fact, some of the properties are in conflict with one other, e.g., thermal insulation versus thermal conductivity. The objective is merely to create a material that has only the characteristics needed to perform the design task. In this direction, this Ph.D thesis is focused. The purpose is to evaluate how the acoustical properties of a composite material improve by the use of embedded viscoelastic plyers.

Composite materials have a long history of usage. Their precise beginnings are unknown, but all recorded history contains references to some form of composite material. For example, straw was used by the Israelites to strengthen mud bricks. Plywood was used by the ancient Egyptians when they realized that wood could be rearranged to achieve superior strength and resistance to thermal expansion as well as to swelling caused by the absorption of moisture. Medieval swords and armor were constructed with layers of different metals. More recently, fiber-reinforced, resin-matrix composite materials that have high strength-to-weight and stiffness-to-weight ratios have become important in weight-sensitive applica-

tions such as aircraft and space vehicles.

The first applications of composite materials in aerospace provided only the construction of tertiary structures, or parts not intended to bear heavy loads, or constant stress. Currently these materials are also used for the realization of structural elements. This coincided with the introduction of carbon fibers which, year by year, have made significant improvements to the properties of epoxy resins and composites. The use of composites in the aeronautical has considerably expanded in 1980s years so much to realize the first aircraft extensively built with these materials. The components of the composite must be insoluble to each other. The above is valid at a macroscopic level. Composite materials are biphasic, ie composed of two distinct solid phases; the first one have a reinforcing function (fibers, which are the reinforcement) and the second one with binder function(matrix). The matrix is the material that includes, generally, the fibers; the fibers are responsible for providing the composite strength and stiffness. They can be oriented in appropriate direction and are generally circular in cross section.

2.1 Micromechanical behaviour of a Lamina

As above mentioned, a large enough piece of the lamina was considered so that the fact that the lamina is made of two or more constituent materials cannot be detected. Thus, we were able to say that a composite material has certain stiffnesses and strengths that we measured in various directions. But the basic question of micromechanics is: what is the relationship of the composite material properties to the properties of the constituents? (fig.2.1).

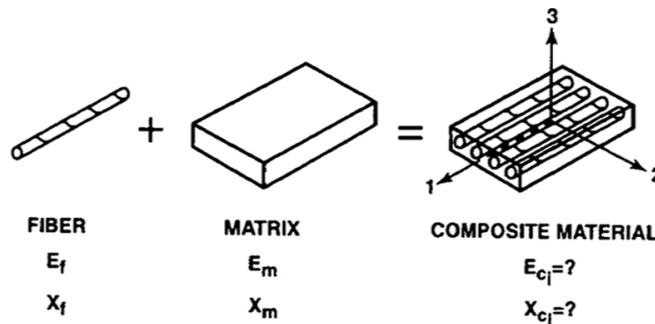


Figure 2.1: Basic question of micromechanics

The micromechanics study the composite materials behaviour wherein the interaction of the constituent materials is examined in detail as part of the definition of the behaviour of the heterogeneous composite material.

Thus the properties of a lamina can be experimentally determined in the *as made* state or can be mathematically estimated on the basis of the properties of the constituent materials. That is, we can predict lamina properties by the procedure of micromechanics, and we can measure lamina properties by physical means and use the properties in a macromechanical analysis of the structure. Thus, micromechanics is a natural adjunction to macromechanics when viewed

in a materials design rather than a structural analysis environment. Real design power is demonstrated when the micromechanical predictions of the properties of a lamina agree with the measured properties. About this, micromechanical analysis has significant, inherent limitations. For example, a perfect bond between fibers and matrix is a usual analysis restriction that might well not be satisfied by some composite materials. Thus micromechanical theories must be validate by careful experimental work.

There are different approach to the micromechanics of composite materials. The most used is the *Mechanics of Materials* [16].

The key feature of the mechanics of materials approach is that certain simplifying assumption must be made regarding the mechanical behaviour of a composite material in order to get an effective solution. Each assumption must be plausible, i.e., there must be a reason why the assumption might be true. The most prominent assumption is that the strain in the fiber direction of a unidirectional fiber-reinforced composite material are the same in the fibers as in the matrix (fig.2.2). If the strains were not the same, then a fracture between the fibers and

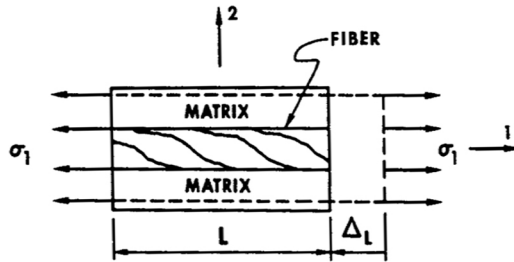


Figure 2.2: Representative volume element loaded in the 1-Direction

the matrix is implied. Thus, the assumption has a plausible reason. Because the strains in both the matrix and fiber are the same, then it is obvious that section normal to the 1-axis, which were plane before being stressed, remain plane after stressing. In the following just we will show, on that basis, the mechanics of materials predictions for the apparent orthotropic moduli of a unidirectionally fiber-reinforced composite material, namely, E_1 , E_2 , ν_{12} and G_{12} .

Determination of E_1

The first modulus to be determined is that of the composite material in the 1-direction, ie in the fiber direction (fig.2.2).

$$\varepsilon_1 = \frac{\Delta L}{L} \quad (2.1)$$

where ε_1 applies for both the fibers and the matrix according to the basic assumption. Then, if both constituent material behave elastically, by the Hooke's law, the stresses in the fiber direction for fibers (σ_f) and matrix σ_m respectively are:

$$\sigma_f = E_f \varepsilon_1 \quad \sigma_m = E_m \varepsilon_1 \quad (2.2)$$

The average stress σ_1 acts on cross-sectional area A of the representative volume element, σ_f acts on the cross-sectional area of the fibers A_f , and σ_m acts on

the cross-sectional area of the matrix A_m . Thus, the resultant force on the representative volume element of composite material is:

$$F = \sigma_1 A = \sigma_f A_f + \sigma_m A_m \quad (2.3)$$

replacing equation 2.2 in equation 2.3 and recognition from macromechanics that:

$$\sigma_1 = E_1 \varepsilon_1 \quad (2.4)$$

we have:

$$E_1 = E_f \frac{A_f}{A} + E_m \frac{A_m}{A} \quad (2.5)$$

But the volume fractions of fibers and matrix can be written as:

$$V_f = \frac{A_f}{A} \quad V_m = \frac{A_m}{A} \quad (2.6)$$

Thus:

$$E_1 = E_f V_f + E_m V_m \quad (2.7)$$

which is known as the rule of mixtures for the apparent Young's modulus of the composite material in the direction of the fibers. The rule of mixtures represents a simple linear variation of apparent Young's modulus E_1 from E_m to E_f as V_f goes from 0 to 1. The fiber modulus is typically many times the matrix modulus. Thus, at usual practical fiber-volume fraction around .6, the fiber modulus dominates the composite modulus E_1 .

Determination of E_2

The apparent Young's modulus, E_2 , of the composite material in the direction transverse to the fibers is considered next. In the mechanics of materials approach, the same transverse stress, σ_2 , is assumed to be applied to both the fiber and the matrix (fig. 2.3). That is, equilibrium of adjacent elements in the com-

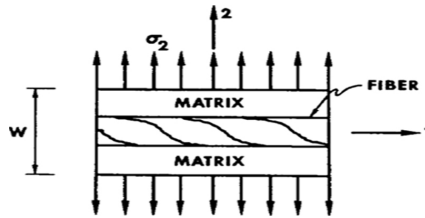


Figure 2.3: Representative volume element loaded in the 2-Direction

posite material (fibers and matrix) must occur.

The strains in the fiber and in the matrix are, therefore, found from the stresses:

$$\varepsilon_f = \frac{\sigma_2}{E_f} \quad \varepsilon_m = \frac{\sigma_2}{E_m} \quad (2.8)$$

The transverse dimension over which, on average, ε_f acts is approximately $V_f W$, whereas ε_m acts on $V_m W$. Thus, the total transverse deformation is:

$$\Delta W = \varepsilon_2 W = V_f W \varepsilon_f + V_m W \varepsilon_m \quad (2.9)$$

or

$$\varepsilon_2 = V_f \varepsilon_f + V_m \varepsilon_m \quad (2.10)$$

which becomes, upon substitution of the strains from equation 2.8,

$$\varepsilon_2 = V_f \frac{\sigma_2}{E_f} + V_m \frac{\sigma_2}{E_m} \quad (2.11)$$

but from the macroscopic stress-strain relation we have:

$$\sigma_2 = E_2 \varepsilon_2 = E_2 \left[\frac{V_f \sigma_2}{E_f} + \frac{V_m \sigma_2}{E_m} \right] \quad (2.12)$$

whereupon:

$$E_2 = \frac{E_f E_m}{E_f V_m + E_m V_f} \quad (2.13)$$

which is known as the rule of mixtures for the apparent transverse Young's modulus of the composite material. Obviously, the assumptions involved in the foregoing derivation are not entirely consistent. In literature [16], better approaches are available for prediction of E_2 , but at the cost of far more complexity.

Determination of ν_{12}

The Poisson's ratio, ν_{12} , is obtained by an approach similar to the analysis for E_1 . First, Poisson's ratio is:

$$\nu_{12} = -\frac{\varepsilon_2}{\varepsilon_1} \quad (2.14)$$

for the stress state $\sigma_1 = \sigma$ and all other stresses are zero. Then, the deformation are depicted in the representative volume element (fig.2.4). There, the fundamental simplifying assumption is that the fiber strains are identical to the matrix strains in the fiber direction, as in the approach to E_1 .

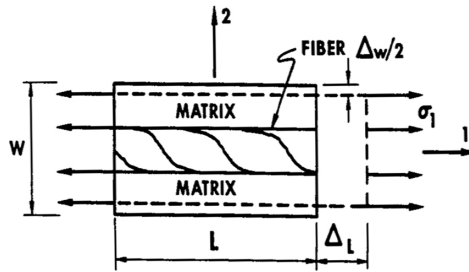


Figure 2.4: Representative volume element loaded in the 1-Direction

The transverse deformation Δ_W is macroscopically equal to:

$$\Delta_W = -W \varepsilon_2 = -W \nu_{12} \varepsilon_1 \quad (2.15)$$

but is also microscopically

$$\Delta_W = \Delta_{mW} + \Delta_{fW} \quad (2.16)$$

In the manner of the analysis for the transverse Young's modulus, E_2 , the transverse deformations Δ_{mW} and Δ_{fW} are approximately:

$$\Delta_{mW} = WV_m\nu_m\varepsilon_1 \quad \Delta_{fW} = WV_f\nu_f\varepsilon_1 \quad (2.17)$$

Combine the last equations and divide by $\varepsilon_1 W$ to get

$$\nu_{12} = \nu_m V_m + \nu_f V_f \quad (2.18)$$

which is a rule of mixtures for the Poisson's ratio. Because the Poisson's ratios ν_m and ν_f are not significantly different from each other, the composite material Poisson's ratio ν_{12} is neutral, i.e., neither matrix-dominated nor fiber-dominated.

Determination of G_{12}

The in-plane shear modulus of a lamina, G_{12} , is determined in the mechanics of materials approach by presuming that the shearing stresses on the fiber and on the matrix are the same (fig.2.5). As we will show in a section 3.1.1, by virtue of the basic presumption, we know that:

$$\gamma_m = \frac{\tau}{G_m} \quad \gamma_f = \frac{\tau}{G_f} \quad (2.19)$$

The nonlinear shear stress-shear strain behavior typical of fiber-reinforced composite materials is ignored, i.e., the behavior is regarded as linear.

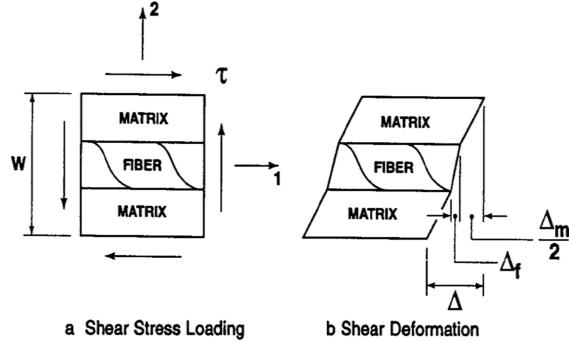


Figure 2.5: Representative volume element loaded in Shear

Generally, the matrix deforms more than the fiber in shear (fig. 2.5) because the matrix has a lower shear modulus. The total shearing deformation is:

$$\Delta = \gamma W \quad (2.20)$$

and is made up of, approximately, microscopic deformations:

$$\Delta_m = V_m W \gamma_m \quad \Delta_f = V_f W \gamma_f \quad (2.21)$$

Then, because $\Delta = \Delta_m + \Delta_f$ division by W yields

$$\gamma = V_m \gamma_m + V_f \gamma_f \quad (2.22)$$

or upon substitution of equation 2.19 and realization that macroscopically

$$\gamma = \frac{\tau}{G_{12}} \quad (2.23)$$

Equation 2.22 can be written as:

$$\frac{\tau}{G_{12}} = V_m \frac{\tau}{G_m} + V_f \frac{\tau}{G_f} \quad (2.24)$$

Finally we have:

$$G_{12} = \frac{G_m G_f}{V_m G_f + V_f G_m} \quad (2.25)$$

which is the same type of expression as was obtained for the transverse Young's modulus.

2.2 Macromechanical behaviour of a Lamina

The lamina is the basic element of the laminate so knowledge of its mechanical behavior is essential to predict and understand the behavior of the composite structure. The macromechanical behavior of a lamina is studied considering only the global mechanical properties of the material assumed homogeneous but not isotropic, regardless of the interactions between components.

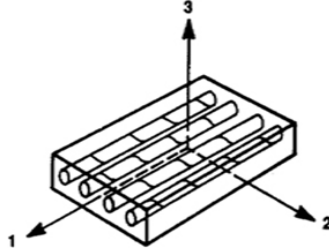


Figure 2.6: Unidirectionally reinforced lamina

In the first approximation, a lamina may be considered as orthotropic material and it is possible to consider its thickness negligible compared to the other dimensions; therefore for a unidirectionally reinforced lamina in the 1-2 plane (fig.2.6), a plane stress state is defined by setting:

$$\sigma_3 = \tau_{13} = \tau_{23} = 0 \quad (2.26)$$

The plane stress state on a lamina is not merely an idealization of reality, but instead is a practical and achievable objective of how we must use a lamina with its fiber in its plane. In the 1-2 plane (fig.2.6), the lamina is equivalent to 2-D orthotropic thin layer for which we can apply the generalized Hooke's law and the stress-strain relation are obtained as:

$$\begin{bmatrix} \sigma_1 \\ \sigma_2 \\ \tau_{12} \end{bmatrix} = \begin{bmatrix} Q_{11} & Q_{12} & 0 \\ Q_{12} & Q_{22} & 0 \\ 0 & 0 & 2Q_{66} \end{bmatrix} \begin{bmatrix} \varepsilon_1 \\ \varepsilon_2 \\ \frac{\gamma_{12}}{2} \end{bmatrix} \quad (2.27)$$

where the Q_{ij} are the so-called reduced stiffnesses for a plane stress state in the 1-2 plane which are expressed in terms of engineering constants as:

$$\begin{aligned} Q_{11} &= \frac{E_1}{1 - \nu_{12}\nu_{21}} & Q_{22} &= \frac{E_2}{1 - \nu_{12}\nu_{21}} \\ Q_{12} &= \frac{\nu_{12}E_2}{1 - \nu_{12}\nu_{21}} = \frac{\nu_{21}E_1}{1 - \nu_{12}\nu_{21}} & Q_{66} &= G_{12} \end{aligned} \quad (2.28)$$

In the stress-strain relations there are four independent material properties, E_1 , E_2 , ν_{12} and G_{12} when equations 2.28 are considered in addition to the reciprocal relation

$$\nu_{21} = \nu_{12} \frac{E_2}{E_1} \quad (2.29)$$

The preceding stress-strain relations are the basis for stiffness and stress analysis of an individual lamina subjected to forces in its own plane.

If the principal directions of orthotropy do not coincide with coordinate directions that are geometrically natural to the solution of the problem, a relation between the stress and strain in the principal material coordinates are needed. Then, a method of transforming stress-strain relations from one coordinate system to another is also needed.

Recalling from elementary mechanics of materials the transformation equations for expressing stresses in an $x-y$ coordinate system in terms of stresses in a 1-2 coordinate system,

$$\begin{bmatrix} \sigma_x \\ \sigma_y \\ \tau_{xy} \end{bmatrix} = \begin{bmatrix} \cos^2 \theta & \sin^2 \theta & 2 \sin \theta \cos \theta \\ \sin^2 \theta & \cos^2 \theta & -2 \sin \theta \cos \theta \\ -\sin \theta \cos \theta & \sin \theta \cos \theta & \cos^2 \theta - \sin^2 \theta \end{bmatrix} \begin{bmatrix} \sigma_1 \\ \sigma_2 \\ \tau_{12} \end{bmatrix} \quad (2.30)$$

where θ is the angle from the x-axis to the 1-axis (fig.2.7). Note especially that the transformation has nothing to do with the material properties but is merely a rotation of stress directions. Also, the direction of rotation is crucial. Similarly,

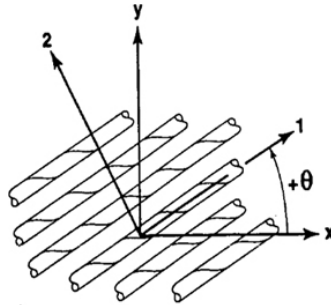


Figure 2.7: Positive Rotation of Principal Material Axes from x-y Axes

the strain-transformation equation are:

$$\begin{bmatrix} \varepsilon_x \\ \varepsilon_y \\ \frac{\gamma_{xy}}{2} \end{bmatrix} = \begin{bmatrix} \cos^2 \theta & \sin^2 \theta & 2 \sin \theta \cos \theta \\ \sin^2 \theta & \cos^2 \theta & -2 \sin \theta \cos \theta \\ -\sin \theta \cos \theta & \sin \theta \cos \theta & \cos^2 \theta - \sin^2 \theta \end{bmatrix} \begin{bmatrix} \varepsilon_1 \\ \varepsilon_2 \\ \frac{\gamma_{12}}{2} \end{bmatrix} \quad (2.31)$$

where we observe that strains do transform with the same transformation as stresses if the tensor definition of shear strain is used (which is equivalent to dividing the engineering shear strain by two).

The transformations are commonly written as:

$$\begin{bmatrix} \sigma_x \\ \sigma_y \\ \tau_{xy} \end{bmatrix} = [T] \begin{bmatrix} \sigma_1 \\ \sigma_2 \\ \tau_{12} \end{bmatrix} \quad (2.32)$$

$$\begin{bmatrix} \varepsilon_x \\ \varepsilon_y \\ \frac{\gamma_{xy}}{2} \end{bmatrix} = [T] \begin{bmatrix} \varepsilon_1 \\ \varepsilon_2 \\ \frac{\gamma_{12}}{2} \end{bmatrix} \quad (2.33)$$

Thus, given the stress-strain relation in the principal material coordinates, the stress-strain relation in x-y coordinate are:

$$\begin{bmatrix} \sigma_x \\ \sigma_y \\ \tau_{xy} \end{bmatrix} = [T] \begin{bmatrix} \sigma_1 \\ \sigma_2 \\ \tau_{12} \end{bmatrix} = [T] [Q] [T]^{-1} \begin{bmatrix} \varepsilon_x \\ \varepsilon_y \\ \frac{\gamma_{xy}}{2} \end{bmatrix} \quad (2.34)$$

Then, if we use the abbreviation

$$[\bar{Q}] = [T] [Q] [T]^{-1} \quad (2.35)$$

the stress-strain relation in x-y coordinate are:

$$\begin{bmatrix} \sigma_x \\ \sigma_y \\ \tau_{xy} \end{bmatrix} = [\bar{Q}] \begin{bmatrix} \varepsilon_x \\ \varepsilon_y \\ \gamma_{xy} \end{bmatrix} = \begin{bmatrix} \bar{Q}_{11} & \bar{Q}_{12} & \bar{Q}_{16} \\ \bar{Q}_{12} & \bar{Q}_{22} & \bar{Q}_{26} \\ \bar{Q}_{16} & \bar{Q}_{26} & \bar{Q}_{66} \end{bmatrix} \begin{bmatrix} \varepsilon_x \\ \varepsilon_y \\ \gamma_{xy} \end{bmatrix} \quad (2.36)$$

or in the abbreviated form:

$$\{\sigma\} = [\bar{Q}] \{\varepsilon\} \quad (2.37)$$

where the bar over the \bar{Q}_{ij} matrix denotes that we are dealing with the transformed reduced stiffnesses instead of the reduced stiffnesses, Q_{ij} . Moreover, the transformed reduced stiffness matrix \bar{Q}_{ij} has terms in all nine positions in contrast to the presence of zeros in the reduced stiffness matrix Q_{ij} . However, there are still only four independent material constants because the lamina is orthotropic. In body coordinate, even an orthotropic lamina appears to be anisotropic. The equation 2.36 is the stress-strain relation in a *generally orthotropic lamina* or equivalently in a orthotropic lamina whose principal material axes are not aligned with the natural body axes.

2.3 Macromechanical behaviour of a Laminate

A laminate is two or more laminae bonded together to act as an integral structural element (fig.2.8). The various laminae are oriented with (local) principal material directions at different angles to the global laminate axes to produce a structural element capable of resisting to loads in several directions. The stiffnesses and strengths of such structural configuration are obtained from the properties of the constituent laminae. There are procedures enable the analysis of

laminates that have individual laminae with principal material directions oriented at arbitrary angle to the chosen or natural axes of the laminate. As a consequence of the arbitrary laminae orientations, the laminate might not have definable principal directions.

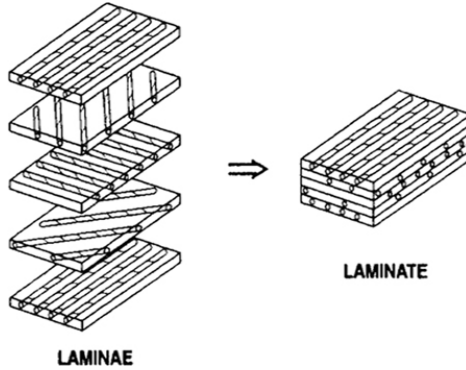


Figure 2.8: Laminate

Starting from the knowledge of the stress-strain relation (eq.2.37) for the K^{th} lamina of a multilayered laminate

$$\{\sigma\}_k = [\bar{Q}]_k \{\varepsilon\}_k \quad (2.38)$$

and after some stress and deformation hypotheses (that would be shown later), a classical lamination theory (CLT) can be defined.

About the strain and stress variation in a laminate, its knowledge through the laminate thickness is essential to the definition of the extensional and bending stiffnesses of a laminate. The first hypothesis is that a laminate is presumed to consist of perfectly bonded laminae. Moreover, the bonds are presumed to be infinitesimally thin as well as non-shear-deformable. That is, the displacements are continuous across lamina boundaries so that no lamina can slip relative to another. Thus, the laminate acts as a single layer with very special properties. Accordingly, if the laminate is thin, a line originally straight and perpendicular to the middle surface of the laminate, i.e., a normal to the middle surface, is assumed to remain straight and perpendicular to the middle surface when the laminate is deformed. It is equivalent to ignoring the shearing strains in a plane perpendicular to the middle surface, that is, $\gamma_{xz} = \gamma_{yz} = 0$ where z is the direction of the normal to the middle surface (fig.2.9). In addition, the normals are presumed to have constant length so that the strain perpendicular to the middle surface is ignored as well, that is, $\varepsilon_z = 0$.

The foregoing assumptions of the behavior of the single layer that represents the laminate constitutes the Kirchhoff hypothesis for plates and shells [20]. The implications of the Kirchhoff hypothesis on the laminate displacements u, v and w in the x, y and z directions are derived by use of the laminate cross section in the $x - z$ plane (fig.2.9). The displacement in the x -direction of point B from the undeformed middle surface to the deformed middle surface is u_0 (where the symbol $(\cdot)_0$ is used to indicate middle-surface values of a variable). Because line ABCD remains straight under deformation of the laminate, the displacement at

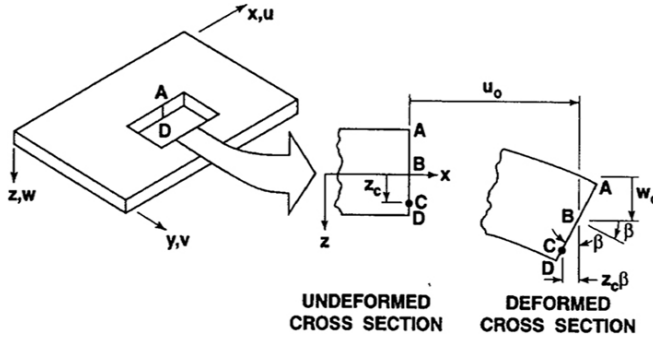


Figure 2.9: Geometry of Deformation in the x-z Plane

point C is:

$$u_c = u_0 - z_c \beta \quad (2.39)$$

But because, under deformation, line ABCD further remains perpendicular to the middle surface, β is the slope of the laminate middle surface in the x-direction, that is:

$$\beta = \frac{\partial w_0}{\partial x} \quad (2.40)$$

Then, the displacement u at any point z through the laminate thickness is:

$$u = u_0 - z \frac{\partial w_0}{\partial x} \quad (2.41)$$

similarly, the displacement v in the y-direction is

$$v = v_0 - z \frac{\partial w_0}{\partial y} \quad (2.42)$$

The laminate strains have been reduced to ε_x , ε_y and γ_{xy} by the Kirchhoff hypothesis. That is, $\varepsilon_z = \gamma_{xz} = \gamma_{yz} = 0$. For small strains (linear elasticity), the remaining strain are defined in terms of displacements as:

$$\begin{aligned} \varepsilon_x &= \frac{\partial u}{\partial x} \\ \varepsilon_y &= \frac{\partial v}{\partial y} \\ \gamma_{xy} &= \frac{\partial u}{\partial y} + \frac{\partial v}{\partial x} \end{aligned} \quad (2.43)$$

thus, for the derived displacements u and v in equations 2.41-2.42, the strains are:

$$\begin{aligned} \varepsilon_x &= \frac{\partial u_0}{\partial x} - z \frac{\partial^2 w_0}{\partial x^2} \\ \varepsilon_y &= \frac{\partial v_0}{\partial y} - z \frac{\partial^2 w_0}{\partial y^2} \\ \gamma_{xy} &= \frac{\partial u_0}{\partial y} + \frac{\partial v_0}{\partial x} - 2z \frac{\partial^2 w_0}{\partial x \partial y} \end{aligned} \quad (2.44)$$

or

$$\begin{bmatrix} \varepsilon_x \\ \varepsilon_y \\ \gamma_{xy} \end{bmatrix} = \begin{bmatrix} \varepsilon_x^o \\ \varepsilon_y^o \\ \gamma_{xy}^o \end{bmatrix} + z \begin{bmatrix} \kappa_x \\ \kappa_y \\ \kappa_{xy} \end{bmatrix} \quad (2.45)$$

where the middle-surface strains are:

$$\begin{bmatrix} \varepsilon_x^o \\ \varepsilon_y^o \\ \gamma_{xy}^o \end{bmatrix} = \begin{bmatrix} \frac{\partial u_0}{\partial x} \\ \frac{\partial v_0}{\partial y} \\ \frac{\partial u_0}{\partial y} + \frac{\partial v_0}{\partial x} \end{bmatrix} \quad (2.46)$$

and the middle-surface curvatures are:

$$\begin{bmatrix} \kappa_x \\ \kappa_y \\ \kappa_{xy} \end{bmatrix} = - \begin{bmatrix} \frac{\partial^2 w_0}{\partial x^2} \\ \frac{\partial^2 w_0}{\partial y^2} \\ \frac{\partial^2 w_0}{\partial x \partial y} \end{bmatrix} \quad (2.47)$$

The last term in equation 2.47 is the twist curvature of the middle surface. We refer only to curvature of the middle surface as a reference surface and not of any other surface. Thus, the Kirchhoff hypothesis has been readily verified to imply a linear variation of strain through the laminate thickness.

Now the stresses in the k^{th} layer can be expressed in terms of the laminate middle-surface strains and curvatures as:

$$\begin{bmatrix} \sigma_x \\ \sigma_y \\ \tau_{xy} \end{bmatrix}_k = \begin{bmatrix} \bar{Q}_{11} & \bar{Q}_{12} & \bar{Q}_{16} \\ \bar{Q}_{12} & \bar{Q}_{22} & \bar{Q}_{26} \\ \bar{Q}_{16} & \bar{Q}_{26} & \bar{Q}_{66} \end{bmatrix}_k \left[\begin{bmatrix} \varepsilon_x^o \\ \varepsilon_y^o \\ \gamma_{xy}^o \end{bmatrix} + z \begin{bmatrix} \kappa_x \\ \kappa_y \\ \kappa_{xy} \end{bmatrix} \right] \quad (2.48)$$

or in the abbreviated form:

$$\{\sigma\}_k = [\bar{Q}]_k \{\varepsilon^o\} + z [\bar{Q}]_k \{\kappa\} \quad (2.49)$$

The \bar{Q}_{ij} can be different for each layer of the laminate, so the stress variation through the laminate thickness is not necessary linear, even though the strain variation is linear. The quantity z represents the distance of the k^{th} layer from the middle surface (fig.2.10). The resultant forces and moments acting on a laminate are obtained by integration of the stresses in each layer or lamina through the laminate thickness as (i.e. in x-direction):

$$N_x = \int_{-t/2}^{t/2} \sigma_x dz \quad M_x = \int_{-t/2}^{t/2} \sigma_x z dz \quad (2.50)$$

Where N_x is a force per unit width of the cross section of the laminate (fig.2.11). Similarly, M_x is a moment per unit width (fig.2.12).

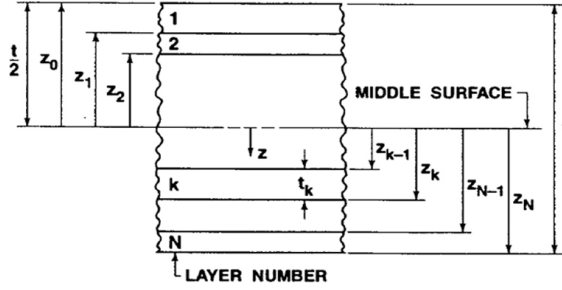


Figure 2.10: Geometry of an N-Layered Laminate

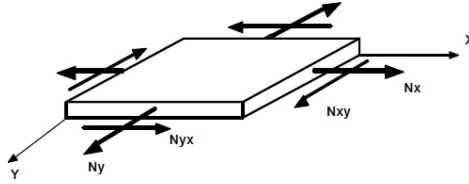


Figure 2.11: In-Plane Force on a Flat Laminate

The entire collection of force and moment resultants for an N-layered laminate (fig.2.11-2.12) is defined as:

$$\begin{bmatrix} N_x \\ N_y \\ N_{xy} \end{bmatrix} = \int_{-t/2}^{t/2} \begin{bmatrix} \sigma_x \\ \sigma_y \\ \tau_{xy} \end{bmatrix} dz = \sum_{k=1}^N \int_{z_{k-1}}^{z_k} \begin{bmatrix} \sigma_x \\ \sigma_y \\ \tau_{xy} \end{bmatrix}_k dz \quad (2.51)$$

and:

$$\begin{bmatrix} M_x \\ M_y \\ M_{xy} \end{bmatrix} = \int_{-t/2}^{t/2} \begin{bmatrix} \sigma_x \\ \sigma_y \\ \tau_{xy} \end{bmatrix} z dz = \sum_{k=1}^N \int_{z_{k-1}}^{z_k} \begin{bmatrix} \sigma_x \\ \sigma_y \\ \tau_{xy} \end{bmatrix}_k z dz \quad (2.52)$$

where z_k and z_{k-1} are defined in the basic laminate geometry (fig.2.10) with the convention that z is positive downward. That is, z_k is the directed distance to the bottom of the k^{th} layer, and z_{k-1} is the directed distance to the top of the k^{th} layer. Moreover, $z_0 = -t/2$ and $z_1 = -t/2 + t_1$. These force and moment resultants do not depend on z after integration, but are functions of x and y , the coordinate in the plane of the laminate middle surface.

Substituting equation 2.48 into equations 2.51-2.52, the resultant forces and moments acting on a laminate can be expressed in terms of the laminate middle-surface strains and curvatures as:

$$\begin{bmatrix} N_x \\ N_y \\ N_{xy} \end{bmatrix} = \sum_{k=1}^N \begin{bmatrix} \bar{Q}_{11} & \bar{Q}_{12} & \bar{Q}_{16} \\ \bar{Q}_{12} & \bar{Q}_{22} & \bar{Q}_{26} \\ \bar{Q}_{16} & \bar{Q}_{26} & \bar{Q}_{66} \end{bmatrix}_k \begin{bmatrix} \int_{z_{k-1}}^{z_k} \begin{bmatrix} \varepsilon_x^o \\ \varepsilon_y^o \\ \gamma_{xy}^o \end{bmatrix} dz \\ \int_{z_{k-1}}^{z_k} \begin{bmatrix} \kappa_x \\ \kappa_y \\ \kappa_{xy} \end{bmatrix} z dz \end{bmatrix} \quad (2.53)$$

and:

$$\begin{bmatrix} M_x \\ M_y \\ M_{xy} \end{bmatrix} = \sum_{k=1}^N \begin{bmatrix} \bar{Q}_{11} & \bar{Q}_{12} & \bar{Q}_{16} \\ \bar{Q}_{12} & \bar{Q}_{22} & \bar{Q}_{26} \\ \bar{Q}_{16} & \bar{Q}_{26} & \bar{Q}_{66} \end{bmatrix}_k \begin{bmatrix} \int_{z_{k-1}}^{z_k} \begin{bmatrix} \varepsilon_x^o \\ \varepsilon_y^o \\ \gamma_{xy}^o \end{bmatrix} z dz \\ \int_{z_{k-1}}^{z_k} \begin{bmatrix} \kappa_x \\ \kappa_y \\ \kappa_{xy} \end{bmatrix} z^2 dz \end{bmatrix} \quad (2.54)$$

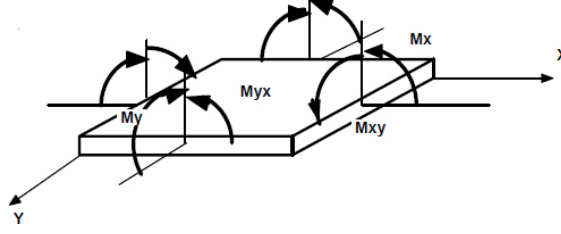


Figure 2.12: Moments on a Flat Laminate

Generally the stiffness matrix for a lamina $[\bar{Q}_{ij}]_k$ is not constant through the thickness of a lamina but is a function of z and must be left inside the integral. Moreover, the quantities ε_x^o , ε_y^o , γ_{xy}^o , κ_x , κ_y and κ_{xy} are not functions of z , but are middle-surface values so they can be removed from within the summation signs. Thus, the last equations can be rewritten as:

$$\begin{bmatrix} N_x \\ N_y \\ N_{xy} \end{bmatrix} = \begin{bmatrix} A_{11} & A_{12} & A_{16} \\ A_{12} & A_{22} & A_{26} \\ A_{16} & A_{26} & A_{66} \end{bmatrix} \begin{bmatrix} \varepsilon_x^o \\ \varepsilon_y^o \\ \gamma_{xy}^o \end{bmatrix} + \begin{bmatrix} B_{11} & B_{12} & B_{16} \\ B_{12} & B_{22} & B_{26} \\ B_{16} & B_{26} & B_{66} \end{bmatrix} \begin{bmatrix} \kappa_x \\ \kappa_y \\ \kappa_{xy} \end{bmatrix} \quad (2.55)$$

$$\begin{bmatrix} M_x \\ M_y \\ M_{xy} \end{bmatrix} = \begin{bmatrix} B_{11} & B_{12} & B_{16} \\ B_{12} & B_{22} & B_{26} \\ B_{16} & B_{26} & B_{66} \end{bmatrix} \begin{bmatrix} \varepsilon_x^o \\ \varepsilon_y^o \\ \gamma_{xy}^o \end{bmatrix} + \begin{bmatrix} D_{11} & D_{12} & D_{16} \\ D_{12} & D_{22} & D_{26} \\ D_{16} & D_{26} & D_{66} \end{bmatrix} \begin{bmatrix} \kappa_x \\ \kappa_y \\ \kappa_{xy} \end{bmatrix} \quad (2.56)$$

where:

$$\begin{aligned} A_{ij} &= \sum_{k=1}^N (\bar{Q}_{ij})_k (z_k - z_{k-1}) \\ B_{ij} &= \frac{1}{2} \sum_{k=1}^N (\bar{Q}_{ij})_k (z_k^2 - z_{k-1}^2) \\ D_{ij} &= \frac{1}{3} \sum_{k=1}^N (\bar{Q}_{ij})_k (z_k^3 - z_{k-1}^3) \end{aligned} \quad (2.57)$$

The quantities A_{ij} are extensional stiffnesses, the B_{ij} are bending-axtension coupling stiffness, and the D_{ij} are bending stiffness. The presence of the B_{ij} implies coupling between bending and extension of a laminate.

Chapter 3

Viscoelastic materials

3.1 Linear response of materials

Unlike many other damping mechanisms most homogeneous isotropic polymeric materials exhibit damping behaviour which depends strongly upon temperature and frequency, but is linear with respect to vibration amplitude, at least within limits. Polymers are materials composed of long intertwined and cross-linked molecular chains, each containing thousands or even millions of atoms.



Figure 3.1: Network of entangled polymers [21]

The internal molecular interactions which occur during deformation in general, and vibration in particular, give rise to macroscopic properties such as stiffness and energy dissipation during cyclic deformation, which is the mechanism of damping.

If the polymers are homogeneous (properties are the same throughout the volume of the sample) and isotropic (properties are the same in all directions), the stiffness and damping characteristics vary with temperature and, to a lesser degree, with frequency, but are otherwise qualitatively similar to those displayed by nominally elastic materials such as metal alloys, apart the fact that the damping levels are much higher and the behaviour is linear. The shear, extensional (Young's) and bulk moduli are closely related to each other for homogeneous, isotropic, polymers. Some polymers are not homogeneous or isotropic and, in

that case, the modulus and damping properties are more complicated functions of direction and position within the material.

The class of polymeric materials is extremely wide, and induce many commercially available products ranging from natural rubber, through various adhesives to stiff plastic, such as Plexiglas. Table 3.1 lists some of the categories of available polymers to be employed in stable material damping systems [22][23]. Special

Table 3.1: List of some polymer types

1	Acrylic rubber
2	Butadiene rubber (BR)
3	Butyl rubber
4	Chloroprene
5	Chlorinated Polyethylenes
6	Ethylene-Propylene-Diene
7	Fluorosilicone rubber
8	Fluorocarbon rubber
9	Natural rubber
10	Polyethylene
11	Polystyrene
12	Polyisobutylene (PIB)
13	Silicone rubber

products can be formulated to meet almost any needs by combining or modifying polymers. The stiffness and damping characteristics of these various polymeric materials vary widely, according to the composition and processing.

The polymers provide the basis for designing damping treatments or systems for application in a wide variety of structures and machines, over wide frequency and temperature ranges.

The behaviour of the viscoelastic materials can be obtained as a mix between elastic and viscous behaviour, both taken as ideal materials.

Elasticity is a property of matter typical of the solid state. An elastic solid can be deformed by applying suitable forces, and recovers the original shape when those forces are removed. In the immediate proximity of a material point, elasticity is described by a relationship, or constitutive equation, that links stresses and strains in that point. Such a relationship is generally nonlinear and only if small strains (or small stresses) are considered, the relationship becomes linear. Contrarily, viscosity is a property of matter typical of the fluid state. The viscous fluids do not maintain a fixed shape and so the stresses are directly connected with the deformation time.

The behaviour of the elastic solids and the viscous fluids identifies the limits of a wide spectrum in which the viscoelastic materials behaviour are enclosed.

3.1.1 Elasticity

If a tensile strength F is applied to an elastic solid it will be subject to a strain $\Delta\varepsilon$ proportional to it ($F \propto \Delta\varepsilon$) as it is described by *Hooke's law* and the strain is not dependent on time; this behaviour is called *linear elasticity*.

Elasticity is a property of matter typical of the solid state: an elastic solid can be

deformed by applying suitable forces, and recovers the original shape when those forces are removed. This behaviour is true if the external loads are lower than the yield strength; it is strongly dependent on the material type and temperature [24].

For small deformations, all solid materials are linearly elastic. Moreover an ideally elastic material absorbs all the energy cumulated in the deformation of the body and this energy is completely stored inside the deformed material. When the external loads are removed the body releases completely the stored energy, therefore it does not dissipate energy so the elastic deformation is a completely reversing cycle.

Locally, the elasticity is described by a constitutive equation that ties stress and strain for each point. Such relationship generally is not linear, but, as already said, if small deformations are considered, the relationship becomes linear; in fact when an elastic material starts to deform, the initial response is always linear and it becomes not linear only if the deformations overcome the yield limit. Therefore, the stress σ is directly connected with the strain ε through Young's modulus E by the equation:

$$\sigma = E\varepsilon \quad (3.1)$$

where the modulus of elasticity, or Young's modulus (E), describes the tendency of the material to deform along directions when opposing forces are applied along that directions; it is the slope of the stress-strain curve in the elastic region (fig. 3.2) and it depends only from the material and from the temperature (it slowly decreases to increase some temperature).

Another important quantity named shear modulus G explain (in the same condition of small deformations) the linear relation between the shear stress τ and the shear strain γ . It is defined as:

$$\tau = G\gamma \quad (3.2)$$

The figure 3.2 show the stress-strain curve for an ideal elastic material.

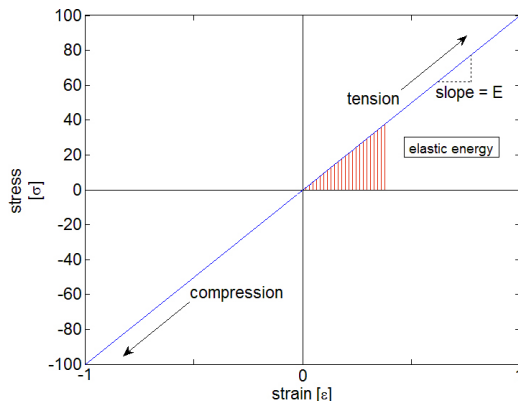


Figure 3.2: Stress-Strain curve

The energy developed by the external load and entirely stored inside the deformed material, before being release once the external load is taken off, is defined by the integral in eq. 3.3:

$$U = \int \sigma d\varepsilon \quad (3.3)$$

3.1.2 Viscosity

The viscosity is a property of matter typical of the fluid state where the generic term of fluid is referred to the liquid and gaseous state. Unlike solids, fluids do not have a proper shape, they can change form and can get deformed irreversibly when external strengths act on it. Moreover, under an external load, the velocity with which fluids change their shape is strongly dependent on the type of fluid because some of them offer a stronger resistance to the flow than others. This resistance is generally known as *viscosity*. The real fluids introduce therefore resistance to the motion of slide or rather to the free movement of the molecules inside it. As for friction in a relative motion of solid surfaces, the viscosity change part of the kinetic energy of motion in a thermic energy and so generates energy dissipation; this does not allow it to recover the original shape when the external forces are removed.

Then, in every real fluid dissipation effects are present and the characteristic of the fluid responsible of them it is the viscosity. Viscosity can be defined as the strength in opposition to the relative motion of the fluid fillets. More generally the viscosity is the parameter that explains the resistance opposed by the fluid to get deformed under the action of a mechanical sollicitation. To define it, let us consider to have a real liquid in quiet confined in two parallel plates of area A at l length between them (fig. 3.3a). For simplicity we suppose that the inferior plate is fixed and the superior one has a constant velocity v so that to induce motion in the fluid. To describe the motion we suppose to divide the fluid in so many strips or thin layers (fig. 3.3b) in order to define for each of them a velocity in comparison to the fixed inferior plate. Moreover we assume that the motion is unsteady and the flow is laminar (simplest case).

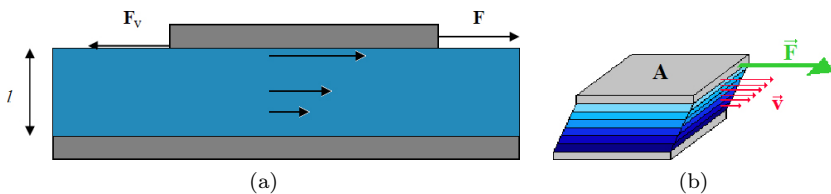


Figure 3.3: Example of viscous flow

Due to the molecular strengths, each thin layer will tend to be attached to the adjacent layer. To maintain the plate at constant speed v , it is necessary to apply a tangential strength F to win the viscous strength F_v explained by the fluid on the superior plate so that opposes it to the motion. Each thin layer applies a resistant strength on those adjacent so that the speed of the latest thin layer, that one very close to the superior plate, is equal to v and decrease linearly with l until zero near the fixed plate. At the equilibrium, the tangential strength F is balanced by the viscous strength F_v . Moreover, the tangential strength F is proportional to the area A and velocity gradient v in the fluid and inversely proportional to the distance between the plates l as following:

$$F = \mu \frac{Av}{l} \quad (3.4)$$

where μ is the proportionality factor called *viscosity*.

The viscosity is strongly dependent by the type of fluid (i.e. water,etc.) and the

environmental conditions, principally the temperature.

In 1687 Isaac Newton was the first to explain the proportionality relation between F/A , known as shear stress τ , and v/l known as velocity gradient[26].

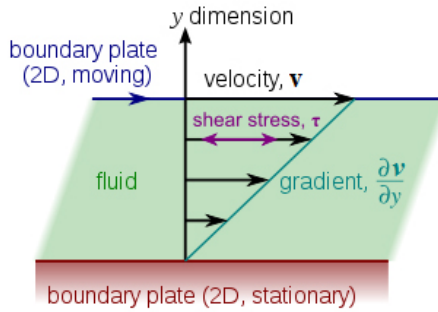


Figure 3.4: Laminar shear of fluid between two plates

In a differential form, if two consecutive parallel thin layers in uniform viscous flow at distance dy are considered (fig. 3.5a), the shear stress between the layers is proportional to the velocity gradient in the direction perpendicular to the layers:

$$\tau = \mu \frac{dv}{dy} \tag{3.5}$$

if A is the contact area, in accord to eq.3.4, the tangential strength is:

$$F = \mu A \frac{dv}{dy} \tag{3.6}$$

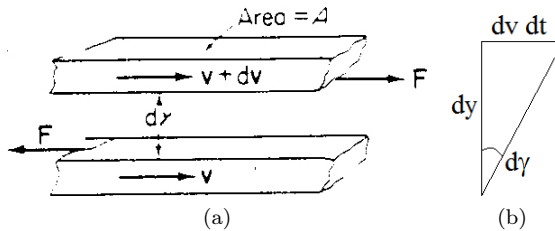


Figure 3.5: Fluid thin layers

Generally, the eq.3.6 is referred to another quantity equivalent to the velocity gradient known as *rate of shear deformation* or *shear rate*. The relative velocity between the upper and the lower thin layer (fig.3.5a) is dv . The rate of the shear deformation is defined as the velocity of variation of the $d\gamma$ angle in a time and so $\frac{d\gamma}{dt}$. In the same time, the deformation between the two thin layers can be defined as $dvdt$ (fig.3.5b) and in the hypothesis that $d\gamma$ is small, we have:

$$dyd\gamma = dvdt \rightarrow \frac{dv}{dy} = \frac{d\gamma}{dt} = \dot{\gamma} \tag{3.7}$$

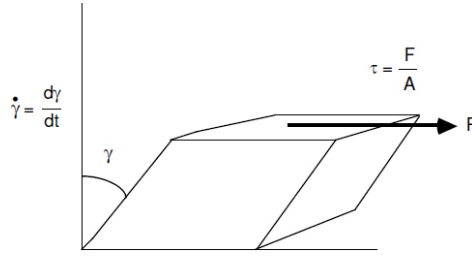


Figure 3.6: Shear rate

Therefore the velocity gradient is equivalent to the shear rate(fig.3.6) by the equation 3.7.

The *Newton's law* (eq.3.6) can be written as:

$$\frac{F}{A} = \tau = \mu \frac{dv}{dy} = \mu \frac{dy}{dt} = \mu \dot{\gamma} \quad (3.8)$$

hence:

$$\tau = \mu \dot{\gamma} \quad (3.9)$$

Until now the viscosity coefficient μ has been considered as a scalar value independent by the velocity of the deformation. There are fluids, however, in which it is a function of the shear rate and the velocity gradient $\mu(\dot{\gamma})$. Therefore, it is possible to distinguish newtonians and non-newtonians fluids. In newtonian fluids the viscosity is a scalar value independent on the shear strength and the shear rate; the viscosity is always dependent on temperature, pressure and chemical composition of the fluid. In other words, the graph of the shear strength vs shear rate show a straight line (fig.3.7) where the ratio $\tau/\dot{\gamma}$ is constant for every value and so the viscosity is constant.

In non-newtonian fluids the graph of the shear strength vs shear rate show a non linear relation between τ and $\dot{\gamma}$; the viscosity is a function of the shear rate and consequently of the shear strength (fig.3.7).

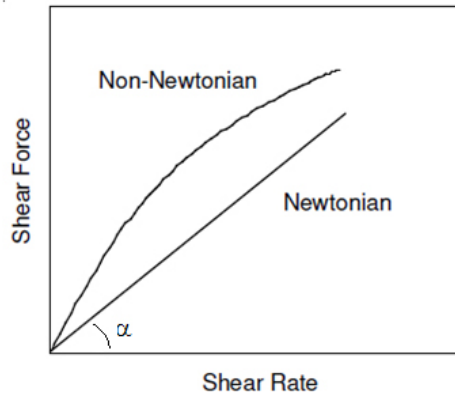


Figure 3.7: Shear rate for newtonian and non-newtonian fluids

3.1.3 Viscoelasticity

Viscoelastic materials are not purely elastic materials because, in reality, all materials deviate from *Hooke's law* in some way. Viscoelastic materials have elements of both of elastic and viscous properties. Whereas elasticity is usually the result of bond-stretching along crystallographic planes in an ordered solid, viscoelasticity is the result of the diffusion of atoms or molecules inside of an amorphous material, e.g., glasses, rubbers and high polymers. Much of the viscoelastic behavior can be described in terms of a simple combination of elastic and viscous phenomena discussed in subsections 3.1.1-3.1.2.

The concept of viscoelasticity introduces a certain ambiguity in the classifications of the materials state. The distinction between solid and liquid state, therefore, doesn't appear so clear anymore if the same material can manifest predominantly solid or liquid characteristic according to the state of solicitation to which it is submitted. In this way a *Deborah* number can be defined. It is a dimensionless number, often used in rheology to characterize the fluidity of materials under specific flow conditions. It was originally proposed by Markus Reiner, a professor at Technion in Israel, inspired by a verse in the Bible, stating The mountains flowed before the Lord in a song by prophetess Deborah (Judges 5:5). It is based on the premise that given enough time even the hardest material, like mountains, will flow. Thus the flow characteristics is not an inherent property of the material alone, but a relative property that depends on two fundamentally different characteristic times.

Formally, the Deborah number is defined as the ratio of the relaxation time characterizing the time it takes for a material to adjust to applied stresses or deformations, and the characteristic time scale of an experiment (or a computer simulation) probing the response of the material. It incorporates both the elasticity and viscosity of the material. It is defined as:

$$De = \frac{t_c}{t_p} \quad (3.10)$$

where t_c refers to the stress relaxation time, and t_p refers to the time scale of observation.

The smaller Deborah number, the material behaves more fluid like with an associated Newtonian viscous flow. At higher Deborah numbers, the material behavior changes to non-Newtonian regime, increasingly dominated by elasticity, reaching solid like behavior with very high Deborah numbers.

- $DE \rightarrow 0$ viscous fluid behaviour
- $DE \gg 1$ elastic solid behaviour
- $DE \cong 1$ viscoelastic behaviour

The behaviour of viscoelastic materials subjected to an external load, on first approximation, can be considered as the sum of viscous and elastic behaviour (as mentioned above). In other words, if a shear strength F is applied to a viscoelastic area A , the compressive shear stress is:

$$\frac{F}{A} = G\tau + \mu \frac{d\gamma}{dt} \quad (3.11)$$

3.1. LINEAR RESPONSE OF MATERIALS

where G is the shear modulus and μ is the viscosity coefficient. A possible solution to this equation is:

$$\theta = \left(1 - e^{-\frac{G}{\mu}t}\right) \frac{F}{AG} \quad (3.12)$$

that explains how the material deformation tend to $\frac{F}{AG}$ for a long time. This quantity is the shear strain at the equilibrium for an ideal elastic material with a shear modulus equal to G and subjected to a shear strength equal to $\frac{F}{A}$. The quantity $\frac{\mu}{G}$ have a time dimension and is called time delay of the material. The trend of the equation 3.12 is showed in a fig.3.8.

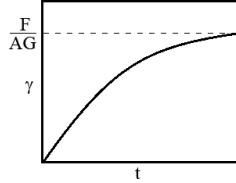


Figure 3.8: Shear strain vs time

Viscoelastic materials can be deformed by applying suitable forces, and not always it is possible to recover the original shape when those forces are removed. This because the shear strain, as above mentioned, is strongly dependent on the time of application of the strength. Therefore, a viscoelastic material can assume a behaviour of a pure elastic material if subjected to a short time stress; on the contrary, it can assume a behaviour of a pure viscous material if subjected to a long time stress (fig.3.9).

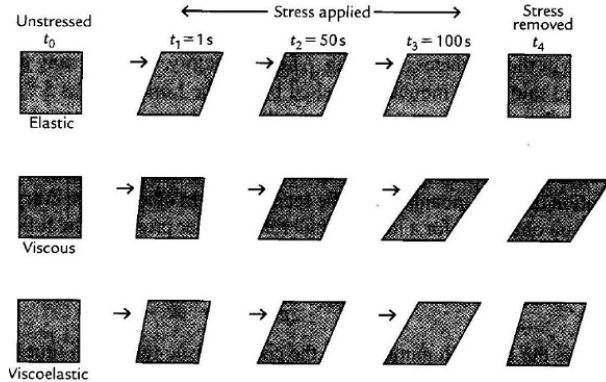


Figure 3.9: Elastic, Viscous and Viscoelastic behaviour to an applied stress

In fig.3.10 the responses of different materials during creep recovery tests is showed. In a creep test, a material is subjected to a sudden stress σ_{step} at time zero, and this stress is then held constant for a period of time and then released while measuring the deformation over time. For an ideal solid, the deformation will be seen immediately when the stress is applied and will disappear immediately once the stress is removed. In other words, the structure of an ideal solid can be recovery completely. An ideal liquid flows with this applied stress,

and strain thus increases with time. In accord with the Newton's law the strain at the time t is equal to $Strain = (t - t_0) \frac{Stress}{\mu}$ and when this stress is removed, an ideal liquid stays at the deformed position without going back to its initial position to any degree, that is, there is no recovery because it reaches its new equilibrium state in no time. The behavior of a viscoelastic material lies between

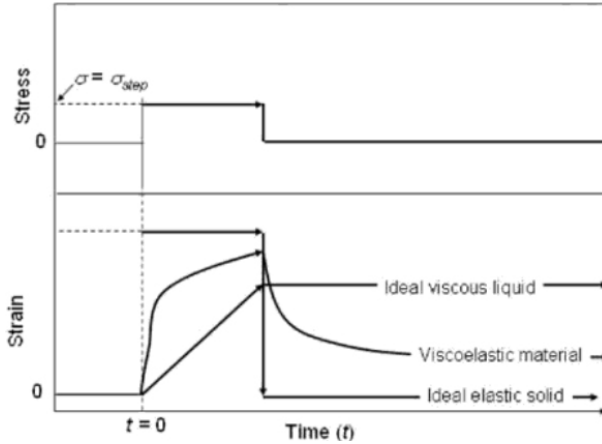


Figure 3.10: Responses of different materials during creep recovery tests

these two extremes. The deformation will be seen when the stress is applied, it increases not linearly with the time, and when the stress is removed the material recover part of the deformation in time. Ideally, it could recover the original shape in an infinite time.

Another test, very useful to characterize the viscoelastic materials is the *stress relaxation test*. In this test, a material is subjected to a sudden strain γ at time t_0 , and this strain is then held constant for a period of time and then released while measuring the stress over time. For the elastic materials the behavior is

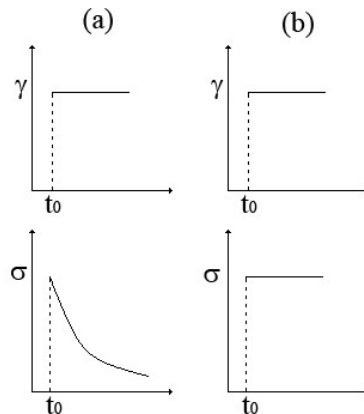


Figure 3.11: Viscoelastic and Elastic behavior to a stress relaxation test

entirely similar to that previously observed in a creep test (fig.3.11b) or rather the stress is a constant and independent by the time of application of the strain. Contrarily, in a viscoelastic case (fig.3.11a), the stress induced in the material

decreases in the time; it will relax with time.

If the stress is time dependent and the deformation is a constant, we have that:

$$E(t) = \frac{\sigma(t)}{\varepsilon_0} \quad (3.13)$$

where $E(t)$ is defined as viscoelastic relaxation modulus. Equivalently we can write:

$$\sigma(t) = E(t)\varepsilon_0 \quad (3.14)$$

that is the equation that bind the uniaxial stress with the deformation in a viscoelastic materials. It is equivalent to the Hooke's law for the elastic materials but it is valid only if the deformation is constant as in the relaxation test. Similarly, if a constant shear strain γ_0 is applied, a shear stress equal to $\tau(t) = G(t)\gamma_0$ is obtained.

Some common phenomena in viscoelastic materials are [29]:

- If the stress is held constant, the strain increases with time (creep).
- If the strain is held constant, the stress decreases with time (relaxation).
- The effective stiffness depends on the rate of application of the load.
- If cyclic loading is applied, hysteresis (a phase lag) occurs, along with a dissipation of mechanical energy.
- Acoustic waves experience attenuation.
- Rebound of an object following an impact is less than 100%.

Among the common viscoelastic phenomena, two types of behavior are of major engineering interest: transient properties (creep and relaxation) and dynamic response to alternating load.

3.2 Constitutive models of linear viscoelasticity

For *Hookean* solids and *Newtonian* fluids, linear relationships are defined to link stress-strain and stress-shear rate, due to mathematical modeling of extreme ideal cases (sections 3.1.1-3.1.2). In this relationships, the proportionality coefficients (elastic modulus and viscosity) are not dependent on the strain and shear rate. When this applies for the viscoelastic materials as well, it is called *linear viscoelasticity*.

Some constitutive models have been developed to simulate the linear viscoelasticity through the linear combination of springs and dashpots, to represent elastic and viscous components respectively.

3.2.1 Maxwell model

One of the first constitutive models of linear viscoelasticity was proposed in 1867 by James Clerk Maxwell [31]. This model, also known as Maxwell model, can be represented by a purely viscous damper and a purely elastic spring connected in series (fig.3.12).

In this configuration, under an applied axial stress, the total stress σ and the total strain ε , can be defined as follows:

$$\sigma = \sigma_1 = \sigma_2 \quad (3.15)$$

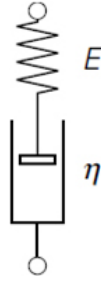


Figure 3.12: Element in a Maxwell model

$$\varepsilon = \varepsilon_1 + \varepsilon_2 \quad (3.16)$$

were 1,2 indicate the spring and damper elements, respectively. Therefore, if an axial stress is applied to the structure, both elastic and viscous elements are subjected to the same stress. About the deformations instead, the total strain is equal to the sum of both elastic and viscous strain ($\varepsilon_1, \varepsilon_2$) (fig. 3.13).

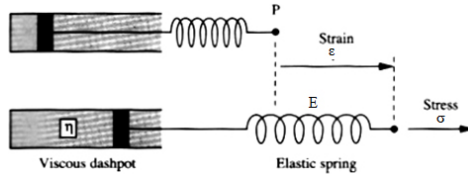


Figure 3.13: Deformed element in a Maxwell model

If E is the elastic modulus of the spring element, by the Hooke's law it is subjected to a stress equal to:

$$\sigma_1 = E\varepsilon_1 \quad (3.17)$$

Equivalently, if μ is the viscosity of the viscous damper element, by the Newton's law it is subjected to a stress equal to:

$$\sigma_2 = \mu \frac{d\varepsilon_2}{dt} \quad (3.18)$$

A time derivative of the equation 3.15 is:

$$\frac{d\sigma}{dt} = \frac{d\sigma_1}{dt} = \frac{d\sigma_2}{dt} \quad (3.19)$$

and replacing the spring's term we have:

$$\frac{d\sigma}{dt} = \frac{d\sigma_1}{dt} = E \frac{d\varepsilon_1}{dt} \quad (3.20)$$

and so:

$$\frac{d\varepsilon_1}{dt} = \frac{1}{E} \frac{d\sigma}{dt} \quad (3.21)$$

replacing it into the equation 3.16 and deriving the last in a time, we have:

$$\frac{d\varepsilon}{dt} = \frac{d\varepsilon_1}{dt} + \frac{d\varepsilon_2}{dt} = \frac{1}{E} \frac{d\sigma}{dt} + \frac{\sigma}{\mu} \quad (3.22)$$

This is the constitutive equation of the Maxwell model. By this equation, the behavior of the Maxwell model in relaxation and creep tests can be evaluated. Consider first the case where a constant strain ε_0 is applied to an initially unstressed material specimen at time $t = 0$. Then $\frac{d\varepsilon}{dt} = 0$ and eq.3.22 give

$$\frac{d\varepsilon}{dt} = 0 = \frac{1}{E} \frac{d\sigma}{dt} + \frac{\sigma}{\mu} \quad (3.23)$$

and so

$$\frac{d\sigma}{\sigma} = -\frac{E}{\mu} dt \quad (3.24)$$

if $t_0 = 0$ and $\sigma(0) = \sigma_0$ the differential equation, opportunely integrated in time, become

$$\sigma = \sigma_0 e^{-\frac{E}{\mu} t} \quad (3.25)$$

where σ_0 is the instantaneous elastic stress.

For a time smaller then t_0 ($t < t_0$) (fig.3.14), $\varepsilon = \varepsilon_0$ and remembering that the ratio between the viscosity coefficient and the modulus have a time dimension, it is possible replace the last equation introducing the relaxation time t_{relax} as follows:

$$\sigma = \sigma_0 e^{-\frac{t}{t_{relax}}} \quad (3.26)$$

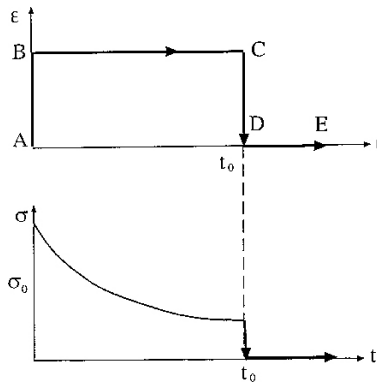


Figure 3.14: Relaxation in a Maxwell model

Therefore, the Maxwell model show that the stress needed to guarantee the same strain level (ε_0) in a viscoelastic material decrease progressively to zero when the time extends to the endless one. In other words, a Maxwell model subjected to a constant deformation give an instantaneous elastic stress that gradually decrease thereafter. Indeed this is how much it is observed qualitatively for the real viscoelastic materials and so the Maxwell model is able to describe the behavior in a relaxation test. The relaxation time is defined as the time to which the stress will be reduced of $1/e$ respect to the initial stress σ_0 .

Consider now the case where a constant stress σ_0 is applied to an initially unstressed material specimen at time $t = 0$. Then $\frac{d\sigma}{dt} = 0$ and eq.3.22 give:

$$\frac{d\varepsilon}{dt} = \frac{\sigma}{\mu} \quad (3.27)$$

this equation opportunely integrated in time, become

$$\varepsilon(t) - \varepsilon_0 = \frac{\sigma_0}{\mu}(t - t_0) \quad (3.28)$$

and if $t_0 = 0$, we have

$$\varepsilon(t) = \varepsilon_0 + \frac{\sigma_0}{\mu}t \quad (3.29)$$

therefore at time $t = 0$ there is an instantaneous elastic strain $\varepsilon_0 = \frac{\sigma_0}{E}$ due to the spring; increasing the time $t > 0$ the dashpot is subjected to the same stress of the spring and so the strain increase linearly with the time.

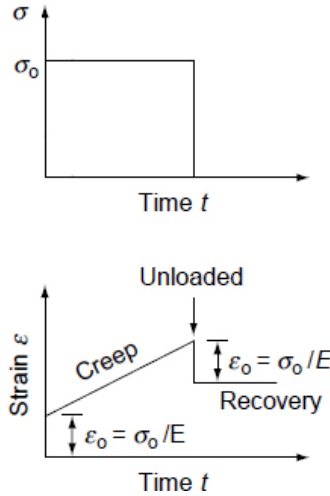


Figure 3.15: Creep in a Maxwell model

In reality, for a long time the strain tend to an asymptotic value and so the Maxwell model is not proper to simulate the creep test. Finally, the Maxwell model allow to simulate the viscoelastic behaviour in a relaxation test but not those in a creep test (if not limited in time).

3.2.2 Kelvin-Voigt model

Another model to describe the behavior of a viscoelastic material was proposed by Kelvin and Voigt [31]. This model combines a spring (characterized by a parameter E) and a dashpot (characterized by a parameter μ) connected in parallel (fig.3.16). In this configuration, under an applied axial stress, the total stress σ in a Kelvin-Voigt model is broken down on both spring and dashpot, namely:

$$\sigma = \sigma_1 + \sigma_2 \quad (3.30)$$

thus, the total stress is equal to the sum of both spring and dashpot stresses. Contrarily, the total strain is the same for the spring and the dashpot; both elastic and viscous elements are subjected to the same strain.

$$\varepsilon = \varepsilon_1 = \varepsilon_2 \quad (3.31)$$

As done for Maxwell model and by the Hooke and Newton's laws we have:

$$\sigma_1 = E\varepsilon_1 \quad (3.32)$$

$$\sigma_2 = \mu \frac{d\varepsilon_2}{dt} \quad (3.33)$$

combine the last equation to get:

$$\sigma = E\varepsilon_1 + \mu \frac{d\varepsilon_2}{dt} \quad (3.34)$$

This differential equation is the constitutive equation of the Kelvin-Voigt model and describes the material behavior under certain stress conditions. Similarly to the Maxwell model, we can describe the relaxation and creep phenomena. In the first case, we assume to have a constant applied strain over time. Then, $\varepsilon = \text{constant}$ so $\frac{d\varepsilon}{dt} = 0$ and consequently $\sigma = E\varepsilon_1$. This means that if the deformation is kept constant the stress remains constant, the Kelvin-Voigt model is not able to predict the stress relaxation and therefore cannot be used to simulate a relaxation behavior. Suppose now to have the second case, i.e. we want to simulate a creep test, where the stress is applied with the same intensity for a long time. If σ is constant, its derivative in time $\frac{d\sigma}{dt} = 0$ for which the general equation of the model reduces to:

$$\sigma_0 = E\varepsilon + \mu \frac{d\varepsilon}{dt} \quad (3.35)$$

and integrating:

$$\varepsilon(t) = \frac{\sigma_0}{E} \left(1 - e^{-\frac{E}{\mu}t} \right) \quad (3.36)$$

remembering that the ratio between viscosity and a modulus is dimensionally a time, the equation can be rewritten by introducing the delay time, t_{delay} , as:

$$\varepsilon(t) = \frac{\sigma_0}{E} \left(1 - e^{-\frac{t}{t_{delay}}} \right) \quad (3.37)$$

and this means that to a initial instantaneous stress σ_0 the material responds with an instantaneous strain σ_0/E plus a strain that grows over time tending to an asymptotic value as expected in reality.

When a Kelvin-Voigt model is loaded, part of the energy is stored in the deformed spring, while the remainder is dissipated by the dashpot and gives rise to the deformation delayed. If the load is suppressed, the original shape is fully recovered by spring but similarly a delay occurs due to dashpot. As it is clear by equation 3.37, when a K-V model is loaded, the deformation is not instantaneous, but increases gradually approaching to an asymptotic value. Similarly, when the load is removed, the deformation slowly fades and the material recovers its original shape. Thus, the Kelvin-Voigt model is able to describe the viscoelastic behavior in a creep tests, but not in those of relaxation.

3.2.3 SLS (Standard Linear Solid) or Zener model

Both Maxwell and Kelvin-Voigt models are limited in their representation of the real viscoelastic behavior. Many other studies have proposed different models, more complex, in order to describe more completely with a single model the

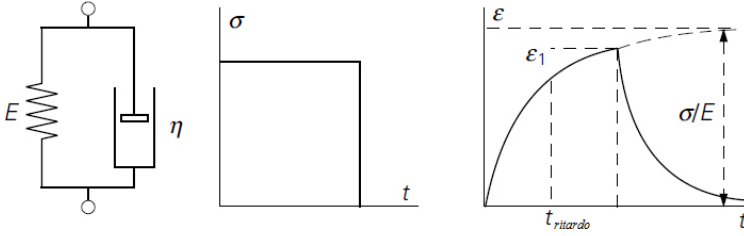


Figure 3.16: Creep in a Kelvin-Voigt model

behavior of materials. Among these the simplest, but still be able to explain qualitatively the most important viscoelastic behavior, is the model SLS (Standard Linear Solid) or Zener[32]. The SLS model provides a combination of both elements and thus offers more possibilities to simulate the real behavior of viscoelastic materials. It provides a Kelvin-Voigt (K-V) element in series with a spring, or with equivalent results, a Maxwell element in parallel with a spring (fig.3.17).

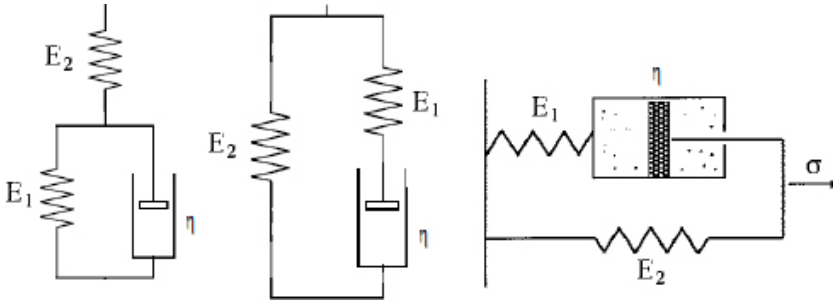


Figure 3.17: Elements in a Zener model

Consider now the case in which the Zener model is composed by K-V element (E_1, μ) in series with a spring element (E_2) (fig.3.17). In this configuration, under an applied axial stress, both elements are subjected to the same stress:

$$\sigma = \sigma_1 = \sigma_2 \quad (3.38)$$

where σ_1 is referred to a K-V element and σ_2 is referred to a spring element. The total strain, instead, is given by the sum of both element strains as:

$$\varepsilon = \varepsilon_1 + \varepsilon_2 \quad (3.39)$$

A time derivative of last equation is:

$$\dot{\varepsilon} = \dot{\varepsilon}_1 + \dot{\varepsilon}_2 \quad (3.40)$$

In the spring we have that: $\dot{\varepsilon}_2 = \frac{\dot{\sigma}_2}{E_2}$.

Replacing the stress-strain relation of the K-V model

$$\sigma_1 = E_1 \varepsilon_1 + \mu \dot{\varepsilon}_1 \quad (3.41)$$

and ε_2 in equation 3.40 we have:

$$\dot{\varepsilon} = \frac{\dot{\sigma}}{E_2} - \frac{E_1}{\mu} \varepsilon_1 + \frac{\sigma}{\mu} \quad (3.42)$$

substituting the equation 3.39 in the last equation:

$$\dot{\varepsilon} = \frac{\dot{\sigma}}{E_2} + \left(1 + \frac{E_1}{E_2}\right) \frac{\sigma}{\mu} - \frac{E_1}{\mu} \varepsilon \quad (3.43)$$

thus:

$$\sigma + \frac{\mu}{E_1 + E_2} \dot{\sigma} = \frac{E_1 E_2}{E_1 + E_2} \varepsilon + \frac{\mu E_2}{E_1 + E_2} \dot{\varepsilon} \quad (3.44)$$

and so:

$$\sigma + p_1 \dot{\sigma} = q_0 \varepsilon + q_1 \dot{\varepsilon} \quad (3.45)$$

where: $p_1 = \frac{\mu}{E_1 + E_2}$, $q_0 = \frac{E_1 E_2}{E_1 + E_2}$, $q_1 = \frac{\mu E_2}{E_1 + E_2}$

This last is the general equation of the SLS model.

As it was done for the two previous models, a constant strain $\varepsilon = \varepsilon_0$ at time $t = 0$ is applied at the SLS model to study its behaviour at relaxation test. Stress due to instantaneous strain is equal to $\sigma_0 = E_2 \varepsilon_0$, because only the spring answers instantaneously. For a time $t > 0$, the strain is constant and so $\frac{d\varepsilon}{dt} = 0$. The general equation of the SLS model becomes:

$$\dot{\sigma} + \frac{E_1 + E_2}{\mu} \sigma = \frac{E_1 E_2}{\mu} \varepsilon_0 \quad (3.46)$$

solving this differential equation, with the given initial condition we get:

$$\sigma(t) = \varepsilon_0 \left(\frac{E_2^2}{E_1 + E_2} e^{-\frac{E_1 + E_2}{\mu} t} + \frac{E_1 E_2}{E_1 + E_2} \right) = \varepsilon_0 G(t) \quad (3.47)$$

and the relaxation function $G(t)$ of the SLS model is expressed as:

$$G(t) = G_\infty + (G_0 - G_\infty) e^{-\beta t} \quad (3.48)$$

where:

- $G_0 = E_2$ is the unrelaxed shear modulus or short-term shear modulus
- $G_\infty = \frac{E_1 E_2}{E_1 + E_2}$ is the relaxed shear modulus or long-term shear modulus
- $\beta = \frac{E_1 + E_2}{\mu}$ is the decay constant

For a viscoelastic materials, the relaxation function $G(t)$ decays to an asymptotic value G_∞ . Contrarily, for a pure viscous fluid the relaxation function tends to zero ($G_\infty = 0$) for a long time; the same equation also says that its value is equal to G_0 for a very small time.

Thus, given these three parameters (G_0, G_∞, β), it is possible to calculate the value of the relaxation modulus at any time. The SLS model is the only capable of simulating both relaxation and creep tests.

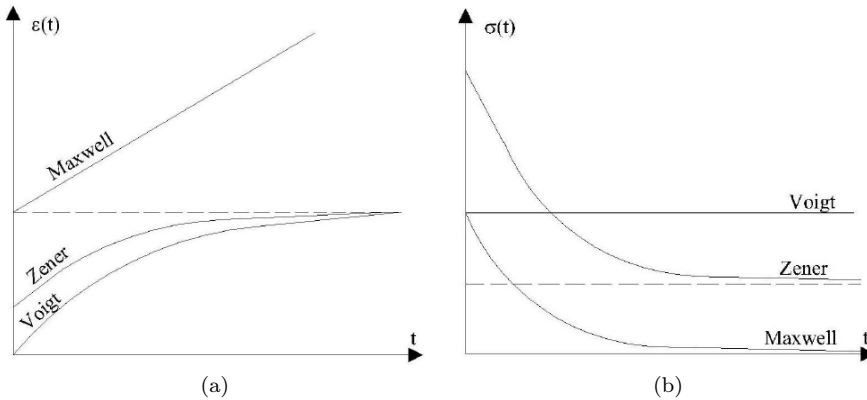


Figure 3.18: Creep (a) and Relaxation (b) tests for Maxwell, Kelvin-Voigt and Zener models

3.3 The dynamic behavior

3.3.1 The DMA (Dynamic Mechanical Analysis)

The response of a material to an oscillatory loads is called dynamics behavior. For viscoelastic materials, the dynamic behavior is of great interest because they are used where vibration damping or sound absorption is very important. A viscoelastic material subjected to a load, due to damping effect, dissipates part of the strain energy and so a phase shift between stress and strain is induced. The phase angle or loss angle δ is thus introduced. The hysteresis loop (fig.3.19) shows the amount of energy lost (as heat) in a loading and unloading cycle. Some materials show a time-dependent elastic behaviour. Although, in the elastic

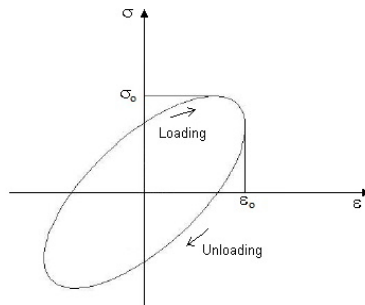


Figure 3.19: Hysteresis loop in a viscoelastic materials

regime, the strain is recoverable, the stress-strain curve is not the same for loading and unloading. Such materials instead exhibit viscoelasticity, involving both elastic and viscous components, which at normal loading and unloading rates leads to hysteresis. A typical hysteresis curve is shown in a figure 3.19, and the energy absorbed during one loading-unloading cycle is given by the area within the loop. The shape of the loop depends on the rates of loading and unloading (unlike normal time-independent elasticity).

Dynamic Mechanical Analysis, otherwise known as DMA, is a technique where a

material is subjected to a sinusoidal deformation γ of small amplitude γ_0 at fixed pulse ω [rad/s]: $\gamma = \gamma_0 \sin(\omega t)$.

The rapidity of deformation or rapid shear is the first derivative respect to time of the deformation:

$$\frac{d\gamma}{dt} = \dot{\gamma} = \omega\gamma_0 \cos(\omega t) \quad (3.49)$$

For a pure Hookian solid, the stress is directly related with the strain $\tau = G\gamma$, but in the case of sinusoidal deformation becomes:

$$\tau = G\gamma_0 \sin(\omega t) \quad (3.50)$$

For a pure Newtonian fluid, instead, where $\tau = \mu\dot{\gamma}$, in the case of sinusoidal deformation becomes:

$$\tau = \mu\omega\gamma_0 \cos(\omega t) \quad (3.51)$$

In other words, the shear wave for an elastic solid will be in phase with the shear deformation, while the shear wave for a viscous fluid will be 90° out of phase compared to the shear deformation. For a viscoelastic materials, a phase shift is confined between 0 and 90 degrees and it reflects the elastic and viscous nature of the material.

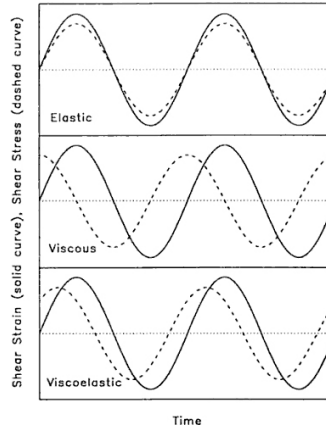


Figure 3.20: DMA of Elastic, Viscous and Viscoelastic materials

3.3.2 Loss Modulus, Storage Modulus, Complex Modulus and Loss Factor

Let us now apply a sinusoidal deformation:

$$\varepsilon = \varepsilon_0 \sin(\omega t) \quad (3.52)$$

where ε_0 is the maximum deformation amplitude for each cycle and ω is the pulsation. The stress will be:

$$\sigma = \sigma_0 \sin(\omega t + \delta) \quad (3.53)$$

where σ_0 is the maximum stress and $\delta(\omega)$ is the phase angle. Defined $E = \sigma_0/\varepsilon_0$, the last equation can be rewritten as:

$$\sigma = \varepsilon_0 E \sin(\omega t + \delta) \quad (3.54)$$

then:

$$\sigma = \varepsilon_0 E \cos(\delta) \sin(\omega t) + \varepsilon_0 E \sin(\delta) \cos(\omega t) \quad (3.55)$$

Similarly, for shear deformation $\gamma = \gamma_0 \sin(\omega t)$ we have:

$$\tau = \gamma_0 G \cos(\delta) \sin(\omega t) + \gamma_0 G \sin(\delta) \cos(\omega t) \quad (3.56)$$

It is clear that the term $\sin(\omega t)$ is in phase with ε (or γ) and the term in $\cos(\omega t)$ is 90° out of phase; therefore, the first term represents the component of the stress that is in phase with the deformation (elastic contribution) and it is also a measure of the energy elastically stored and recovered during each cycle. The term $E' = E \cos(\delta)$ (or $G' = G \cos(\delta)$) is known as dynamic storage elastic modulus or storage modulus.

The second term represents the component of the stress out of phase (phase shifted of 90°) with the deformation (viscous contribution) and it is a measure of the energy dissipated (as heat) in each deformation's cycle. The term $E'' = E \sin(\delta)$ (or $G'' = G \sin(\delta)$) is known as dynamic loss viscous modulus or loss modulus.

Then the viscoelastic materials stores energy during the deformation (expressed by the storage modulus and E') and releases part of the energy during unloading with losses (expressed by the loss modulus E''). The phase angle between stress and strain is expressed as a tangent:

$$\tan \delta = \frac{E''}{E'} = \eta \quad (3.57)$$

it is known as loss factor or loss tangent or dissipation factor; it is an alternative measure of the dissipation energy because expressed as ratio between the loss modulus and the storage modulus in a deformation cycle.

For a pure elastic material (phase angle= 0°), the loss factor is equal to zero; contrarily for a pure viscous material the phase angle is equal to 90° , the energy is fully dissipated.

It is often convenient to express the stress as a complex quantity, whose complex modulus is given by:

$$\frac{\sigma^*}{\varepsilon^*} = \frac{\sigma_0}{\varepsilon_0} e^{i\delta} = E^* = E' + iE'' \quad (3.58)$$

where E^* is known as Complex Young Modulus or Complex Modulus.

As done in the time domain, the constitutive equation of viscoelastic materials can be expressed in the frequency domain, through the use of complex modulus. The constitutive equation is given as a relation between E' and E'' defined directly in a frequency domain. The determination of these coefficients must be done experimentally for each materials.

Thus:

$$|E^*| = \frac{\sigma_0}{\varepsilon_0} = \sqrt{(E')^2 + (E'')^2} \quad (3.59)$$

finally, given $E'' = E' \tan \delta$, we have:

$$E^* = (E' (1 + \tan^2 \delta)) \quad (3.60)$$

3.3. THE DYNAMIC BEHAVIOR

An expression similar to complex Young's modulus can be used for the complex shear modulus G^* defined as:

$$G^* = (G' + jG'') \quad (3.61)$$

where the real part G' is due to pure elastic behavior, while the imaginary part G'' is due to pure viscous behavior and it is linked to the material's shear strain. For most of viscoelastic materials is:

$$E' = 3G', \quad \tan \delta = \tan \delta_G \quad (3.62)$$

where $\tan \delta_G = G''/G'$. These relations show that the complex Young's modulus and the complex Shear modulus have the same frequency dependence and the loss factor to the extensional stress is the same as on the shear deformation. Real and imaginary parts of the complex modulus depends on temperature, frequency (fig.3.21) and the environment.

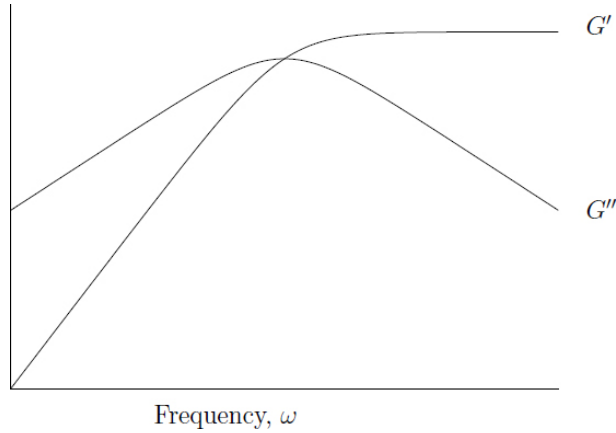


Figure 3.21: Storage modulus and loss modulus

3.3.3 Other consideration about Loss Factor

The damping capacity of a system is defined as the energy dissipated during a load cycle:

$$\Delta U = \oint f_d dx \quad (3.63)$$

This quantity can also be interpreted as the area within the hysteresis cycle in the force-displacement plan.

If U_{max} is the total initial energy of the system, the specific damping D is then defined by the ratio:

$$D = \frac{\Delta U}{U_{max}} \quad (3.64)$$

And so the loss factor η , that is the the damping capacity per radian:

$$\eta = \frac{\Delta U}{2\pi U_{max}} \quad (3.65)$$

U_{max} is approximately equal to the maximal kinetic energy and the maximal potential energy of the system, when the damping is low. If those relations are applied in a viscoelastic material under an armonic sollicitation (or deformation), it is:

$$\Delta U = \pi E'' \varepsilon_0^2 \quad (3.66)$$

and since $E'' = \eta E'$ it is:

$$\Delta U = \pi \eta E' \varepsilon_0^2 \quad (3.67)$$

The maximal potential energy absorbed by the material is:

$$U = \frac{1}{2} E' \varepsilon_0^2 \quad (3.68)$$

Hence, from eq 3.67 and 3.68, it is possible to derive the loss factor as:

$$\eta = \frac{\Delta U}{2\pi U} \quad (3.69)$$

It is clear that a material characterized by a high loss factor has a strong capacity in dissipating energy, and so strong damping properties.

It should not be forgotten that the loss factor depends on temperature and frequency. For each material, in a fixed temperature range, it is possible to observe convenient values of the dynamic parameters only in a certain frequency range, and, vice versa, in a fixed frequency range, it is possible to observe convenient values of the dynamic parameters only in a certain temperature range.

3.3.4 Temperature effects on viscoelastic behavior

The properties of polymeric materials which are used as damping treatments are generally much more sensitive to temperature than metals or composites. Thus, their properties, namely the complex moduli represented by E , G , and the loss factor η , can change fairly significantly over a relatively small temperature range. There are three main temperature regions in which a viscoelastic material can effectively operate, namely the glassy region, transition region, and rubbery region [1, 10]. Figure 3.22 shows how the loss factor and the storage modulus can vary with temperature. The glassy region is representative of low temperatures where the storage moduli are generally much higher than for the transition or rubbery regions. This region is typical for polymers operating below their brittle transition temperature. However, the range of temperatures which define the glassy region of a polymeric material is highly dependent on the composition and type of viscoelastic material (fig.3.23). Thus, different materials can have much different temperature values defining their glassy region. Because the values of the storage moduli are high, this inherently correlates to very low loss factors. The low loss factors in this region are mainly due to the viscoelastic material being unable to deform (having high stiffness) to the same magnitude per load as if it were operating in the transition or rubbery regions where the material would be softer. On the other material temperature extreme, the rubbery region is representative of high material temperatures and lower storage moduli. However, though typical values of storage moduli are smaller, like the glassy region the material loss factors are also typically very small. This is due to the increasing breakdown of material structure as the temperature is increased. In this region,

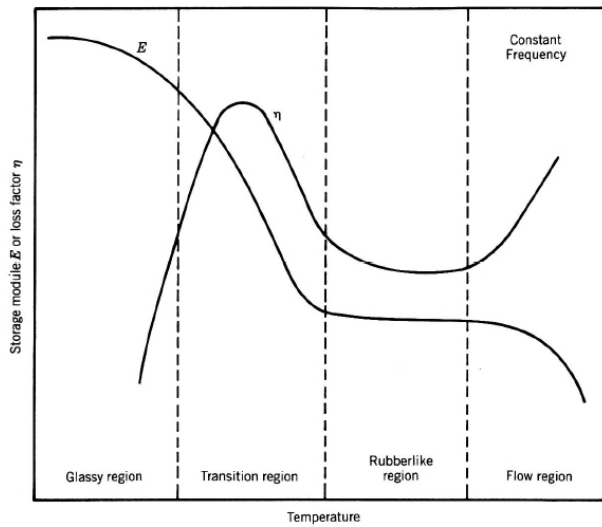
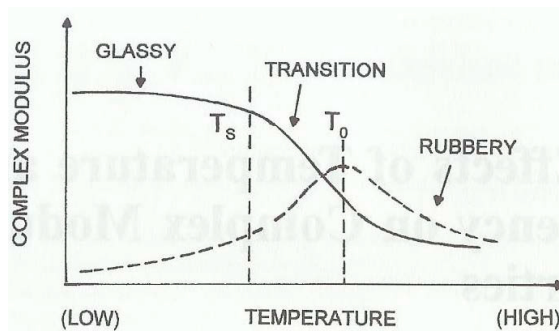
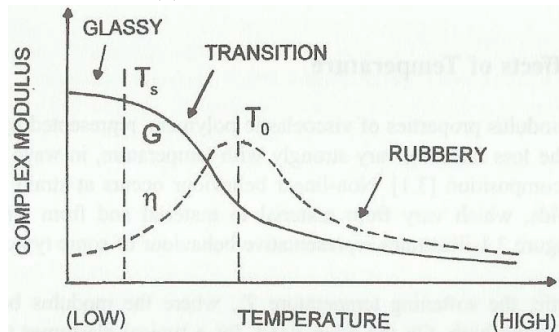


Figure 3.22: Temperature effects on Storage Modulus and Loss Factor



(a) Typical plastic material



(b) Typical elastomer material

Figure 3.23: Temperature effects on different materials: plastic (a), elastomer (b)

the viscoelastic material is easily deformable, but has lower interaction between the polymer chains in the structure of the material. Cross-linking between polymer chains also becomes a less significant property as temperature is increased. A lower interaction between the chains results in the material taking longer to

reach equilibrium after a load is removed. Eventually, as the temperature hits an upper bound critical value (also known as the flow region temperature), the material will begin to disintegrate and have zero effective loss factor and zero storage modulus. The region falling between the glassy and rubbery regions is known as the transition region. Materials which are used for practical damping purposes generally should be used within this region because loss factors rise to a maximum. In more detail, if a material is within the glassy region and the temperature of the material is increased, the loss factor will rise to a maximum and the storage modulus will fall to an intermediate value within the transition region. As the material temperature is further increased into the rubbery region, the loss factor will begin to fall with the storage modulus. This behavior is illustrated in Figure 2.2. Therefore, it is extremely important to know the operating temperature range during the design phase of a host structure to which a viscoelastic damping treatment will be applied so that the viscoelastic treatment will be maximally effective. Figure 3.24 shows the optimum regions for various damping treatments. The region A is optimum for the free-layer treatments,

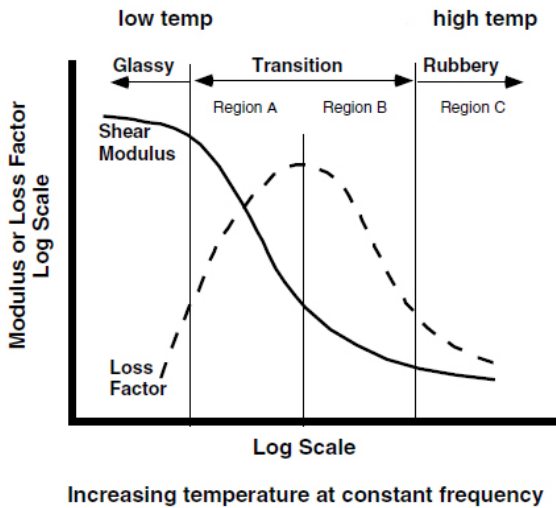


Figure 3.24: Optimum regions for the Loss Factor

characterized by high shear modulus and high loss factor. The region B is optimum for the constrained-layer treatments, characterized by low shear modulus and high loss factor. The region C is good for harmonic absorbers (tuned-mass dampers), having a low shear modulus and low loss factor, while the regions A and B are also excellent for many other types of dampers.

3.3.5 Frequency effects on viscoelastic behavior

Like temperature, frequency also has a profound effect on the complex modulus properties of a viscoelastic polymer, though to a much higher degree with an inverse relationship. The three regions of temperature dependence (glassy, transition, rubbery) can sometimes be a few hundred degrees, more than covering a typical operational temperature range of an engineered structure. But the range of frequency within a structure can often be several orders of magnitude.

The frequency dependence on complex moduli can be significant from as low as $10^{-8} Hz$ to $10^8 Hz$, a range much too wide to be measured by any single method [1]. Furthermore, relaxation times after deformation of a viscoelastic material can be anywhere from nanoseconds to years and will greatly effect one's measurement methods, especially at low temperatures [1, 10].

Frequency has an inverse relationship to complex moduli with respect to temper-

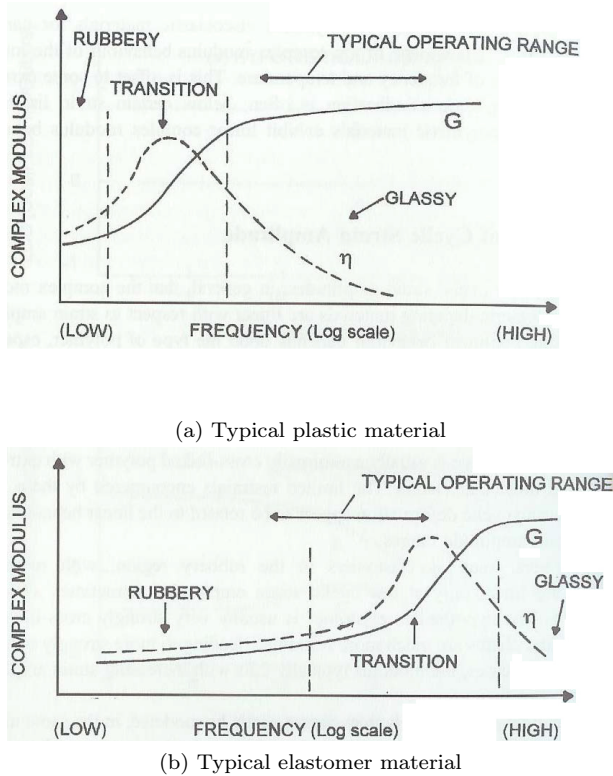


Figure 3.25: Frequency effects on Storage Modulus and Loss Factor

ature (fig.3.25). At low frequency, the storage moduli are low and the loss factors are low. This region is synonymous with the rubbery region (high temperatures). This is due to the low cyclic strain rates within the viscoelastic layer. As the frequency is increased, the material hits the transition region where the loss factor hits a maximum value. As the frequency is increased further, the storage moduli increase as the loss factor decreases. Thus, the transition region is again the range of frequency for which a material should be chosen to correspond to a host structure's typical operating range. Figure 3.26 illustrates this behavior.

3.3.6 Cyclic Strain Amplitude Effects on Complex Modulus

The effect of cyclic strain amplitude on polymeric complex moduli is highly dependent on the composition and type of the polymer, particularly the molecular structure [1, 10]. Experiments have shown that the complex moduli of polymers

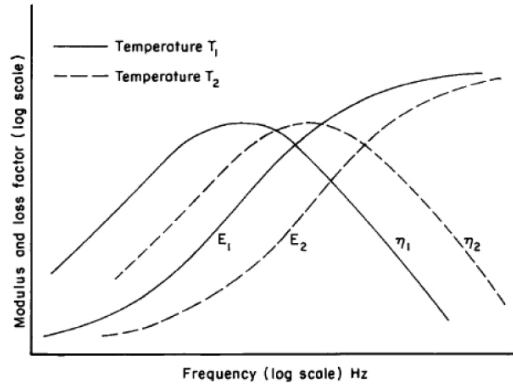


Figure 3.26: Both Temperature and Frequency effects

generally behave linearly only at low cyclic strain amplitudes [1]. There are, however, polymers such as pressure sensitive adhesives, which exhibit linearity even at high cyclic strain amplitudes. These polymers usually have very few cross links between long, entangled polymer chains. Therefore, the low interaction between these chains seems to have an effect on the linear behavior over wide strain amplitude ranges [1]. However, most viscoelastic polymers used in typical damping applications behave nonlinearly at high strain amplitudes. This nonlinearity is very difficult to model accurately and involves very complicated theories and a significant number of tests, many more than for linear complex modulus behavior, to gather data sufficient to establish trends for a specific material [1, 10].

3.3.7 Environmental effects on complex modulus

The environment plays a significant role in all outdoor engineering applications. Temperature ranges, climate, amount of rainfall or direct exposure to sunlight, as well as foreign substance exposure (such as petroleum products, alkalis, harmful chemicals, etc.) are necessary design factors to take into consideration for any outdoor engineering project. The same holds true when considering applying a viscoelastic treatment to an engineered structure. Temperature dependence on the behavior of viscoelastic complex moduli has already been discussed. But depending on the application, polymer type, and composition of the material, exposure to foreign substances must also be addressed. Oils and other petros can penetrate into some materials and alter the behavior as well as jeopardize the bond between a material and the host structure, something which will be shown to be very important. Therefore, it is important to study the effects of these foreign elements on the behavior of the material which will be used in a particular application. Some elements may be more important than others depending on the operating environment, so these elements should hold the highest interest of the designer.

Chapter 4

Experimental Approach

The objective of this research activity is to evaluate the damping of composite structures realized with embedded viscoelastic damping treatments (as discussed in section 1.2) and then, subsequently, to develop a numerical analysis technique that correctly represents what occurs experimentally. The structures analyzed in this work are two typical aircraft composite fuselage skin made by carbon fiber/epoxy resin pre-preg laminate; the first one treated with viscoelastic damping treatments (HPLT) and the second without treatment (will be our reference). The activities were performed in the frame of the project A.R.C.A. (DM24436) granted to IMAST S.c.a.r.l. and funded by the M.I.U.R.. Defined a flight altitude in a range of about 0-8000m and considering to an international standard atmosphere (ISA), to simulate the behavior of such structures in a temperature range similar to the flight conditions different tests in a temperature range from 15°C to -35°C were performed.

A number of damping measures and criteria are used in practice to characterize structural damping [37, 38]. It appears in practice that damping parameters in multi-degree-of-freedom (MDOF) systems are the most critical to estimate. It is well known that they are the most sensitive to noise, measurement errors, inadequate excitation, etc. There exist different techniques for measuring damping values and properties [38, 39]. Different methods of damping identification have also been developed in dynamics; a review can be found in references [38, 40]. These methods can be classified into time and frequency domain. The logarithmic decrement is the simplest time-domain method used for single-degree-of-freedom (SDOF) systems. More elaborate time-domain techniques are used for MDOF systems. The most popular techniques include the Smith least squares (SLS) algorithm [41] and the least squares complex exponential (LSCE) method [41] which basically fit the impulse response function (IRF) of a MDOF system. A modification of the SLS method based on an initial estimate obtained from the logarithmic decrement can be found in reference [40]. Other time domain techniques used for SDOF and MDOF systems include limit envelopes [42] and Hilbert transform [43, 44, 46, 47, 48].

Frequency domain methods are based on the frequency response function (FRF). The 3-dB method [37] uses the amplitude of the FRF. This method can be improved when the phase information from the Nyquist plot is used additionally [37]. The methods can be extended to MDOF systems for lightly coupled modes

with minimal crossovers. They also give significant errors in the case of lightly damped systems. More accurate results can be obtained when curve-fitting techniques are applied to the FRF. This can be done by using, for example, a linear least squares technique for the SDOF system and a non-linear least squares technique for the MDOF system. A comparison between various time and frequency domain methods is given in reference [40]. A combined time-frequency approach can be applied to estimate the damping of the system by using, for example, the Wigner-Ville distribution [44, 48]. The main use of a time-frequency approach to the study of vibration signals is made on time variations of the spectral characteristics.

The presence of viscoelastic material, as in this case, increases the modal density of the whole structure. This does not allow to use methods based on the frequency domain, such as 3-dB method, since it is impossible to isolate each resonance peak because the structural response at a resonance is influenced by contribution of the neighbouring resonances (heavily coupled modes). A time-domain's method based on the Hilbert transform and the identification of the extinction curve of the signal was then used, in this work. This method is the so-called Impulse Response Decay Method (IRDM).

4.1 Impulse Response Decay Method (IRDM)

The Impulse Response Decay Method (IRDM) is a time-domain methods for damping measurement based on decay of oscillations[49, 51].

The damping characterization for a structure can be made through different parameters, all related and equivalent to each other. For experimental damping evaluation it is customary to refer to a dimensionless quantity, called loss factor η . It represents the fraction of mechanical energy dissipated (generally as heat) in a vibration cycle [53, 54]. The main point of the procedure is that the impulse response is obtained directly in time domain and not as inverse frequency response of the structure. This is the situation in which the impulse response function is prone to a Bias error when calculated via an inverse Fourier transform from a leakage free measurement of the frequency response function using DFT/FFT technique [50]. When the system under investigation contains lightly damped resonances, the estimated impulse response function will be biased in both amplitude and phase. Lightly damped resonances in a system cause the impulse response function to be long with decaying oscillations, which in the frequency domain corresponds to sharp, narrow peaks in the frequency response function. If the record length in the FFT analysis is not sufficiently long compared to the time constant of the decay in the impulse response function, the bias error is observed [49]. In the frequency domain this means that above-mentioned bias error is observed if the resonance peak in the frequency response function is narrower than the resolution in the analysis even though the calculated samples of the frequency response function are free of the influence of leakage. One of the assumptions underlying the application of this method is that the structural response is an IRF (Impulse Response Function). This claim allows to extract information from signal by applying the Hilbert transform such as the decay rate D that is directly related to loss factor η .

In the standard IRDM procedure, the Hilbert transform must be applied on each

resonance peak and then this procedure evaluates the loss factor at resonance [50]. For highly damped structures, such as skins in advanced composite materials where the modal density is very high, it is not possible to separate each resonance peak because the structural response at a resonance is influenced by contribution of the neighbouring resonances (heavily coupled modes). In this case, it is assumed to obtain the loss factor in a frequency band as average loss factor in the band. This is not a modal approach, often known as Impulse Response Decay Method (IRDM) and allows a realistic estimate of damping to high frequencies. Once acquired the Time History, the first step is to filter the signal in a 1/3 octave bands in order to isolate the contributions to various bands; then the Hilbert transform is applied to the various bands and the Hilbert's envelope is evaluated. The final step is to evaluate the regression line, and then the decay rate of the response for each analysis band.

4.1.1 Excitation type

The assumption underlying the application of the Hilbert transform is that the excitation is impulsive [49]. Theoretically the unit impulse function or Dirac function ($\delta(t)$) is a generalized function representing an infinitely sharp peak bounding unit area; this function has the value zero everywhere except at $t = t_0$ where its value is infinitely large in such a way that its total integral is 1.

$$\delta(t) = \begin{cases} +\infty, & t = t_0 \\ 0, & t \neq 0 \end{cases} \quad (4.1)$$

$$\int_{-\infty}^{+\infty} \delta(t) dt = 1 \quad (4.2)$$

In frequency-domain, an impulsive signal has a constant spectrum and so excites the structure with the same amplitude at all frequencies. An impulsive signal is not easily reproducible experimentally due to both constructive problems and physical problems (friction, etc.). Since vibration tests require a lot of

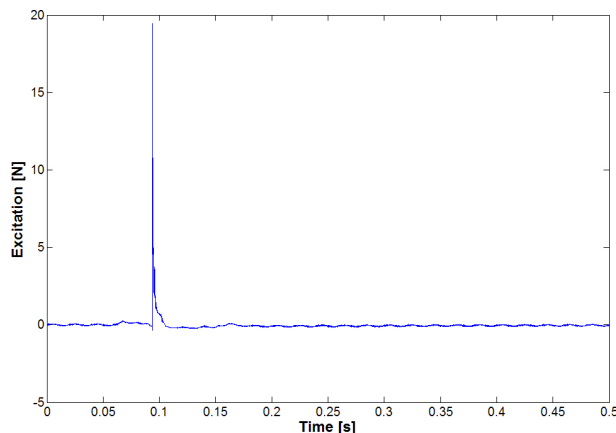


Figure 4.1: Excitation

excitations with the same amplitude and because the tests were conducted in a

climatic chamber, in order to characterize the damping behavior in a temperature range similar to the flight conditions, an excitation system has been developed ad-hoc.

A programmable excitation system was thus developed by Department of Aerospace Engineering at University of Naples Federico II in order to overcome the limitations given by standard excitation devices and to obtain a signal that is as close as possible to the impulsive one. The obtained excitation signal (fig.4.1) has an application time about $2.5 \cdot 10^{-4}$ s and so its frequency spectrum is constant up to around 4 kHz.

4.1.2 Hilbert Transform

The Hilbert transform [45] for a real signal $x(t)$ in time domain is defined as:

$$\tilde{x}(t) = H[x(t)] = \int_{-\infty}^{+\infty} \frac{x(\alpha)}{\pi(t - \alpha)} d\alpha \quad (4.3)$$

It is easy to see (fig.4.2) that the Hilbert transform leads to phase delay ($\pi/2$ radians for each frequency component of input signal) and produces no change in input amplitude signal. Defined a complex analytical signal $\hat{x}(t)$, whose real part

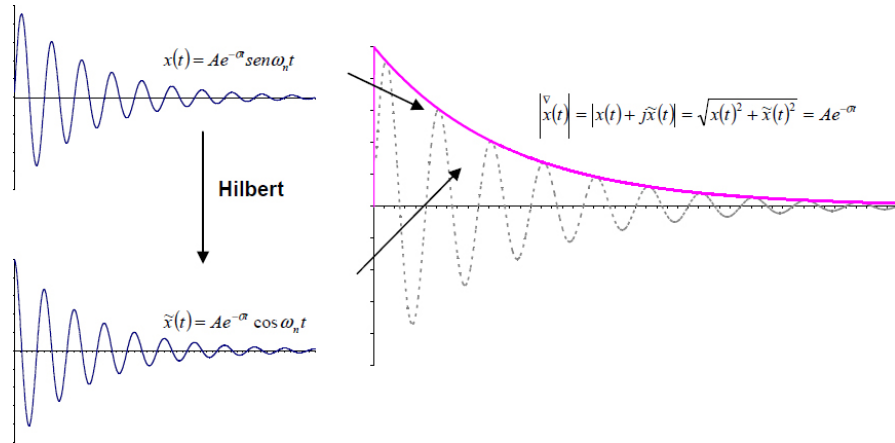


Figure 4.2: The use of Hilbert transform to determine a signal envelope

is the signal $x(t)$ and its imaginary part is the Hilbert transform of the signal $\tilde{x}(t)$, as follows:

$$\hat{x}(t) = x(t) + j\tilde{x}(t) \quad (4.4)$$

the module of the function so defined, provides the envelope function, as shown in figure 4.2 for a simple signal like a damped sinusoid. The envelope of impulsive response gives all the information necessary to calculate damping. In the case of MDOF system, the same method can be used if, in the frequency response, it is possible to distinguish every modal behaviour. An example is the system represented in figure 4.3 with frequency response and relative impulsive response on right side. The impulsive response can not be used because it is a sum of five different damped sinusoids, each of them corresponding to an own vibration mode. Through an opportune filtering, it is possible to isolate the peak of interest

in the FRF so to obtain the impulsive response corresponding to a SDOF system (4.3c, 4.3d). Do that, it is possible to analyze the system as seen before. The use

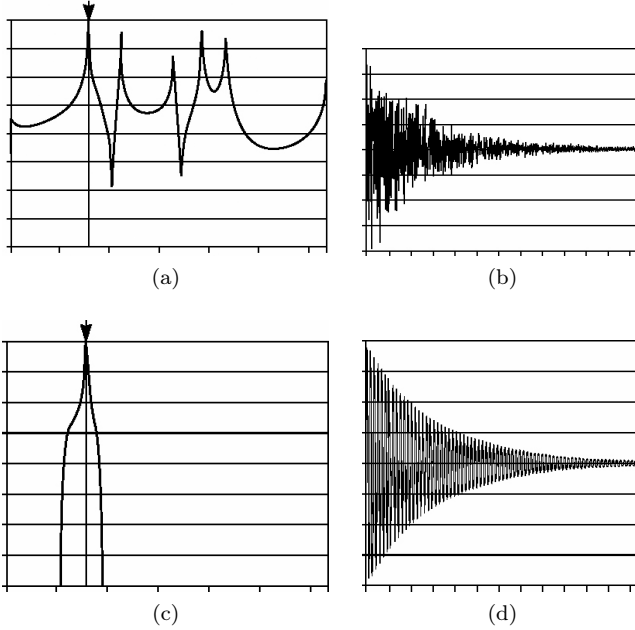


Figure 4.3: Example of MDOF system

of Hilbert transform to determine damping, requires the knowledge of impulsive response (in time domain) of the structure for the analysis. If $h(t)$ is the impulse response function (IRF), the analytic function $\hat{h}(t)$ defined such as equation 4.4, is equal to:

$$\hat{h}(t) = h(t) + j\tilde{h}(t) \quad (4.5)$$

whose modulus is:

$$|\hat{h}(t)| = \sqrt{h^2(t) + \tilde{h}^2(t)} \quad (4.6)$$

The modulus of the function \hat{h} is simply the envelope of the function $h(t)$ (fig.??).

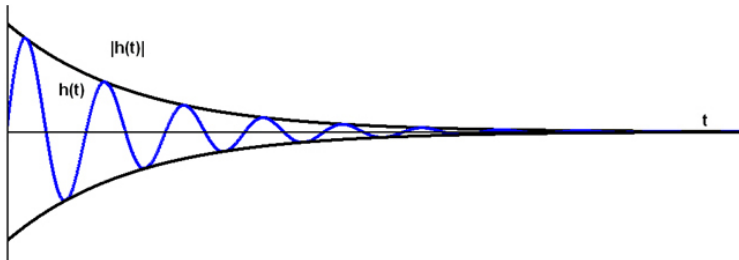


Figure 4.4: IRF for a SDOF system

For a SDOF system (Single Degree Of Freedom system) the modulus of IRF transform is [49]:

$$h(t) = A_0 e^{-\sigma t} \sin(\omega_d t) \rightarrow |\hat{h}(t)| = A_0 e^{-\sigma t} \quad (4.7)$$

where A_0 is the amplitude; $e^{-\sigma t}$ is the exponentially decaying term, determined by the viscous damping and called the damping term; $\sin(\omega_d t)$ is the term that oscillates at a frequency which is the damped natural frequency.

If the system is underdamped the impulse response has a trend like that shown in fig.4.4, where the bold curves are called *extinction curves* and are described by the equation:

$$y = \pm A_0 e^{-\sigma t} \quad (4.8)$$

where σ is the decay constant or decay rate. Known the decay constant, it easy to obtain the loss factor as:

$$\eta = \frac{2\sigma}{\omega_n} \quad (4.9)$$

where ω_n is the central frequency of each analysis band.

4.1.3 Decay Rate evaluation

The viscoelastic layer give rise to an increase in modal density due to its link with the viscoelastic characteristics and frequency [55]. When the frequency of analysis increases, the modal density increases too. For this reason, in this case, applying the procedure described in section 4.1.2, the Hilbert envelope is not very smooth as in the SDOF (fig.4.4). Consider what happens in figure 4.5 where

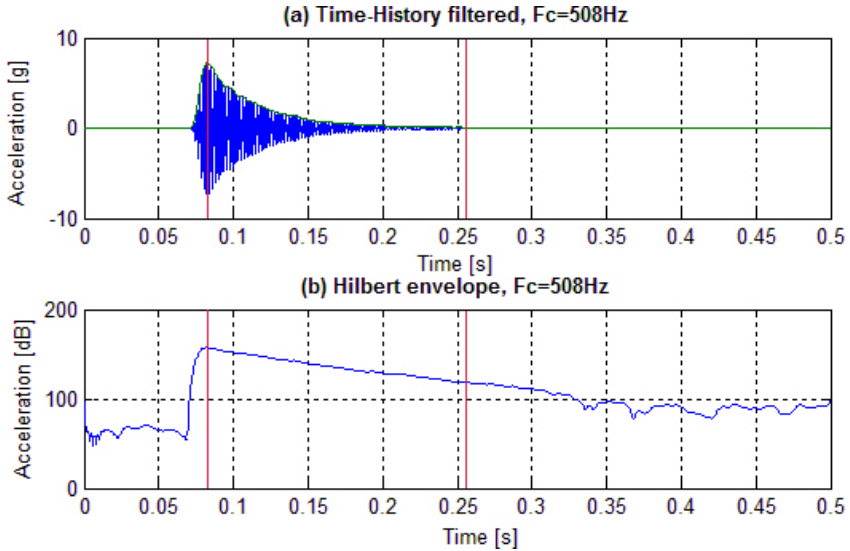


Figure 4.5: Filtered time-history and its Hilbert envelope, Fc=508Hz

the filtered time-history (with central-band frequency equal to 508Hz) and its Hilbert envelope is shown; this last have generally a large number of peaks (local maxima) due to high modal density. The area of interest in the Hilbert's envelope curve useful to decay rate evaluation is contained between red lines (fig.4.5) and coincides with time history extinction length. The decay evaluation is achieved by the least squares method considering the values identified by the peaks in the area of interest. Another assumption is to neglect the valleys (local minima) since they are related to the sampling used to calculate the Hilbert envelope. If the

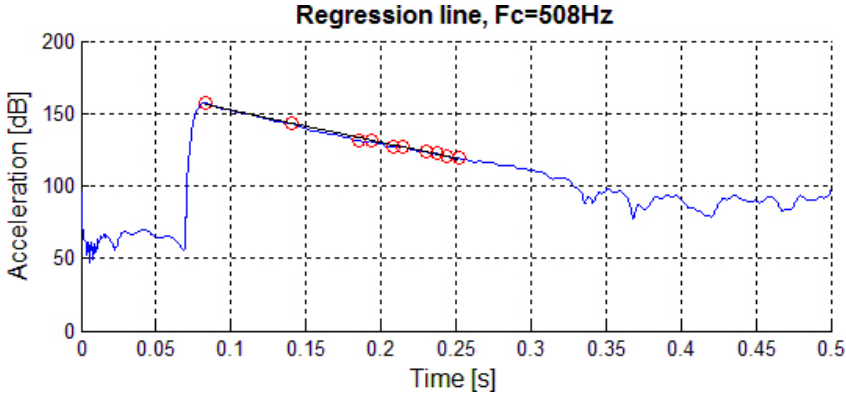


Figure 4.6: Regression line, Fc=508Hz

peaks (red circles in fig.4.6) are identified by couples of random variable (x_i, y_i) where x_i is the time and y_i is the acceleration in dB, the regression line is given by:

$$y = ax + b \quad (4.10)$$

where the terms a, b are estimated in order to minimize the squared residuals S given by:

$$S = \sum_{i=1}^n z_i^2 = \sum_{i=1}^n (y_i - ax_i - b)^2 \quad (4.11)$$

The estimation of parameters a, b is computed imposing that the partial derivatives of the squared residuals S respect to a, b are equal to zero as follows:

$$\frac{\partial S}{\partial a} = 2 \left(- \sum_{i=1}^n x_i y_i + a \sum_{i=1}^n x_i^2 + b \sum_{i=1}^n x_i \right) = 0 \quad (4.12)$$

$$\frac{\partial S}{\partial b} = 2 \left(- \sum_{i=1}^n y_i + a \sum_{i=1}^n x_i + nb \right) = 0$$

hence

$$\hat{b} = \frac{1}{n} \sum_{i=1}^n y_i - \hat{a} \frac{1}{n} \sum_{i=1}^n x_i = \bar{y} - \hat{a} \bar{x} \quad (4.13)$$

$$\hat{a} = \frac{\frac{1}{n} \sum_{i=1}^n (x_i y_i) - \bar{x} \bar{y}}{\frac{1}{n} \sum_{i=1}^n x_i^2 - \bar{x}^2} \quad (4.14)$$

and finally, the regression line (fig.4.6) becomes:

$$y = \hat{a}x + \hat{b} \quad (4.15)$$

and its slope \hat{a} is the decay rate D . The equation 4.9 give the loss factor η .

4.2 Experimental set-up

In this section, the experimental set-up used to perform tests is described. It can be divided into an excitation system, a climatic room and an acquisition system.

4.2.1 Excitation system

The excitation system used in this activity has been entirely designed and built at Dias's laboratory. It is the result of numerous experiments accompanied by corresponding changes in order to obtain an excitation system more performing. This system (fig.4.7) is composed by pneumatic actuator (cylinder), hydraulic electrovalves, and it is automated through the use of a programmable control unit. The pneumatic actuator was chosen because it compared to other excitation

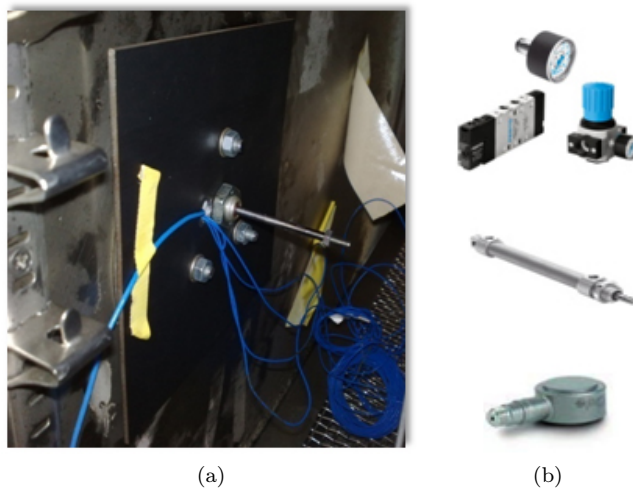


Figure 4.7: Excitation system (a) and some of its components (b)

systems, such as impact hammer, it is able to provide a lot of excitations with the same intensity (avoiding the overload of the channel in the acquisition system) and above keeping the same position for the excitation. Electromagnetic actuators were discarded due to their high inertia. In addition, only the pneumatic actuator can operate automatically without problems up to low temperatures, as in this case. The obtained signal (fig.4.8) has an excitation time about $2.5 \cdot 10^{-4}$ s and

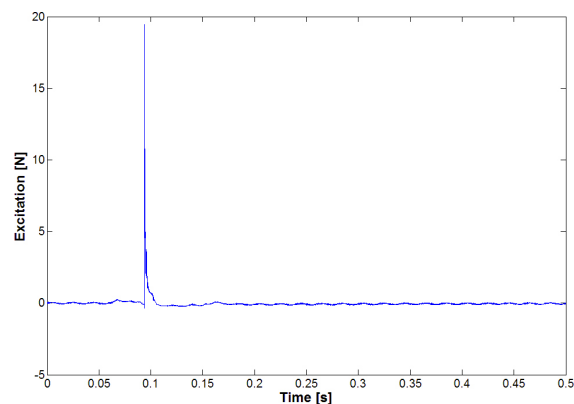


Figure 4.8: Excitation signal

so its frequency spectrum is constant up to around 4 kHz.

4.2.2 Climatic room

Defined a flight altitude in a range of about 0-8000m and considering the international standard atmosphere (ISA), in order to simulate the damping behavior of these composite fuselage structures in a temperature range similar to the flight conditions, different tests in a temperature range from 15°C to -35°C were performed. The device able to reproduce the environmental flight conditions in terms of temperature is the climatic room (fig.4.9). These tests have been performed in the climatic room of the acoustic laboratory of the Alenia Aeronautica which allows temperature variations in a wide range of values (-75°C , $+180^{\circ}\text{C}$) with a rate of change of $8^{\circ}\text{C}/\text{min}$).



Figure 4.9: Climatic room of Alenia Aeronautica laboratories

4.2.3 Acquisition system

The acquisition system is composed by four monoaxial accelerometers, PCB Piezotronics, (fig.4.10b) located in a different positions on the panel surface skin. The acceleration time histories are showed and registered in a real time by signal analyzer device *LMS scadas mobile SCM01* (fig.4.10a).



(a) scadas mobile



(b) accelerometer

Figure 4.10: Acquisition system

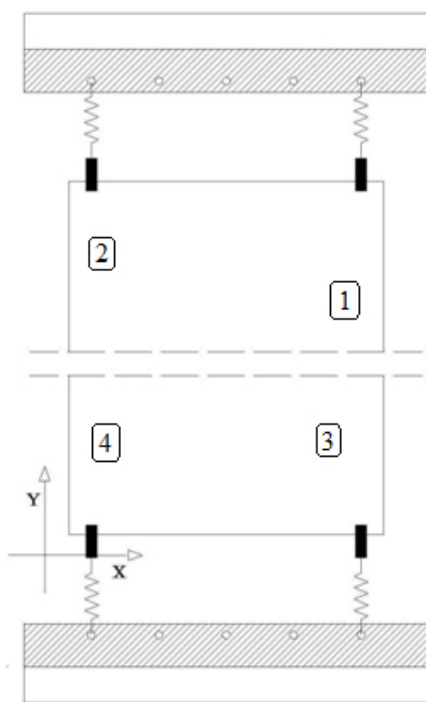
4.3 Structure lay-up

Two typical aircraft composite fuselage panels made by carbon fiber/epoxy resin pre-preg laminate have been analyzed in this work; the first one treated with viscoelastic damping treatments (HPLT) and the second without treatment (fig.4.11). About the boundary conditions, the panels are suspended into the



Figure 4.11: Panels lay-up: (a) treated, (b) no-treated

climatic room through four springs (fig.4.12b) in order to realize a free-free condition. The stiffness of the springs are such that the first natural frequency of the springs-panel system is much lower than the first natural frequency of the panel. The dimensions of the panels are equal to 200x600mm. The position of the four accelerometers is like in figure 4.12a.



(a) Cad view



(b) Coupon

Figure 4.12: Test Panel

4.4 Results

Thanks to the excitation system opportunely developed for this test campaign, a lot of signal acquisitions have been performed at different temperature conditions for both no-treated and treated panels as follows:

- 212 tests for no-treated panel at temperature condition of -35°C ;
- 168 tests for treated panel at temperature condition of 15°C ;
- 100 tests for treated panel at temperature condition of -20°C ;
- 50 tests for treated panel at temperature condition of -25°C ;
- 50 tests for treated panel at temperature condition of -35°C .

A first result of the viscoelastic effect, it already can be seen from the comparison of the time histories. These curves (fig. 4.13) show that the treated panel has a decay rate much faster than the untreated panel.

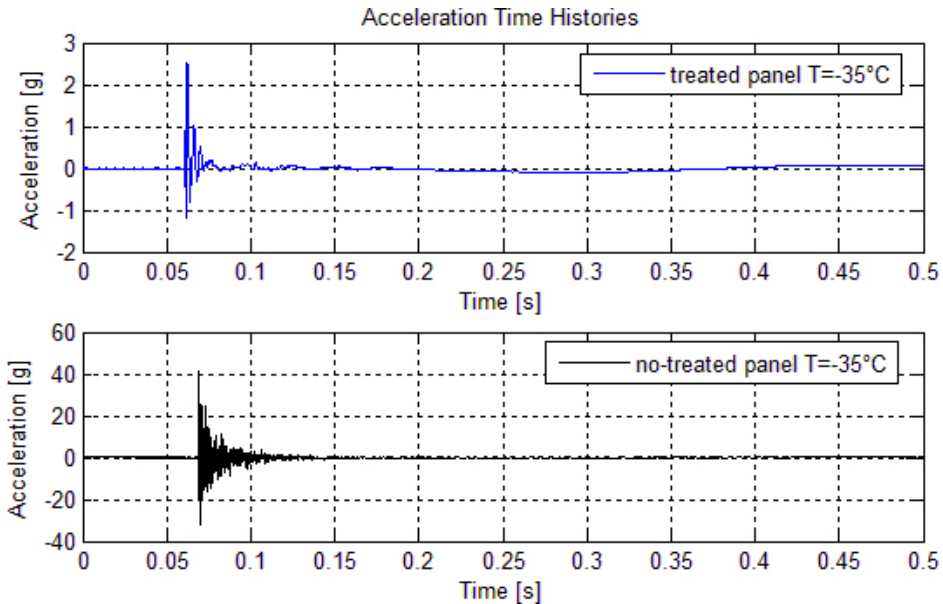
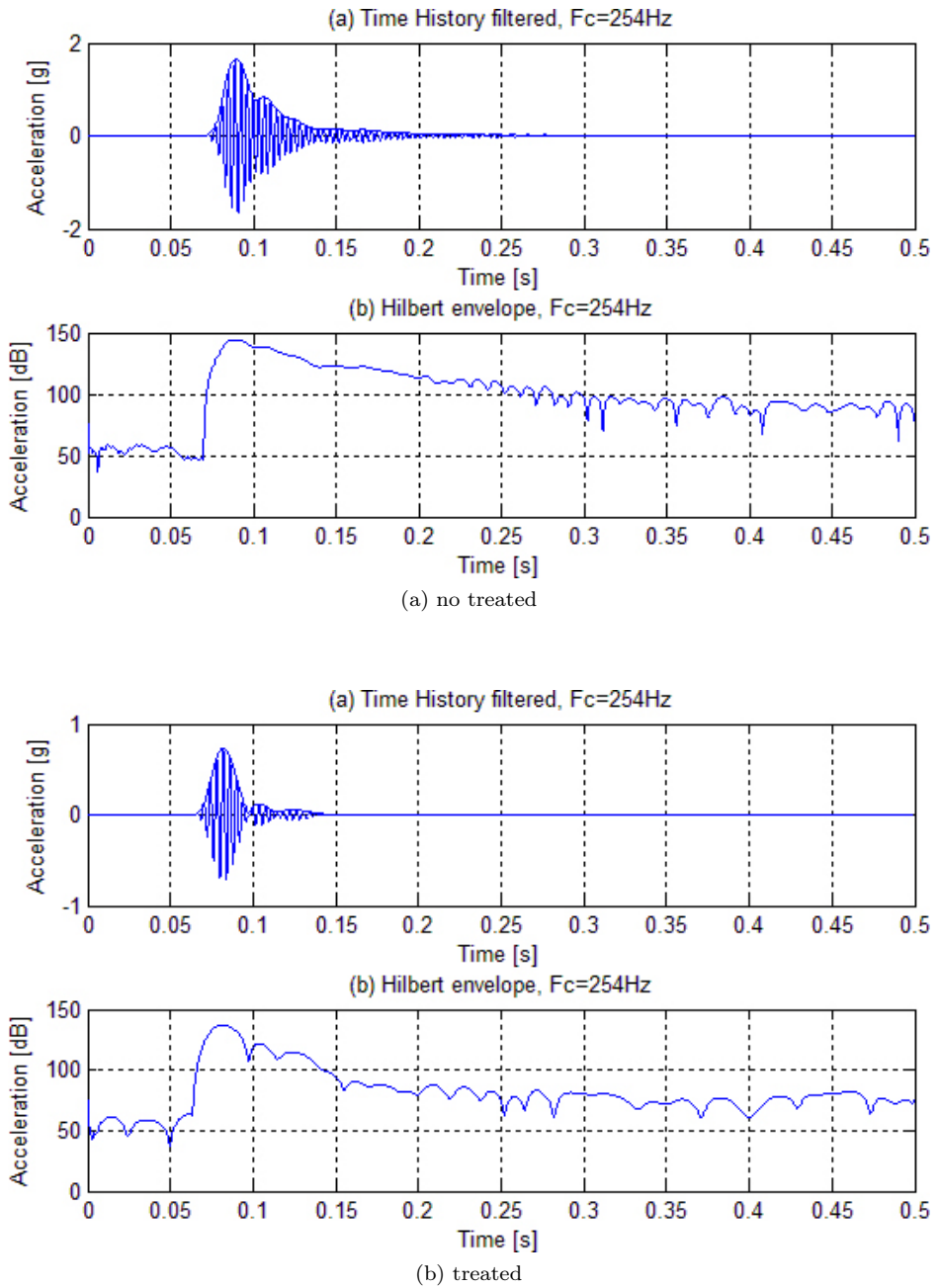


Figure 4.13: Acceleration time histories for treated and no-treated panels

This effect is much more clear in the filtered signals and their Hilbert transforms. A comparison between the filtered accelerations and their Hilbert transforms, for the two analyzed cases (treated and no-treated panels) in the analysis band with the central frequency equal to 254Hz , 508Hz , 806Hz , 1016Hz , 2032Hz and 3225Hz are shown in figures 4.14-4.19, respectively.

Figure 4.14: No-treated (a) vs treated (b) time histories, $F_c=254\text{Hz}$

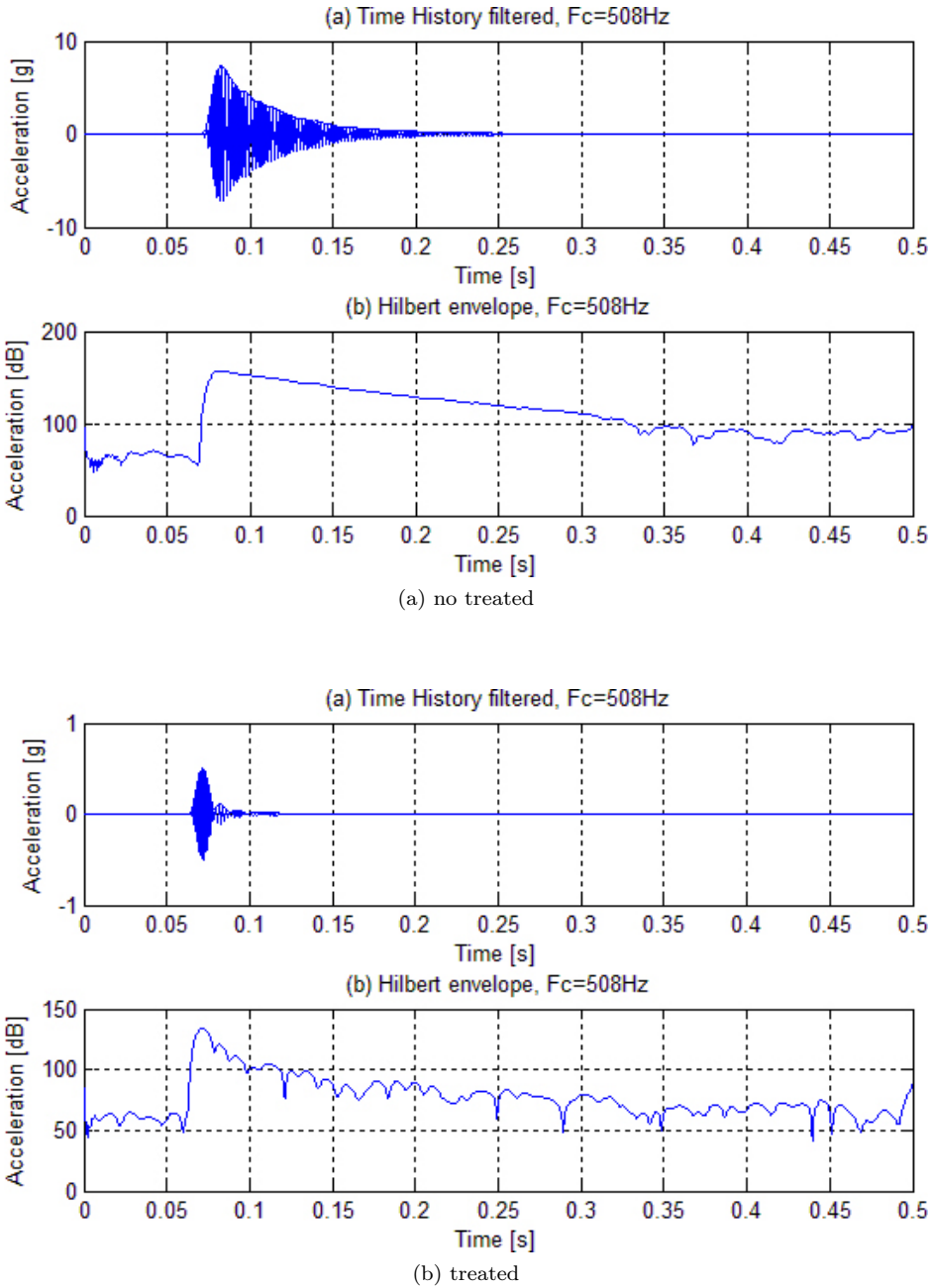
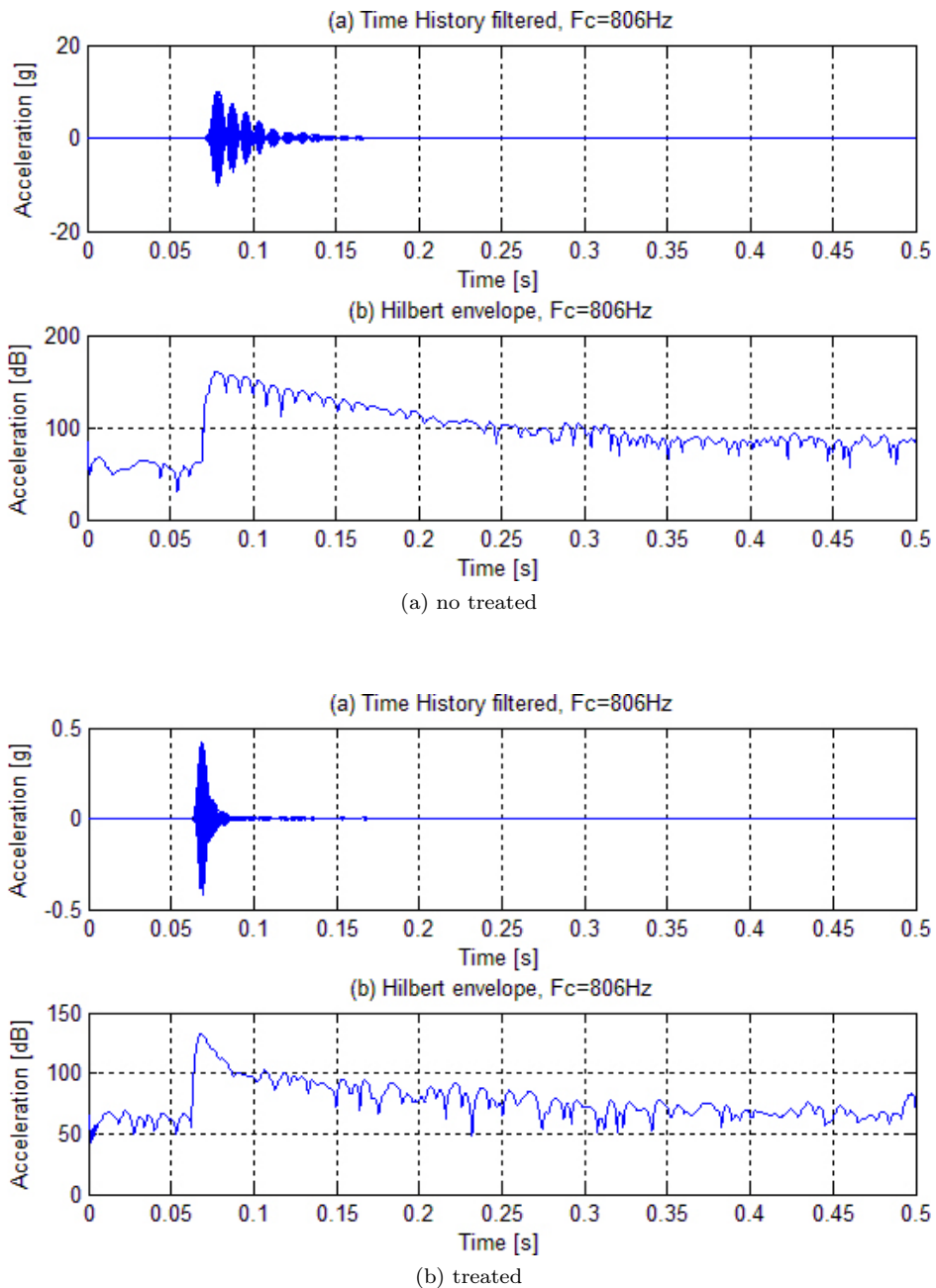
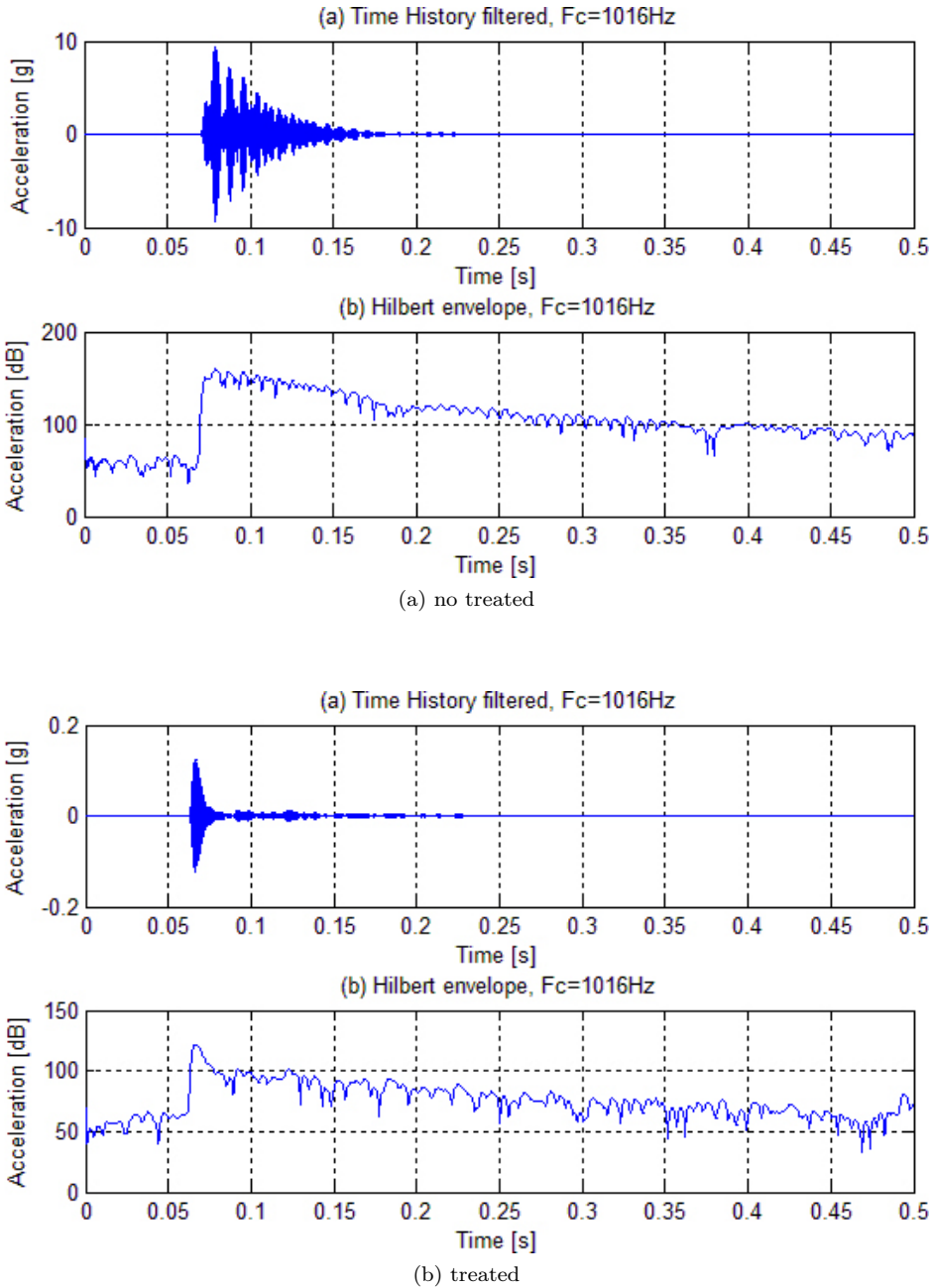


Figure 4.15: No-treated (a) vs treated (b) time histories, $F_c=508\text{Hz}$

Figure 4.16: No-treated (a) vs treated (b) time histories, $F_c=806\text{Hz}$

Figure 4.17: No-treated (a) vs treated (b) time histories, $F_c = 1016\text{Hz}$

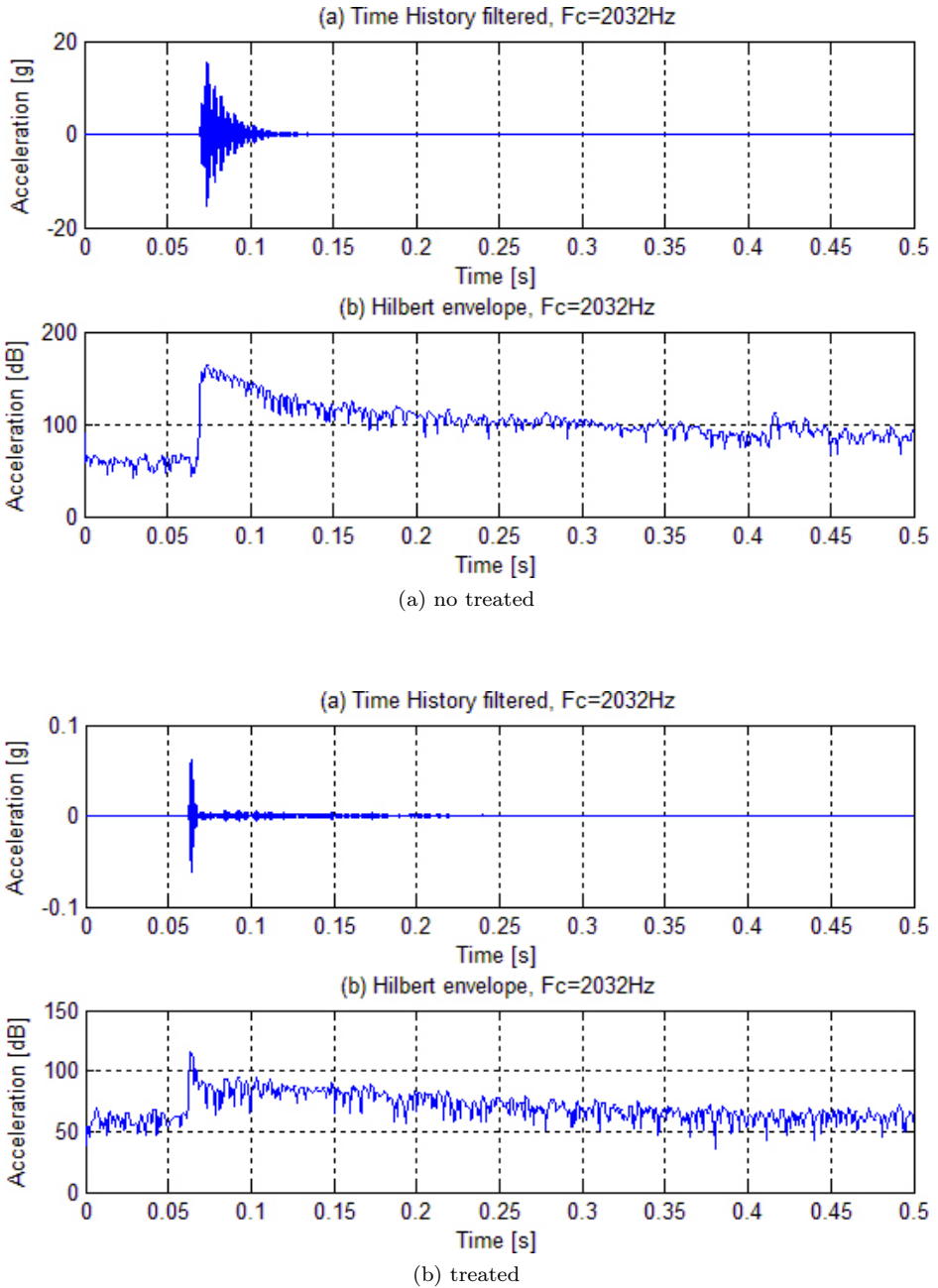


Figure 4.18: No-treated (a) vs treated (b) time histories, $F_c=2032\text{Hz}$

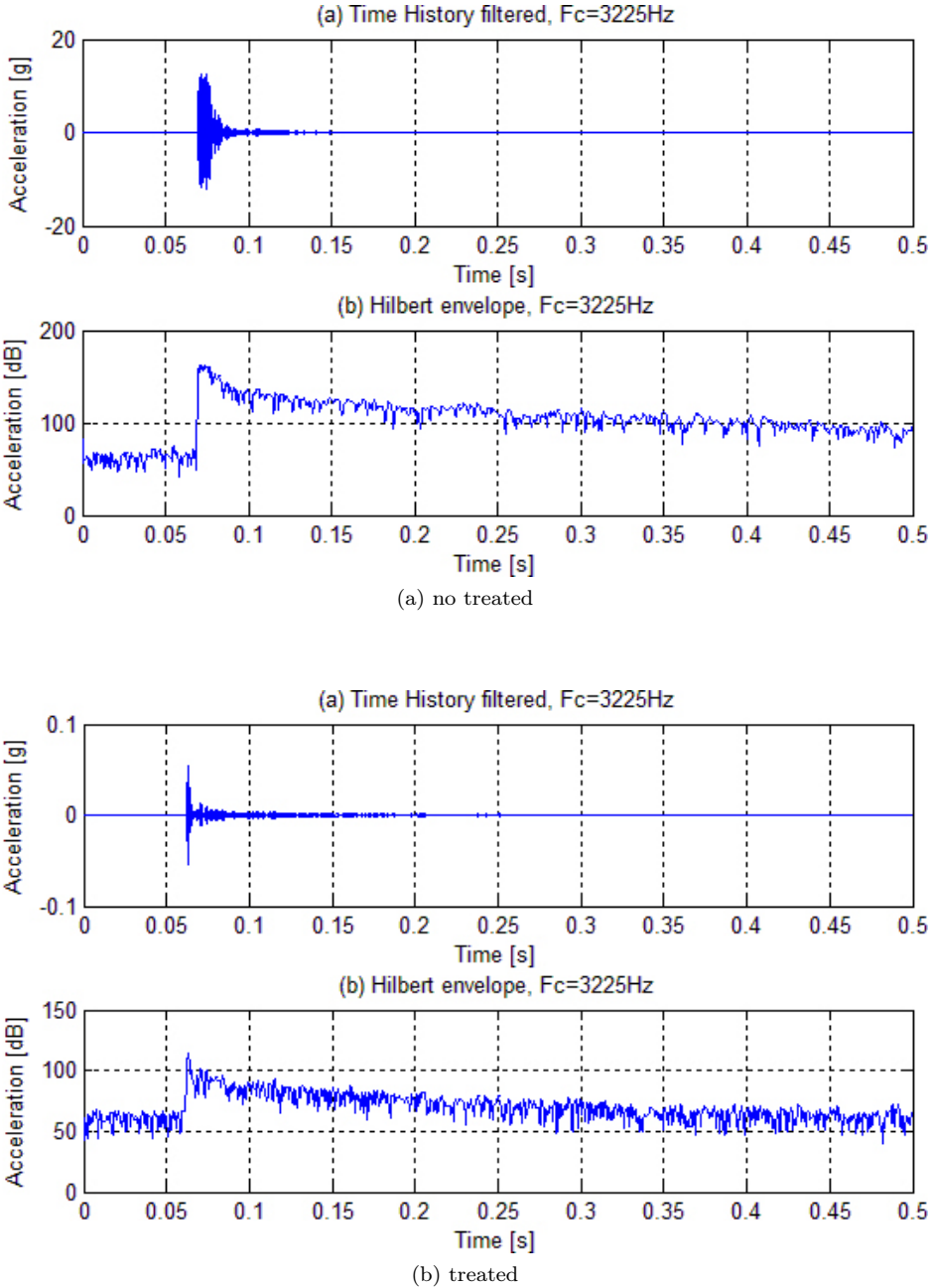


Figure 4.19: No-treated (a) vs treated (b) time histories, $F_c = 3225\text{Hz}$

4.4.1 Position effect

Four accelerometers for each test have been utilized. Considering a coordinate system as shown in a figure 4.12a, in the table 4.1 the accelerometers positions are reported. For each tests and for both test panels, these positions do not change. The use of four accelerometers, therefore, allows to avoid that the acquired signals are affected by systematic errors, such as the bias error. In fact, in the case of a suspended panel, a typical systematic error could be caused by the placement of the accelerometer in a lines of zero out-of-plane displacement [56]. In this case the sensor cannot detect the real behavior of the structure, and consequently its measurement is wrong. The figures 4.20-4.21, show the loss factor evaluated for

Table 4.1: Position of the accelerometers

	x [mm]	y [mm]
accelerometer 1	129	450
accelerometer 2	55	525
accelerometer 3	169	280
accelerometer 4	30	235

each accelerometer at temperature condition of $T = -35^{\circ}\text{C}$ and for both test panels (treated and no-treated). It is possible to see that the loss factor have

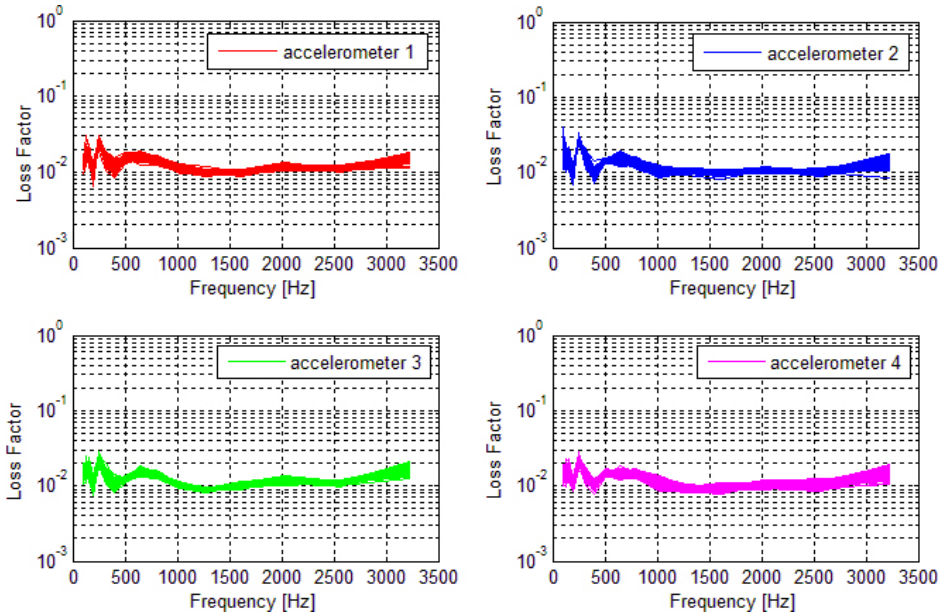


Figure 4.20: Loss factor for each accelerometers in a no-treated panels at $T = -35^{\circ}\text{C}$

the same curve progress thus are not be dependent on accelerometer positions. So the bias error can be excluded.

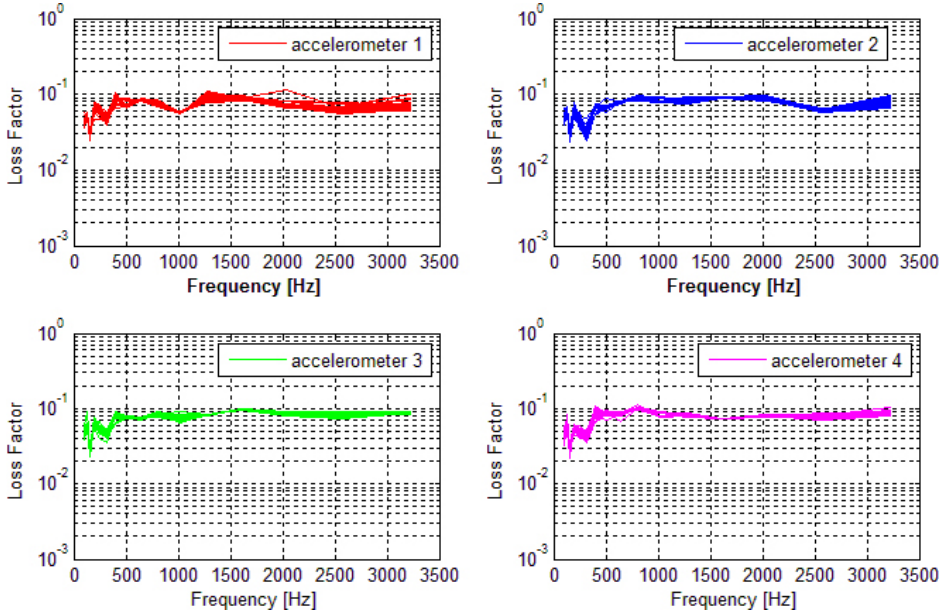


Figure 4.21: Loss factor for each accelerometers in a treated panels at $T = -35^{\circ}\text{C}$

4.4.2 Temperature effect

Generally, the viscoelastic materials change their mechanical properties with frequency and temperature as shown in sections 3.3.4-3.3.5.

In this work, the investigation was focused on the characterization of the overall damping for two typical aircraft composite fuselage skin made by carbon fiber/epoxy resin pre-preg laminate; the first one treated with viscoelastic damping treatments (HPLT) and the second without treatment.

Considering that in aerospace application from cruise and climb/descent conditions the temperature ratio is very high, it is very important to appraise the range of temperature in which the composite structures give an optimal noise and vibration reduction (best loss factor). To get this, many tests have been performed.

Assessed the absence of systematic errors due to the positioning of the accelerometers, the loss factor curves were obtained as average value of a loss factor evaluated for each accelerometers and for all tests, at fixed temperature condition. The first result of damping versus frequency for both test panels (treated and no-treated) is shown in figure 4.22. At the same temperature (-35°C) the loss factor of the treated panel is almost one order of magnitude higher than that of the no-treated panel (about 10^{-1} versus 10^{-2}). This highlights how the viscoelastic damping treatments are very efficient for noise and vibration control.

The evaluated loss factor versus frequency at different temperature conditions, for treated panel are shown in figure 4.23. The analyzed temperature conditions, for treated panel, have been $T = 15^{\circ}\text{C}$, $T = -20^{\circ}\text{C}$, $T = -25^{\circ}\text{C}$, $T = -35^{\circ}\text{C}$.

Decreasing the temperature from 15°C to -25°C , the loss factor increases of about 5 logarithmic levels reaching the optimal value. At the temperature of -35°C , the loss factor has the same curve progress referred to these at -20°C

4.4. RESULTS

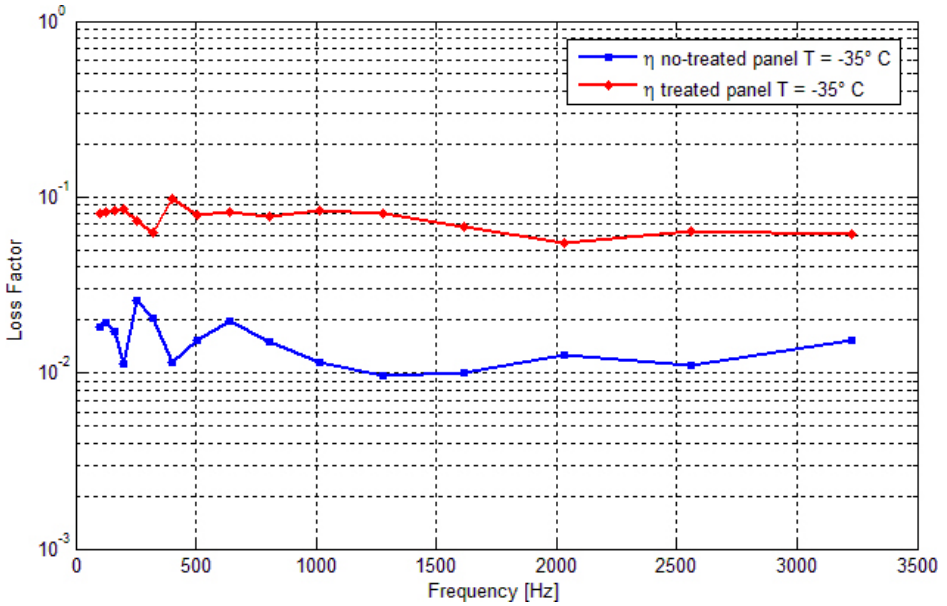


Figure 4.22: Loss factor for both test panels (treated and no-treated) at $T = -35^{\circ}\text{C}$

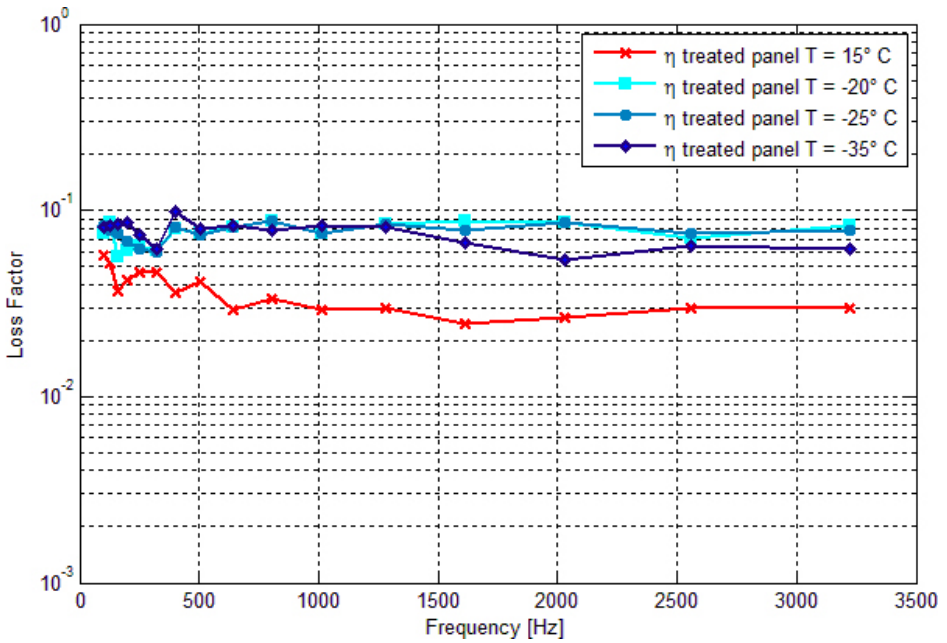


Figure 4.23: Treated panel: loss factor vs frequency at different temperature conditions

and -25°C up to 1500Hz, but it decreases of about 2 logarithmic levels for the other frequencies. This behavior is in compliant to viscoelastic properties curves (fig.3.22) where the optimal temperature range in which the composite structure show the greatest damping is about from -20°C to -35°C .

4.4.3 Statistical analysis

In order to estimate the uncertainty level of our tests and thanks to high number of acquired signals, a statistical analysis has been made.

Defined the standard deviation as follows:

$$\sigma = \sqrt{\frac{\sum_{i=1}^N (\eta_i - \bar{\eta})^2}{N}} \quad (4.16)$$

where N is the number of the performed tests (as reported in a section 4.4), η_i is the loss factor at i -th test and $\bar{\eta}$ is the mean loss factor, the standard deviations curves have been calculated (fig.4.24). By equation 4.16, is clear that increasing

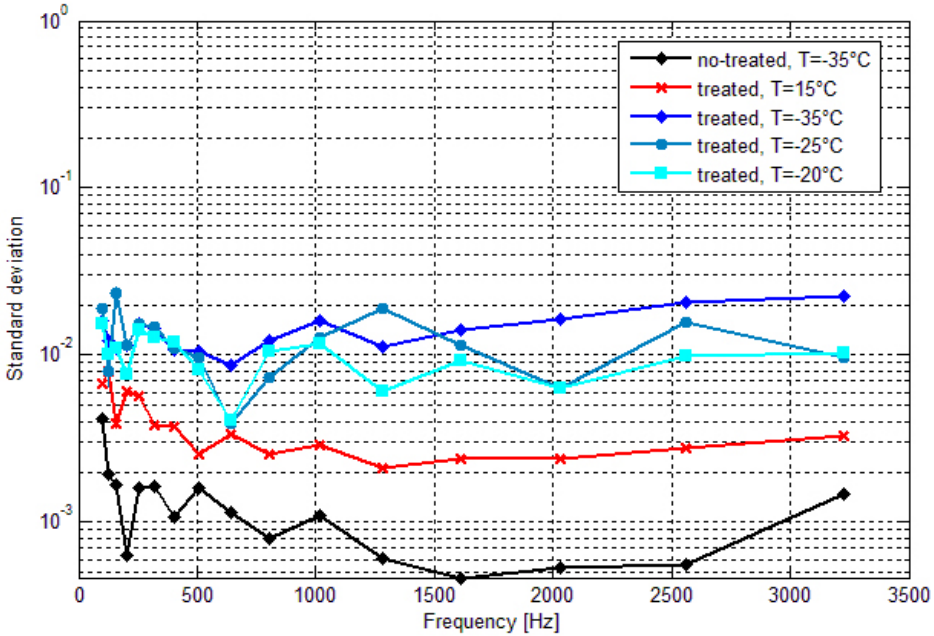


Figure 4.24: Standard deviation for each temperature condition

the number of tests N , decreases the value of the standard deviation and so the estimated loss factor tends to be very close to the mean. This is perfectly what appears by our tests; for no-treated panel at temperature condition of $T = -35^\circ\text{C}$, where we have the greatest number of tests (212), a minimum value of the standard deviation (about 10^{-3}) occurs. However, the maximum standard deviation occurs for treated panel at temperature condition of -35°C and frequencies greater than 1500Hz, but its value is relatively low (about 10^{-2}). For these two test cases (treated and no-treated panels at temperature of -35°C), a confidence intervals at 95% were calculated (fig.4.25, 4.26). Defined the mean value as:

$$\bar{\eta} = \frac{\sum_{i=1}^N \eta_i}{N} \quad (4.17)$$

the probability at 95% can be expressed as:

$$P\left(\bar{\eta} - 1.96 \frac{\sigma}{\sqrt{N}} < \eta < \bar{\eta} + 1.96 \frac{\sigma}{\sqrt{N}}\right) = 0.95 \quad (4.18)$$

4.4. RESULTS

and so, the confidence interval is:

$$IC = \bar{\eta} \pm 1.96 \frac{\sigma}{\sqrt{N}} \quad (4.19)$$

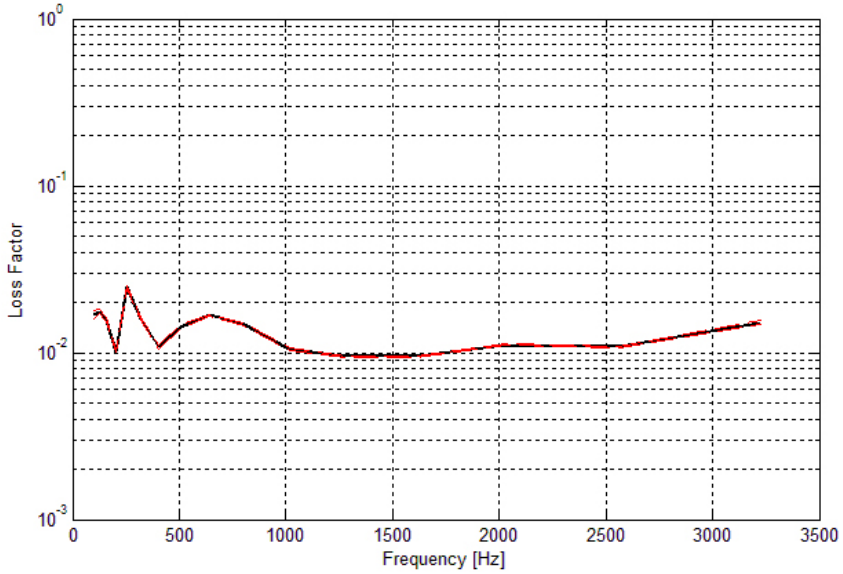


Figure 4.25: Confidence interval for no-treated panel, T=-35°C

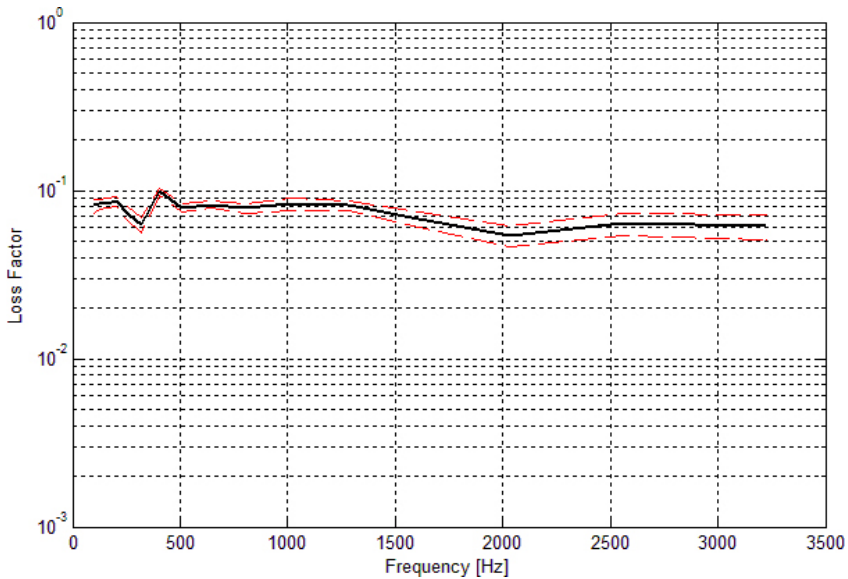


Figure 4.26: Confidence interval for treated panel, T=-35°C

The maximum interval with 95% confidence interval is 0.0019 for the untreated panel and it is 0.0211 for the treated panel; the first one occurs at low frequencies

while the second occurs around $3200Hz$. At high frequencies the evaluated loss factor is influenced by the excitation system, as seen in section 4.1, while at low frequencies, such as $0 - 500Hz$, the values of the loss factor are unstable. This is related to the IRDM method that when the modal density is low gives instable results [51].

Chapter 5

Numerical approach

The objective of the numerical part of this research activity is to create a numerical approach able to provide the same experimental results in terms of damping, as shown in chapter 4.

There are different analytical and numerical methods, as described in chapter 1, able to characterize the dynamic behavior of structures realized with constrained layer treatments. The analytical methods are applicable only on relatively simple structures, while the need to analyze complex structures turn our attention to the methods based on finite element analysis. The use of the traditional FEM approaches, such as the Modal Strain Energy (MSE) or the Complex Eigenvalue Analysis, is limited by the material models; many FEM software, in fact, does not allow to use the viscoelastic material models. The assumption of this chapter is to simulate the same experimental test, in terms of load and boundary's conditions, in order to reproduce the same dynamic behaviour of the panel in terms of accelerations and so to apply the IRDM like in the experimental tests. Two approaches (Explicit non linear analysis and Direct frequency response analysis) in time and frequency domains have been used and two different models for viscoelastic material, Herman and Peterson and Hysteretic formulation respectively, have been utilized.

5.1 Finite Element modelling

The composite structures realized with embedded viscoelastic damping treatments can be represented like the sandwich structures where the viscoelastic layer is like the sandwich core. The dissipation energy in the structure is given only by viscoelastic material and it is almost exclusively linked to shear deformation [59]; modeling composite structures with viscoelastic layer requires that the shear deformation be accurately represented.

There are three commonly-used finite element models for composite structures with viscoelastic core, as shown in figure 5.1. Briefly, the features of the above three models can be summarized as:

- Model (a) is commonly-used for its relatively simple FEM modelling and for its low computational cost required;

- Model (b) is the most complex one and can be used to model curved plates, because the offset plate elements in model (a) do not correctly represent the curved inside and outside layers [61];
- Model (c) exhibits a better convergence rate than model (a), but due to the extra nodes, the computational cost increases.

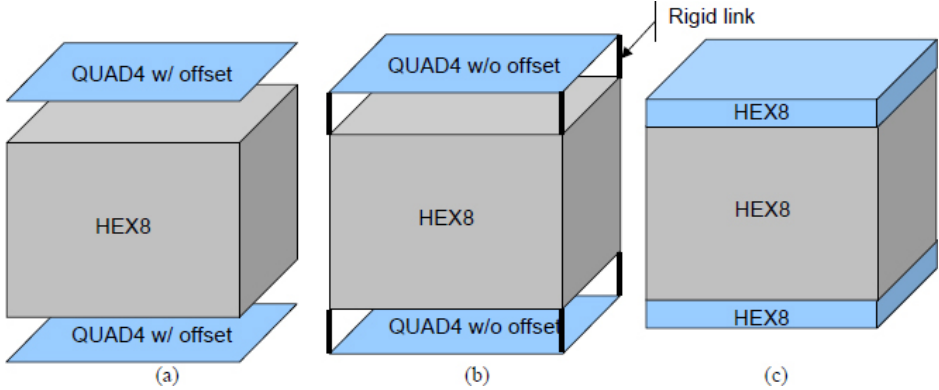


Figure 5.1: Finite element models for composite structures with viscoelastic core

One thing that needs to be avoided in finite element modeling is shear locking. Shear locking is caused by an inaccurate displacement field of linear quadrilateral or hexahedral elements. Illustrated on the left of figure 5.2 is the real deflection

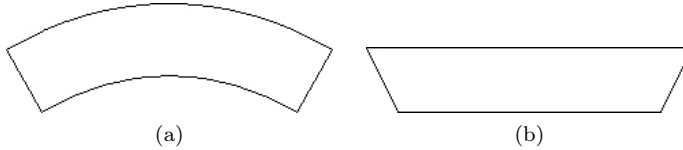


Figure 5.2: Shear locking: real (a) and approximate (b) linear representations of bending deflections

shape of a bending element and on the right its linear representation. It can be seen that though the extension on the top and the compression at the bottom are modeled, an unreal shear stress is introduced by the linear model. This excessive shear absorbs strain energy, thus the element reaches equilibrium with smaller nodal displacements because of shear locking. This representation under-predicts the bending displacements and over-predicts the stiffness. To avoid shear locking, the thickness/length ratio of solid elements should be kept above $1/5000$ [62]. This requirement is satisfied in this Finite Element model.

Considering computational cost and that the test panels are no curved plates, model (a) is used in this research. Therefore, shell-solid-shell elements have been used for the FE modelling where the QUAD4 elements (for both upper and lower layers), are modeled by PCOMP scheduled with offset equal to composite mid-thickness; the HEXA elements are, instead, modeled by HEXA8 scheduled

Table 5.1: Number of Nodes and Elements of the FE model

Type	Number
PCOMP	9600
HEXA8	4800
Total Elements	14400
Total Nodes	9922

both in a NASTRAN software. The FE model dimensions are like to test panels (fig.5.3) equal to 200x600[mm] respectively for width and height. The mesh is



Figure 5.3: Test panel: real (a) and FE model(b)

realized with around 15000 elements and around 10000 nodes as reported in table 5.1. The mesh size is equal to 5x5[mm] and it is such that numerical results are reliable up to frequencies of about 5000Hz as required by experimental tests.

The composite lay-up is granted to IMAST S.c.a.r.l. and was developed in the frame of the project A.R.C.A. (DM24436) funded by the M.I.U.R.. Considering the reference system in figure 5.4, where the x-axis is oriented in a longitudinal direction of the plate and the y-axis in a transversal direction, the composite lay-up is equal to:

$$[OF(IWWF)/45/90/ - 45/0/ - 45/Viscoelastic/ - 45/0/ - 45/90/45/OF]$$

The properties of Fabric (OF and $OF(IWWF)$) and Tape are reported in a table 5.2. The thickness of the viscoelastic layer is 0.230mm and so the total thick-

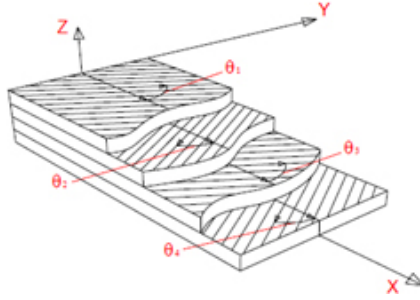


Figure 5.4: Reference system for composite lay-up

Table 5.2: Properties of the Composite plies

	Tape	Fabric	Fabric (IWWF)
E_1 [GPa]	142.0	65.1	65.2
E_2 [GPa]	7.79	65.20	65.20
G_{12} [GPa]	4.00	3.86	3.86
ν_{12}	0.34	0.05	0.05
t [mm]	0.193	0.220	0.220
ρ [Kg/m ³]	1550	1531	1909

ness of the panel is equal to 2.6mm. About the boundary conditions and load conditions, they are made in order to represent correctly the experimental tests. The boundary condition is then free-free, while the load is impulsive. It is simulated with a constant frequency spectrum, such as the Dirac signal. About the

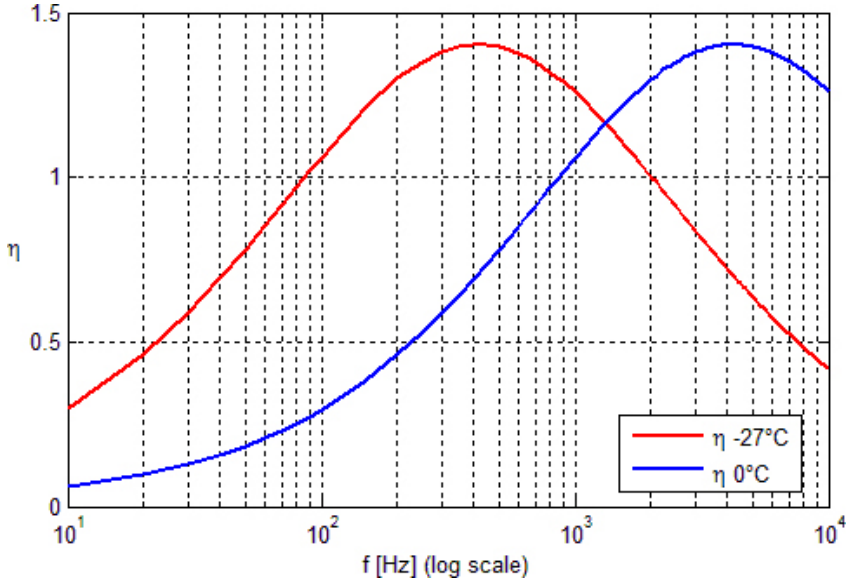


Figure 5.5: Loss Factor for HPLT viscoelastic material

viscoelastic material, soundfoil LT (HPLT) was used. Its properties, only in two

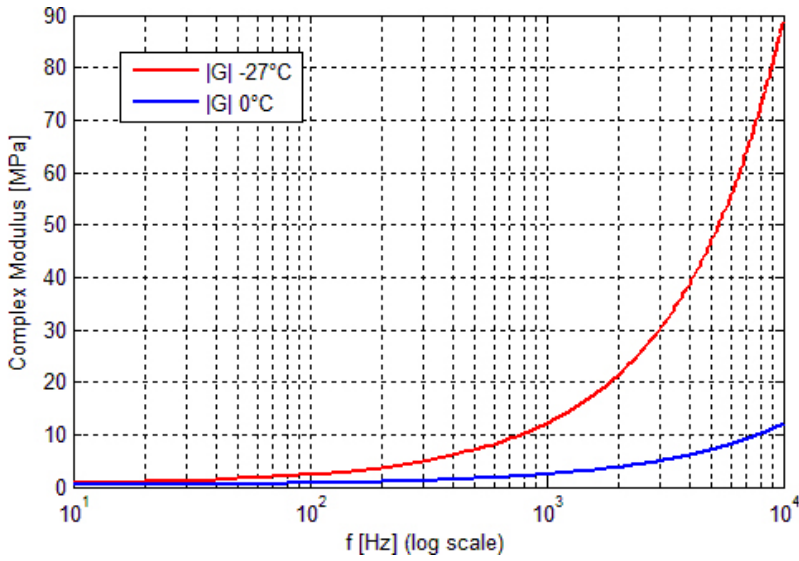
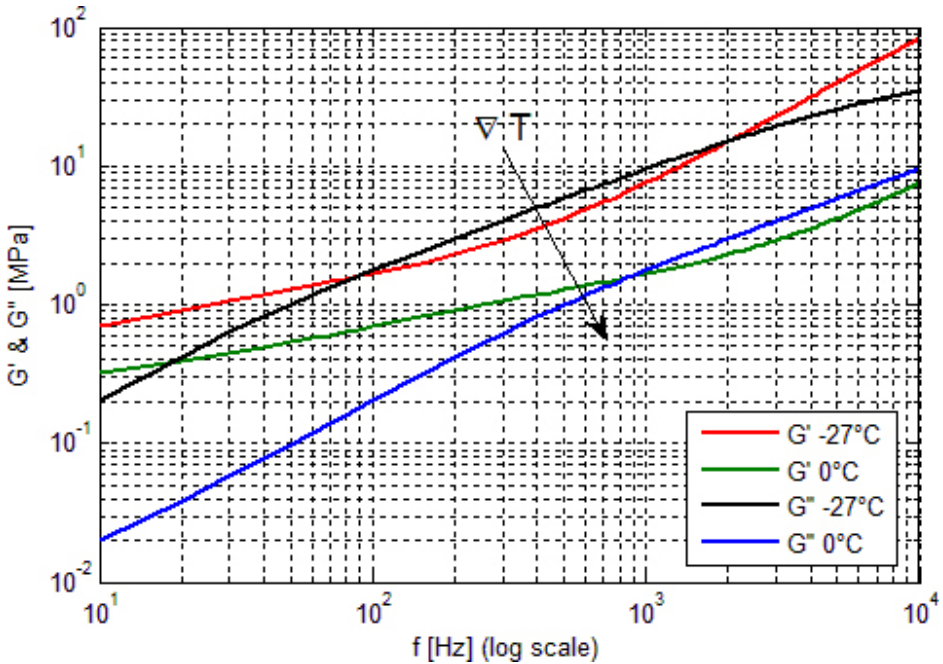


Figure 5.6: Complex Modulus for HPLT viscoelastic material

different temperature conditions (-27°C and 0°C), in terms of loss factor η and complex modulus $|G|$ are granted to IMAST S.c.a.r.l. in the frame of the project A.R.C.A. (DM24436) funded by the M.I.U.R.. Known the loss factor η and the complex modulus $|G|$ and by equations 3.57-3.58, the Loss Modulus and the Storage Modulus can be calculated (fig.5.7). The properties reported in figure 5.7,

Figure 5.7: G' and G'' for HPLT viscoelastic material

show that the viscoelastic material (HPLT) give a maximum performance at low temperature, in accord with experimental results. Decreasing the temperature from 0°C to -27°C, the storage modulus (G') increases, but the loss modulus (G'') increases much more and so the loss factor (η) increases. Therefore at low temperatures the viscoelastic material dissipates a greater quantity of energy.

As previously described, two different approaches have been used. For both the equation of structural dynamics is solved, the first one in time domain and the second in frequency domain.

5.2 Explicit non linear analysis

The application of this method is entirely performed by NASTRAN software. The general equation of motion:

$$[M] \{\ddot{x}\}_n + [C] \{\dot{x}\}_n + [K] \{x\}_n = \{F(t)\}_n^{ext} \quad (5.1)$$

can be rewritten as:

$$[M] \{\ddot{x}\}_n = \{F\}_n^{ext} - \{F\}_n^{int} \quad (5.2)$$

and so:

$$\{\ddot{x}\}_n = [M]^{-1} \{F\}_n^{residual} \quad (5.3)$$

where:

$\{F(t)\}_n^{ext}$ is the vector of externally applied loads;

$\{F\}_n^{int} = [C] \{\dot{x}\}_n + [K] \{x\}_n$ is the vector of internal loads;

$[M]$ is the mass matrix.

The acceleration can be found by inverting the mass matrix and multiplying it by the residual load vector. The mass matrix is lumped which results in a diagonal mass matrix. Since is diagonal, its inversion is trivial, and the matrix equation (eq.5.3) is a set of independent equations for each degree of freedom, as follows:

$$\ddot{x}_{ni} = F_{ni}^{residual} / M_i \quad (5.4)$$

For explicit codes to remain stable, the time step must subdivide the shortest natural period in the mesh. This means that the time step must be less than the time taken for a stress wave to cross the smallest element in the mesh. Because the smallest element in an explicit solution determines the time step, it is extremely important to avoid very small elements in the mesh. Since it is impossible to do a complete eigenvalue analysis every cycle to calculate the timestep, an approximate method, known as the Courant Criterion, is used. This is based on the minimum time which is required for a stress wave to cross each element:

$$\Delta t = \frac{SL}{c} \quad (5.5)$$

where:

Δt is the time step;

S is the time step scale factor (< 1);

L is smallest element dimension;

c is the speed of sound in the element material.

This explicit methods allows to use the formulation of Herman and Peterson for the viscoelastic material, as follows:

$$G(t) = G_\infty + (G_0 - G_\infty)e^{-\beta t} \quad (5.6)$$

where:

- G_0 is the unrelaxed shear modulus or short-term shear modulus
- G_∞ is the relaxed shear modulus or long-term shear modulus
- $\tau = 1/\beta$ is the decay constant

The advantages of this explicit approach are that it gives directly the time-history like the experimental tests and that it has a lower computational cost compared to direct frequency response analysis. The disadvantage of this approach is that it requires that the characteristics of the viscoelastic material are inserted in time domain (NASTRAN material scheduled MATD006). Unfortunately, in this research activity, only two viscoelastic properties are known, ie the Loss Modulus and Loss Factor, and both are expressed in frequency domain. To overcome this limitation, the interconversion methods have been used [63, 64, 65]. The dynamic measurements are mainly used in industry field, because they can be easily made from commercially available equipment, and these allow to obtain the dynamic response functions in terms of $G'(\omega)$ and $G''(\omega)$. As discussed above, $G'(\omega)$ is a measure of elastic energy stored in a cycle of deformation, while $G''(\omega)$ is a measure of energy dissipated in a cycle of deformation.

Many approximate interconversion methods have been developed in the past. Some of these are still used now, especially in laboratories. These methods, given the material properties in frequency domain provide the material properties in time domain. Three are the most common algorithms based on semiempirical formulations; all these consider that a dynamic experiment performed at frequency ω , is equivalent to an experiment performed in time with $t = 1/\omega$ and are following shown:

Ninomiya and Ferry [63]:

$$G(t) \cong \left[G'(\omega) - .4G''(.4\omega) + .014G''(10\omega) \right]_{\omega=1/t} \quad (5.7)$$

Schwarzl and Struik [64]:

$$G(t) \cong \left[G'(\omega) - .337G''(.323\omega) \right]_{\omega=1/t} \quad (5.8)$$

Schwarzl [65]:

$$G(t) \cong \left[G'(\omega) - .00807G''\left(\frac{\omega}{16}\right) - .00719G''\left(\frac{\omega}{8}\right) + .00616G''\left(\frac{\omega}{4}\right) - .467G''\left(\frac{\omega}{2}\right) + .0918G''(\omega) + .0534G''(2\omega) - .08G''(4\omega) + .0428G''(8\omega) \right]_{\omega=1/t} \quad (5.9)$$

Applying these at the viscoelastic material used in this research activity (soundfoil LT (HPLT)), at temperature condition of $T = 0^\circ\text{C}$, the curves in a figure 5.8 have been calculated. All methods give the same results so the terms of Herman and

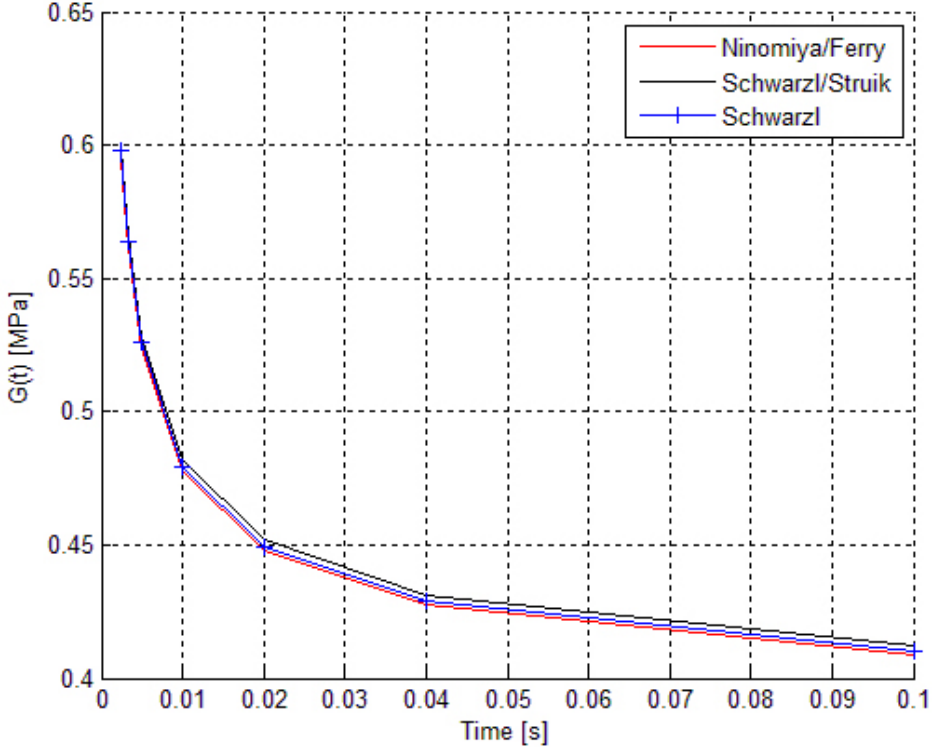


Figure 5.8: Application of interconversion methods to HPLT viscoelastic material

Peterson formulation (eq.5.6) can be chosen as follows:

- $G_0 = 0.6[\text{MPa}]$
- $G_\infty = 0.4[\text{MPa}]$
- $\tau = 0.1[\text{s}]$

Other parameters needed to define the NASTRAN material scheduled (MATD006) are the density ρ and the bulk modulus B . The first one is known and equal to $\rho = 990[\text{Kg}/\text{m}^3]$; the second is unknown, so we chose to place it equal to that of similar materials and thus $B = 1[\text{GPa}]$. The time step calculated by Courant Criterion is equal to $\Delta t = 10^{-5}[\text{s}]$.

5.2.1 Results

A brief summary of the parameters utilized in the first numerical simulation are listed in table 5.3; the result in terms of loss factor vs. frequency is reported in figure 5.9. The numerical result of the test 1 shows a strongly decay in frequency,

Table 5.3: Parameters used in a first numerical simulation

	G_0 [MPa]	G_∞ [MPa]	$Bulk$ [GPa]	τ [s]	Δt [s]	ρ [Kg/m ³]	T °C
test 1	0.6	0.4	1	0.1	10 ⁻⁵	990	0

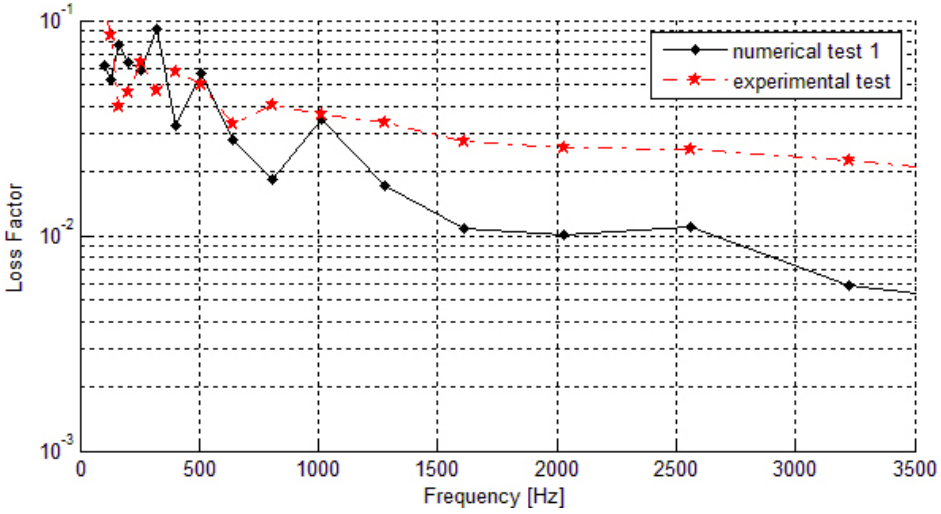


Figure 5.9: Loss Factor vs. frequency result for test 1

abnormal if compared to experimental result. This behavior may be attributed to three different factors: the first related to the erroneous attribution of the bulk modulus. As mentioned above, this parameter is unknown and therefore it has been estimated by viscoelastic materials with similar features; the second related to the incorrect estimation of the viscoelastic material properties in the time domain (G_0 , G_∞ , τ). Thus, interconversion models could be not valid for the present case; the third related to the material model used. The Herman and Peterson formulation could be inappropriate in this case. In order to perform a

Table 5.4: Parameters used in simulations from 1 to 4

	G_0 [MPa]	G_∞ [MPa]	$Bulk$ [GPa]	τ [s]	Δt [s]	ρ [Kg/m ³]	T °C
test 1	0.6	0.4	1	0.1	10 ⁻⁵	990	0
test 2	0.6	0.4	1	20	10 ⁻⁵	990	0
test 3	0.6	0.4	3	0.1	10 ⁻⁵	990	0
test 4	2	0.4	1	0.1	10 ⁻⁵	990	0

sensitivity analysis, three other numerical simulations were conducted by varying

τ , K , G_0 , and keeping all other parameters constant like in test 1. A brief summary of the used parameters are listed in table 5.4. The results in figure 5.10

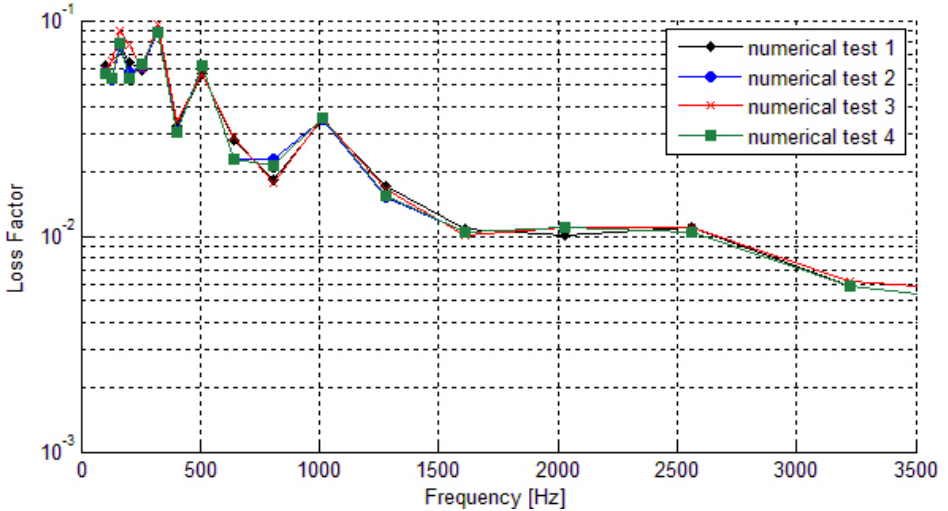


Figure 5.10: Loss Factor vs. frequency results for all explicit non linear simulations

show that the strongly decay in frequency remains yet. Therefore, the variation of material properties does not affect the numerical solution. In fact, varying the Decay constant τ , the Bulk modulus B and the unrelaxed Shear modulus G_0 for the tests 2,3,4 respectively, the loss factor curves have the same trend (fig. 5.10). This is physically not possible. For this reason we can conclude that the material model (Herman and Peterson) is inappropriate in this case. This could be due to several factors such as the type of excitation (impulsive in this case), the embedded viscoelastic configuration with upper and lower plies of composite material, the boundary conditions and much more. Is very difficult to investigate between all these aspects since it would require further experimental tests and so would be very expensive. Beginning to the test results, a new numerical approach based on direct frequency response of the structure has been used.

5.3 Direct Frequency Response Analysis

In direct frequency response analysis, structural response is computed at discrete excitation frequencies by solving a set of coupled matrix equations using complex algebra. Similarly to done with the Explicit method, also the application of this method is entirely performed by NASTRAN software. The damped forced vibration equation of motion with harmonic excitation, can be written as [66]:

$$[M] \{\ddot{x}\} + [B] \{\dot{x}\} + [K] \{x\} = \{P(\omega)\}e^{j\omega t} \quad (5.10)$$

The load in eq. 5.10 is introduced as a complex vector, which is convenient for the mathematical solution of the problem. From a physical point of view, the load can be real or imaginary, or both. The same interpretation is used for response

quantities.

For harmonic motion (which is the basis of a frequency response analysis), assume a harmonic solution of the form:

$$\{x\} = \{X(\omega)\}e^{j\omega t} \quad (5.11)$$

where $\{X(\omega)\}$ is a complex displacement vector. Taking the first and second derivatives of equation 5.11, the following is obtained:

$$\begin{aligned} \{\dot{x}\} &= j\omega\{X(\omega)\}e^{j\omega t} \\ \{\ddot{x}\} &= -\omega^2\{X(\omega)\}e^{j\omega t} \end{aligned} \quad (5.12)$$

When the above expressions are substituted into equation 5.10, the following is obtained:

$$-\omega^2 [M] \{X(\omega)\}e^{j\omega t} + j\omega [B] \{X(\omega)\}e^{j\omega t} + [K] \{X(\omega)\}e^{j\omega t} = \{P(\omega)\}e^{j\omega t} \quad (5.13)$$

which after dividing by $e^{j\omega t}$ simplifies to:

$$[-\omega^2 M + j\omega B + K] \{X(\omega)\} = \{P(\omega)\} \quad (5.14)$$

The equation of motion is solved by inserting the forcing frequency into the equation of motion. This expression represents a system of equations with complex coefficients if damping is included or the applied loads have phase angles.

The Damping simulates the energy dissipation characteristics of a structure. Damping in direct frequency response is represented by the damping matrix $[B]$ and additions to the stiffness matrix $[K]$. The damping matrix is comprised of several matrices:

$$[B] = [B^1] + [B^2] \quad (5.15)$$

where $[B^1]$ is the damping matrix generated through *CVISC* and *CDAMPi* Bulk Data cards (damping elements); $[B^2]$ holds the damping terms generated through direct matrix input, e.g., on the *DMIG* (Direct Matrix Input at Grid points) Bulk Data card. These would be needed to model discrete dampers, which does not apply to this research.

In frequency response analysis, the parameters G and GE on the *MATi* entry do not form a damping matrix. Instead, they form the following complex stiffness matrix:

$$[K] = (1 + jg) [K^1] + [K^2] + j [K^4] \quad (5.16)$$

where g is the overall structural damping coefficient specified through the *PARAM*, G Bulk Data card. $[K^1]$ is the stiffness matrix for structural elements. This would be appropriate if all elements had the same damping properties, which is not the case here. $[K^2]$ is the stiffness terms generated through direct matrix input, e.g., *DMIG* Bulk Data card, which is not done here. $[K^4]$ is the element damping matrix generated by the multiplication of individual element stiffness matrices by an element damping, g_e , entered on the *MATi* Bulk Data card; g_e is the element structural damping coefficient (GE on the appropriate *MATi* entry). The equation 5.16 is of particular interest in the current discussion of viscoelastic material properties because the presence of these properties will be reflected in terms of this equation. For discussion purposes, frequency-dependent

material properties will be denoted as viscoelastic materials. Thus, if the stiffness properties for the viscoelastic elements are initially computed on the basis of a representative reference shear modulus, G_{REF} , the stiffness matrix for the viscoelastic elements (denoted by the subscript v) may be written in the form:

$$[K]_v = \left[\frac{G'(f) + jG''(f)}{G_{REF}} \right] [K^1]_v \quad (5.17)$$

To use the viscoelastic capability in the NASTRAN software, the following conditions are necessary:

1. Assume the $[K^1]$ matrix will be restricted only to the viscoelastic elements. This restriction implies that elastic elements will have a blank or zero entry for g_e on their associated *MATi* Bulk Data entries. Conversely, all viscoelastic materials must have representative reference values of g_e , and G_{REF} entered on their associated *MATi* Bulk Data entries. Then, by definition:

$$[K^4]_v = g_{REF} [K^1]_v \quad (5.18)$$

2. The *TABLEDi* tabular functions TR(f) and TI(f) are defined to represent the complex moduli of all viscoelastic materials.

These two conditions may be combined in equation 5.16 to provide the following expression [68]:

$$\begin{aligned} [K]_v &= (1 + jg) [K^1]_v + \{TR(f) + jTI(f)\} [K^4]_v \\ &= \{[1 + g_{REF}TR(f)] + j[g + g_{REF}TI(f)]\} [K^1]_v \end{aligned} \quad (5.19)$$

A comparison of equation 5.17 and 5.19 yields the form of the tabular functions $TR(f)$ and $TI(f)$:

$$TR(f) = \frac{1}{g_{REF}} \left[\frac{G'(f)}{G_{REF}} - 1 \right] \quad (5.20)$$

$$TI(f) = \frac{1}{g_{REF}} \left[\frac{G''(f)}{G_{REF}} - g \right] \quad (5.21)$$

The advantage of this direct frequency response approach is that it requires as input parameters that the characteristics of the viscoelastic material are inserted directly in frequency domain, so the calculation of TR and TI is simple because G' and G'' are known. The overall structural damping g is fixed equal to zero, so the damping is given only by the viscoelastic material. The reference shear modulus G_{REF} and the reference element damping g_{REF} are chosen so that their product is equal to one [67].

The disadvantage of this approach is that it gives as output the Frequency Response Function (FRF) and then to have the time-history (as in the experimental tests) we must use the Fourier transform. Moreover, it has a higher computational cost compared to explicit non linear analysis.

5.3.1 Results

Two direct frequency response analyses were conducted into two temperature conditions known, i.e. $T = -27^{\circ}\text{C}$ and $T = 0^{\circ}\text{C}$. The data used for $G'(f, T)$ and $G''(f, T)$ are shown in fig. 5.7. The frequency range of analysis is from 10Hz to 6100Hz with a sampling equal to 1Hz so that it provides results, in terms of loss factor, up to about 2500Hz [69]. The results in terms of frequency re-

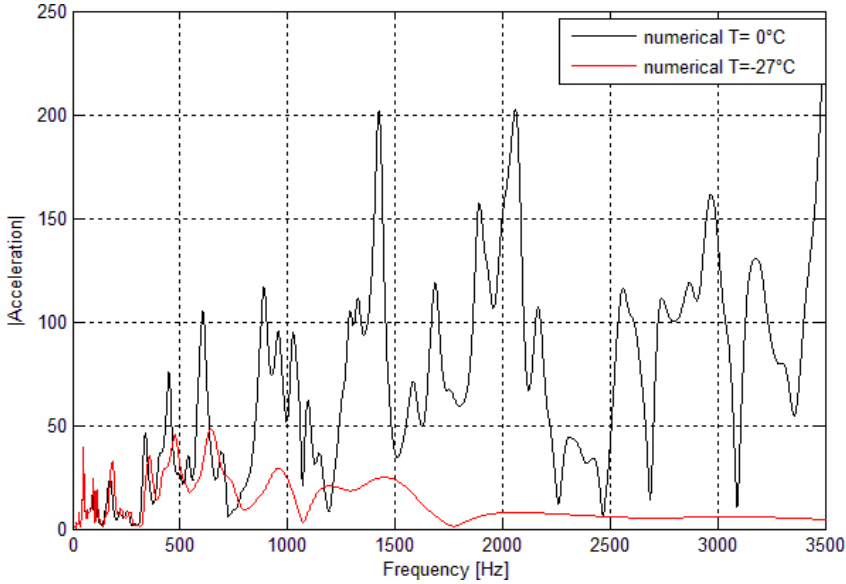


Figure 5.11: Frequency Response Function (FRF) for two temperature conditions

sponse function (FRF) are reported in figure 5.11. They show how the effect of

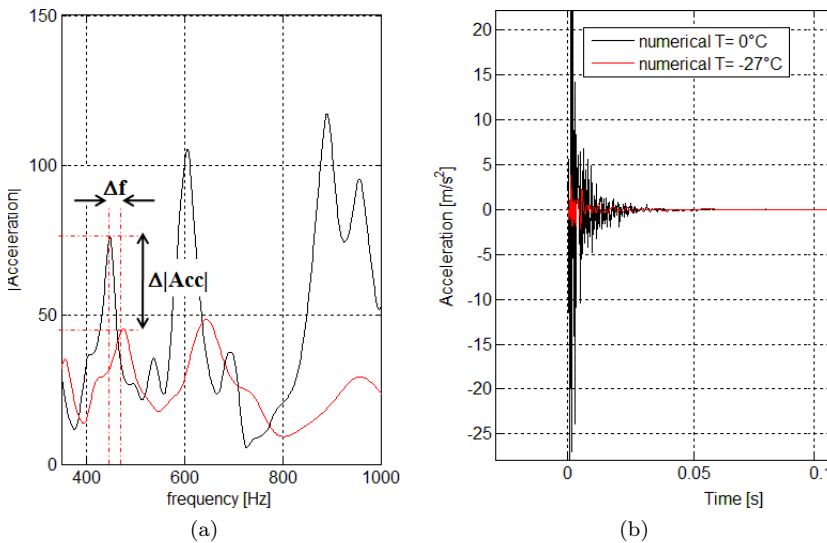


Figure 5.12: FRF (a) and accelerations (b), for both temperature conditions

viscoelastic material on the entire structure is greater at lower temperatures (in accord with the material properties, fig.5.7). In addition to the strong reduction of the amplitude in frequency (that increases with frequency), by zoom in the range 400-1000Hz (fig.5.12a), another clear effect given by viscoelastic material it is possible to see: it is the phase displacement. By fixing the attention on a peak, e.g. that at 450Hz in the temperature condition of 0°C (black line in fig. 5.12a), the numerical simulation carried out in the other temperature condition of -27°C , shows a reduced amplitude (of the quantity $\Delta|Acc|$) and a phase delay of about Δf (red line in fig. 5.12a) for the same peak.

The effect of the amplitudes reduction is also visible in the overlap of the acceleration time histories, obtained from FRF through the inverse Fourier transform (fig.5.12b). Starting from the accelerations time history, was then applied the IRDM procedure, like in the experimental tests, and therefore the loss factor was calculated. As already shown in the FRF, the loss factor curves (fig. 5.13) give

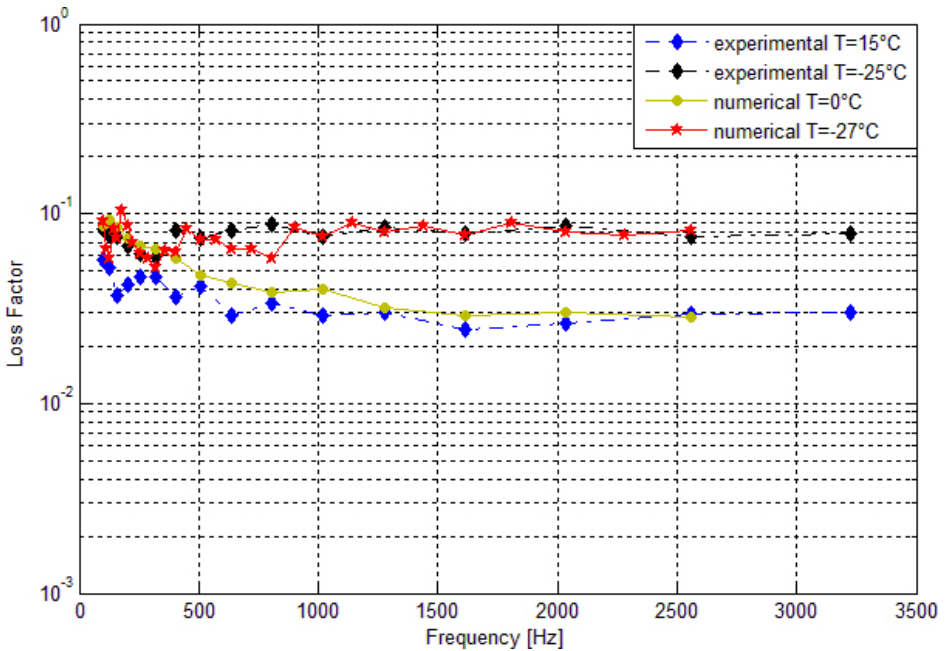


Figure 5.13: Loss Factor vs. frequency results for all direct frequency response simulations

a strong damping, with a magnitude order of about 10^{-1} , in the temperature condition of $T = -27^{\circ}\text{C}$ respect to that at $T = 0^{\circ}\text{C}$, where the magnitude order is about $2 \cdot 10^{-2}$.

About the comparison between numerical and experimental results, the fig. 5.13 shows that in the range of $500 - 2500\text{Hz}$, the numerical results at temperature condition of -27°C are perfectly related with those given experimentally at the same temperature. Moreover, the numerical result, obtained in the temperature condition of 0°C , show that the damping level (expressed in terms of loss factor), is higher than that obtained experimentally at 15°C . This one is agreement with the viscoelastic material properties (fig. 3.22).

Conclusions

Structures subjected to dynamic loads, generally show structural damping values which are just slightly capable of reducing oscillations amplitude. In the aerospace field, low structural damping, or high oscillations amplitudes, may impact negatively on structural stability and emitted noise. This is much evident if applied to structures in composite materials. In force of their stiffness-over-weight ratio, composite materials are deeply used in large assemblies and subassemblies belonging to fuselage and/or lifting surfaces (wing, tail empennages, control surfaces); on the other hand, structural advantages related to composite solutions are accompanied by drawbacks mainly due to materials' high vibration and noise permeability. By increasing structural damping it is possible to obtain a considerable noise and vibration reduction thus augmenting overall composite appeal in aerospace applications. Among the most common damping treatments in the aerospace field, viscoelastic materials embedding are widespread. This research activity was born in the wake of ARCA and COMFORT research projects, within which different types of composite material structures have been built. In particular, typical aircraft composite fuselage skin made by carbon fiber/epoxy resin pre-preg laminate treated with viscoelastic damping treatments have been utilized in this work. This research activity can be split up in two parts: the first one related to experimental tests; the second related to the numerical simulations. About the experimental part, the objectives have been primarily the identification and validation of a procedure to extract the loss factor with a low dispersion of the data in different temperature conditions and, subsequently, to characterize the performance of two test panels in different environmental conditions like flight temperature conditions. About the numerical part, the objective has been the identification of a numerical procedure able to give as output the same result of the experimental tests, in terms of loss factor. In this direction, two ways have been undertaken by two different numerical approaches: explicit in time domain and direct in frequency domain.

In Chapter 4, the experimental approach is described. Two composite fuselage structures have been analyzed; the first one treated with viscoelastic damping treatments (HPLT) and the second without treatment taken as reference panel. The presence of viscoelastic material, as in this case, increases the modal density of the whole structure. This does not allow to use methods based on the frequency domain, such as 3-dB method, since it is impossible to isolate each resonance peak because the structural response at resonance is influenced by the contribution of the neighbouring resonances (heavily coupled modes). A time-domain's method, Impulse Response Decay Method (IRDM), based on the Hilbert transform and

the identification of the extinction curve of the signal was then used (section 4.1). The experimental set-up is characterized by an excitation system entirely developed at the Department of Aerospace Engineering of the University of Naples Federico II, in order to overcome the limitations given by standard excitation devices and to obtain a signal that is as close as possible to the impulsive one. In order to analyze the tests panel in the environmental flight conditions in terms of temperature, the climatic room of the acoustic laboratory of Alenia Aeronautica (section 4.2.2) has been used. Defined a flight altitude in a range of about 0-8000m and considering the international standard atmosphere (ISA), some tests in a temperature range from 15°C to -35°C were performed. About the boundary conditions, the panels are suspended into the climatic room through four springs (fig.4.12b) in order to realize a free-free condition (section 4.3). A first experimental result of the viscoelastic effect, can be seen in the comparison of the time histories (fig. 4.13). They show that the treated panel has a decay rate much faster than the untreated panel. This effect is much more clear in the filtered signals and their Hilbert transforms, so for the two analyzed cases (treated and no-treated panels) in the analysis band with the central frequency equal to 254Hz , 508Hz , 806Hz , 1016Hz , 2032Hz and 3225Hz , in figures 4.14-4.19, their comparisons are respectively shown. Four monoaxial accelerometers located in different positions have been used (fig.4.10b) in order to evaluate if the acquired signals are affected by systematic errors, such as the bias error. A typical systematic error, in the case of a suspended panel, is due to the placement of the accelerometer in a lines of zero out-of-plane displacement [56] so the sensor cannot detect the real behavior of the structure, and consequently its measurement is wrong. The figures 4.20-4.21 show that the loss factor evaluated for each accelerometer at temperature condition of $T = -35^{\circ}\text{C}$ and for both test panels (treated and not-treated) have the same curve progress thus are not dependent on accelerometer positions. So the bias error can be excluded.

Assessed the absence of systematic errors due to the positioning of the accelerometers, the loss factor curves were obtained as average value of loss factor evaluated for each accelerometers and for all tests, at fixed temperature conditions. The first result of damping versus frequency for both test panels (treated and not-treated) is shown in figure 4.22. At the same temperature (-35°C) the loss factor of the treated panel is almost one order of magnitude higher than that of the not-treated panel (about 10^{-1} versus 10^{-2}). This highlights how the viscoelastic damping treatments are very efficient for noise and vibration control.

The evaluated loss factor versus frequency at different temperature conditions, for treated panel are shown in figure 4.23. The analyzed temperature conditions, for treated panel, have been $T = 15^{\circ}\text{C}$, $T = -20^{\circ}\text{C}$, $T = -25^{\circ}\text{C}$, $T = -35^{\circ}\text{C}$.

Decreasing the temperature from 15°C to -25°C , the loss factor increases of about 5 logarithmic levels reaching the optimal value. At the temperature of -35°C , the loss factor has the same curve progress referred to these at -20°C and -25°C up to 1500Hz , but it decreases of about 2 logarithmic levels for the other frequencies. This behavior is compliant to viscoelastic properties curves(fig.3.22) where the optimal temperature range in which the composite structure show the greatest damping is about from -20°C to -35°C .

In order to estimate the uncertainty level of the experimental tests and thanks to high number of acquired signals (section 4.4), a statistical analysis has been made in terms of standard deviation and confidence interval (section 4.4.3). The figure

4.24 shows that for not-treated panel at temperature condition of $T = -35^{\circ}\text{C}$, where we have the greatest number of tests (212), a minimum value of the standard deviation (about 10^{-3}) occurs. However, the maximum standard deviation occurs for treated panel at temperature condition of -35°C and frequencies greater than 1500Hz , but its value is relatively low (about 10^{-2}). Moreover, for these two test cases (treated and not-treated panels at temperature of -35°C), the confidence intervals calculated at 95% (fig.4.25, 4.26) shows that the maximum value is 0.0019 for the untreated panel and it is 0.0211 for the treated panel; the first one occurs at low frequencies while the second occurs at around 3200Hz . At high frequencies the evaluated loss factor is influenced by the excitation system, as seen in section 4.1, while at low frequencies, such as $0 - 500\text{Hz}$, the values of the loss factor are unstable. This is related to the IRDM method that when the modal density is low gives instable results [51].

At the conclusion of this experimental part, we can say that the experimental approach, applied as described in this Ph.D. thesis, provides very reliable results. In addition, the loss factor curves estimated at different temperature conditions are perfectly consistent with the real characteristics of the viscoelastic material.

In Chapter 5 the numerical approach is described. The assumption of this chapter has been to simulate the experimental test, in terms of load and boundary conditions, in order to reproduce the same dynamic behaviour of the panel in terms of accelerations and so applying the IRDM like in the experimental tests, the loss factor has been calculated. Two approaches (Explicit non linear analysis and Direct frequency response analysis) in time and frequency domains have been used and two different models for viscoelastic material, Herman and Peterson and Hysteretic formulation respectively, have been utilized.

The shell-solid-shell elements have been used for the FE modelling (fig. 5.3b) where the QUAD4 elements (for both upper and lower layers) have been modeled by PCOMP Bulk Data card with offset equal to composite mid-thickness and the HEXA elements have been, instead, modeled by HEXA8 Bulk Data card both in a NASTRAN software. The FE model dimensions are like to test panels (fig.5.3) equal to 200×600 [mm] respectively for width and height. The mesh is realized with approximately 15000 elements and around 10000 nodes as reported in table 5.1. The mesh size is equal to 5×5 [mm] and it is such that numerical results are reliable up to frequencies of about 5000Hz as required by experimental tests. The composite lay-up is granted to IMAST S.c.a.r.l. and it is reported in a section 5.1. The laminate properties are reported in a table 5.2. The thickness of the viscoelastic layer is 0.230mm while the total thickness of the panel is equal to 2.6mm . The boundary condition is free-free, while the load is impulsive. It has been simulated with a constant frequency spectrum, such as the Dirac signal. About the viscoelastic material, soundfoil LT (HPLT) was used. Its properties, in two different temperature conditions (-27°C and 0°C) are reported in figure 5.7. As seen in section 5.2, the advantages of the first numerical approach (explicit in a time domain) are that it gives directly the time-history like the experimental tests and that it has a lower computational cost compared to direct frequency response analysis. The disadvantage of this approach is that it requires that the characteristics of the viscoelastic material are inserted in time domain, but unfortunately, in this research activity only two viscoelastic properties are known, ie the Loss Modulus and Loss Factor, both expressed in frequency domain and

so the interconversion methods have been used [63, 64, 65]. A summary of the parameters utilized in these simulations are listed in table 5.4. The numerical result in terms of loss factor vs. frequency of the test 1 shows a strongly decay in frequency, abnormal if compared to experimental result (fig.5.9). This may be attributed to three different factors: the first related to the erroneous attribution of the bulk modulus; the second related to the incorrect estimation of the viscoelastic material properties in the time domain (G_0 , G_∞ , τ). Thus, interconversion models could be not valid for the present case; the third factor is related to the material model used. The Herman and Peterson formulation could be inappropriate in this case. In order to perform a sensitivity analysis; three other numerical simulations were conducted by varying τ , K , G_0 , and keeping all other parameters constant like in test 1. The results in figure 5.10 show that the strongly decay in frequency still remains yet. Therefore, the variation of material properties does not affect the numerical solution. In fact, varying the Decay constant τ , the Bulk modulus B and the unrelaxed Shear modulus G_0 for the tests 2,3,4 respectively, the loss factor curves have the same trend (fig. 5.10). This is physically not possible. For this reason we can conclude that the material model (Herman and Peterson) is inappropriate in this case. This could be due to several factors such as the type of excitation (impulsive in this case), the embedded viscoelastic configuration with upper and lower plies of composite material, the boundary conditions and much more. It is very difficult to investigate among all these aspects since it would require further experimental tests and so would be very expensive. Starting from test results, a new numerical approach based on direct frequency response of the structure has been investigated.

In direct frequency response analysis, structural response is computed at discrete excitation frequencies by solving a set of coupled matrix equations using complex algebra, as reported in a section 5.3. Two direct frequency response analyses were conducted into two temperature conditions known, i.e. $T = -27^\circ\text{C}$ and $T = 0^\circ\text{C}$. The data used for $G'(f, T)$ and $G''(f, T)$ are shown in fig. 5.7. The frequency range of analysis has been from 10Hz to 6100Hz with a sampling equal to 1Hz so that it provides results, in terms of loss factor, up to about 2500Hz [69]. The results in terms of frequency response function (FRF) are reported in figure 5.11. They show how the effect of viscoelastic material on the entire structure is greater at lower temperatures (in accord with the material properties, fig.5.7). In addition to the strong reduction of the amplitude in frequency (that increases with frequency), by zoom in the range 400-1000Hz (fig.5.12a), another clear effect given by viscoelastic material has been observed: it is the phase displacement. Focusing on a peak, e.g. that at 450Hz in the temperature condition of 0°C (black line in fig. 5.12a), the numerical simulation carried out in the other temperature condition of -27°C , has shown a reduced amplitude (of the quantity $\Delta|Acc|$) and a phase delay of about Δf (red line in fig. 5.12a) for the same peak.

The effect of the amplitudes reduction has been also visible in the overlap of the acceleration time histories, obtained from FRF through the inverse Fourier transform (fig.5.12b). Starting from the accelerations time history, the IRDM procedure has been then applied, like in the experimental tests, and therefore the loss factor has been calculated. As already shown in the FRF, the loss factor curves (fig. 5.13) give a strong damping, with a magnitude order of about 10^{-1} , in the temperature condition of $T = -27^\circ\text{C}$ respect to that at $T = 0^\circ\text{C}$, where the magnitude order is about $2 \cdot 10^{-2}$.

About the comparison between numerical and experimental results, the fig. 5.13 shows that in the range of $500 - 2500Hz$, the numerical results at temperature condition of $-27^{\circ}C$ are perfectly related with those given experimentally at the same temperature. Moreover, the numerical result, obtained in the temperature condition of $0^{\circ}C$, have shown that the damping level (expressed in terms of loss factor), is higer than that obtained experimentally at $15^{\circ}C$. This one is agreement with the viscoelastic material properties (fig. 3.22).

At the conclusion of the numerical campaign, we can say that the numerical approach in terms of direct frequency response analysis, applied as described in this Ph.D. thesis, provides results very close with those obtained experimentally.

Therefore, during preliminary phase design of a generic component realized in composite material, with specific damping characteristics, in order to reduce time and costs associated to experimental tests, a possible way could be to use directly the numerical approach described in this thesis, in order to evaluate the damping level of the structure and subsequently proceed to the realization and so the experimental validation only for a single model instead of other not definitive models.

Bibliography

- [1] DAVID I. G. JONES, *Handbook of Viscoelastic Vibration Damping*, John Wiley & Sons, 2001
- [2] VÉR ISTVÁN L., BERANEK LEO L., *Noise and Vibration Control Engineering: Principles and Applications*, John Wiley & Sons, 2005
- [3] H. OBERST, K. FRANKENFELD, *Über die dämpfung der biegeschwingungen dünner bleche durch fest haftende belage*, *Acustica* 2, 181-194, 1952
- [4] ROSS D., UNGAR E.E., KERWIN E.M. JR., *Damping of plate flexural vibrations by means of viscoelastic laminate*, 1959, In ASME (Ed.). *Structural Damping* (pp. 49-88). New York: ASME
- [5] MEAD D.J., MARKUS S., *The forced vibration of a three-layer, damped sandwich beam with arbitrary boundary conditions*, 1969, *Journal of Sound and Vibration*, 10(2), 163-175
- [6] DI TARANTO R.A., *Theory of vibratory bending for elastic and viscoelastic layered finite length beams*, *Transactions of the ASME, Journal of Applied Mechanics*, 1965, 881-886
- [7] YAN M.J., DOWELL E.H., *Governing equations for vibrating constrained-layer damping of sandwich beams and plates*, 1972, *Transactions of the ASME, Journal of Applied Mechanics*, 94, 1041-1047
- [8] RAO Y., SADASIVA V.K., NAKRA B.C., *Vibrations of unsymmetrical sandwich beams and plates with viscoelastic plates*, 1974, *Journal of Sound and Vibration*, 34(3), 309-326
- [9] F. AMOROSO, *Tecniche innovative di modellazione di pannelli di fusoliera in composito ad elevato smorzamento per l'abbattimento del rumore interno e/o esterno*, Ph.D Thesis, University on Naples FEDERICO II, 2004
- [10] SUN C. T., LU Y. P., *Vibration Damping of Structural Elements*, 1995, Englewood Cliffs, NJ: Prentice Hall.
- [11] HU B-G., DOKAINISH M. A., MANSOUR W. M., *A Modified MSE Method for Viscoelastic Systems: A Weighted Stiffness Matrix Approach*, *Journal of Vibration and Acoustics*, Vol.117, 226-231, April 1995
- [12] P. J. SHORTER, *Wave propagation and damping in linear viscoelastic laminates*, *Journal of the Acoustical Society of America*, Vol.115, No.5, Pt.1, May 2004

- [13] ERIC E. UNGAR, EDWARD M. KERWIN, JR., *Loss Factors of Viscoelastic Systems in Terms of Energy Concepts*, Journal of the Acoustical Society of America, Vol.34, Issue 5, 1962
- [14] C. D. JOHNSON, D. A. KIENHOLZ, L. C. ROGERS, *Finite element prediction of damping in beams with constrained viscoelastic layers*, Shock and Vibration Bulletin, Vol.pt 1, No.71-81, 1980
- [15] MD NASTRAN R3, *Quick Reference Guide*, MSC Software
- [16] ROBERT M. JONES, *Mechanics of composite materials*, Taylor & Francis, 1999
- [17] S. P. TIMOSHENKO, J. N. GOODIER, *Theory of Elasticity*, 3rd edition, McGraw-Hill, New York, 1970
- [18] STEPHEN W. TSAI, *Strength Characteristics of Composite Materials*, NASA CR-224, April 1965
- [19] R. BYRON PIPES, N. J. PAGANO, *Interlaminar Stresses in Composite Laminates Under Uniform Axial Extension*, Journal of Composite Materials, October 1970
- [20] S. TIMOSHENKO, S. WOINOWSKY-KRIEGER, *Theory of plates and shells*, McGraw-Hill, New York, 1959
- [21] Y. MASUBUCHI, G. IANNIRUBERTO, F. GRECO, G. MARRUCCI, *Entanglement molar mass and its relationship to plateau modulus of polymer melts: Quantitative comparison of primitive chain network simulations with literature data of linear viscoelasticity*, The Journal of Non-Newtonian Fluid Mechanics, 149, 87-92 (2008).
- [22] J. D. FERRY, *Viscoelastic Properties Of Polymers*, 1st ed., John Wiley & Sons, New York 1961
- [23] H. OBERST, *Material of high inner damping*, Report Phys.-Tech. Assoc. (also Acustica 6, Beiheft 1, 144-153), 1956
- [24] DONALD R. ASKELAND, PRADEEP P. PHULÉ, *The science and engineering of materials*, Cengage Learning., 2006
- [25] STEPHEN H. CRANDALL, NORMAN C. DAHL, THOMAS J. LARDNER, *An Introduction to the Mechanics of Solids*, McGraw-Hill, Boston, 1959
- [26] VICTOR LYLE STREETER, E. BENJAMIN WYLIE, KEITH W. BEDFORD, *Fluid Mechanics*, McGraw-Hill, 1998
- [27] WILLIAM N. FINDLEY, JAMES S. LAI, KASIF ONARAN, *Creep and relaxation of nonlinear viscoelastic materials*, North-Holland Publishing Company, 1989
- [28] ALFRED FOX, *Stress relaxation testing*, American Society for Testing and Materials, 1979

- [29] KOSMATKA J.B., LIGUORE S.L., *Review of Methods to Study Constrained Layer Damping*, ASCE Journal of Aerospace Engineering, Vol. 6, 1993, pp. 268-283
- [30] WARD I. M., *Mechanical Properties of Solid Polymers*, John Wiley & Sons Inc., 1983
- [31] TSCHOEGL W. NICHOLAS, *The Phenomenological Theory of Linear Viscoelastic Behavior*, Springer, 1989
- [32] ATANACKOVIC M. TEODOR, *A modified Zener model of a viscoelastic body*, Continuum Mechanics and Thermodynamics, Volume 14-2, 137-148, Springer, 2002
- [33] SCHIESSEL H., METZLER R., BLUMEN A., NONNENMACHER T. F., *Generalized viscoelastic models: their fractional equations with solutions*, Journal of Physics A: Mathematical and General, Volume 28-23, 1995
- [34] BIRD R. BYRON, MARSH B. DUANE, *Viscoelastic Hysteresis. Part I. Model Predictions*, Journal of Rheology, Volume 12-4, 1968
- [35] MENARD KEVIN P., *Dynamic Mechanical Analysis: A Practical Introduction*, CRC Press, 1999
- [36] AHID D. NASHIF, DAVID I. G. JONES, JOHN P. HENDERSON, *Vibration Damping*, John Wiley & Sons, 1985
- [37] W. T. THOMSON, *Theory of Vibration with Applications (fourth edition)*, Chapman and Hall, London, 1993
- [38] DAVID I. G. JONES, *Application of damping treatments (third edition)*, Shock & Vibration Handbook, McGraw-Hill, New York, 1987
- [39] L. E. GOODMAN, *Material damping and slip damping (third edition)*, Shock & Vibration Handbook, McGraw-Hill, New York, 1987
- [40] J. VAN TOMME, *Evaluation of damping measurements in materials and structures*, The 13th International Seminar on Modal Analysis, Leuven - Belgium, September 1987
- [41] J. E. COOPER, *Parameter estimation methods for flutter testing*, AGARD, SMP Meeting, Rotterdam, May 1995
- [42] A. TONDL, *The application of skeleton curves and limit envelopes to analysis of nonlinear vibration*, Shock and Vibration Digest, 7, 13-17, 1975
- [43] J. K. LEE, Y. S. PARK, *Modal parameter estimation in structural system using complex envelope signal*, Proceedings of the 10th IMAC, San Diego - California, 167-172, 1992
- [44] D. SPINA, F. BRANCALEONI, C. VALENTE, *Damage assessment from the dynamic response of deteriorating structures*, International Workshop on Safety Evaluation of Time-Variant and Nonlinear Structures Using Identification Approaches, Lambrecht - Germany, September 1992

- [45] S. L. HAHN, *Hilbert Transform in Signal Processing*, Artech House, Inc., Boston, 1996
- [46] M. FELDMAN, *Nonlinear system vibration analysis using the Hilbert transform - i. free vibration analysis method freevib.*, Mechanical Systems and Signal Processing, 8, 119-127, 1994
- [47] M. FELDMAN, *Nonlinear system vibration analysis using the Hilbert transform - ii. free vibration analysis method forcevib.*, Mechanical Systems and Signal Processing, 8, 309-318, 1994
- [48] M. FELDMAN, S. BRAUN, *Identification of nonlinear system parameters via the instantaneous frequency: application of the Hilbert transform and Wigner-Ville techniques*, Proceedings of 13th IMAC, 637-642, Nashville - Tennessee, 1995
- [49] BRUEL & KJAER, *Damping Measurements from Impulse Response Function*, The Technical Publications Department
- [50] S. GADE, H. HERLUFSEN, *Digital Filter Techniques vs. FFT Techniques for Damping Measurements (Damping Part I)*, Bruel & Kjaer
- [51] F. AMOROSO, A. DE FENZA, E. MONACO, R. PECORA, L. LECCE, *Improved Impulse Response Decay Method (IRDM) for structural damping measurements*, The 17th International Congress on Sound & Vibration (ICSV), Cairo - Egypt, July 2010.
- [52] F. AMOROSO, A. DE FENZA, E. MONACO, R. PECORA, L. LECCE, *Experimental evaluation of vibro-acoustic behavior of composite fuselage structures realized with embedded viscoelastic damping treatments*, The 18th International Congress on Sound & Vibration (ICSV), Rio De Janeiro - Brazil, July 2011.
- [53] L. CREMER, M. HECKL, *Structure-Borne Sound*, Berlin, Springer-Verlag, 1973
- [54] K. ZAVERI, *Complex Modulus Measurements Using Wide Band Random Excitation*, Proceedings of Internoise, Beijing, China, 1987, pp. 1383-1386
- [55] DAVID A. BIES, COLIN H. HANSEN, *Engineering Noise Control: Theory and Practice (fourth edition)*, Spon Press, 2009
- [56] JIMIN HE, ZHI-FANG FU, *Modal analysis*, Linacre House & Jordan Hill, Oxford, 2001
- [57] P. ERTO, *Probabilità e statistica per le scienze e l'ingegneria (IV edizione)*, McGraw-Hill
- [58] PLOUIN A., BALMES E., *A Test Validated Models of Plates with Constrained Viscoelastic Materials*, International Modal Analysis Conference, Orlando, 1999, pp. 194-200
- [59] PLOUIN A., BALMES E., *Steel/viscoelastic/steel sandwich shells. Computational methods and experimental validations*, International Modal Analysis Conference, 2000, pp. 384-390

- [60] MD R2 NASTRAN, *Explicit Nonlinear (SOL700) User's Guide*
- [61] MOREIRA R., RODRIGUES J. D., *Constrained damping layer treatments: The finite element modeling*, Journal of Vibration and Control, Vol. 10, 2004, pp. 575-595
- [62] JOHNSON C. D., KIENHOLZ D. A., *Finite Element Prediction of Damping in Structures with Constrained Viscoelastic Layers*, AIAA Journal, Vol. 20, No. 9, September, 1982, pp. 1284-1290
- [63] NINOMIYA K., FERRY J. D., *Some approximative equations useful in the phenomenological treatment of linear viscoelastic data*, J. Colloid. Sci. 14,36, 1959
- [64] SCHWARZL F.R., STRUIK L.C.E., *Analysis of relaxation measurements*, Advances in Molecular Relaxation Processes Volume 1, Issue 3, December 1968, Pages 201-255
- [65] SCHWARZL F.R., *The numerical calculation of storage and loss compliance from creep for linear viscoelastic materials*, Rheologica Acta 8, 6Ü17, 1969.
- [66] MSC NASTRAN VERSION 68, *Basic Dynamic Analysis User's Guide*
- [67] MSC NASTRAN VERSION 70, *Advanced Dynamic Analysis User's Guide*
- [68] FLUGGE WILHELM, *Viscoelasticity*, Springer-Verlag, Second Edition, 1975
- [69] ALAN V. OPPENHEIM, ALAN S. WILLSKY, S. HAMID, *Signals and Systems (2nd Edition)*, Prentice Hall, 1997
- [70] G. SCARSELLI, F. AMOROSO, E. MONACO, L. LECCE, *Finite Element Modelling Techniques for Damping Treatments of Fuselage Panel in Composite Material*, XIX congresso nazionale AIDAA, Italy, 2007
- [71] F. AMOROSO, A. DE FENZA, E. MONACO, R. PECORA, L. LECCE, *Evaluation of vibro-acoustic behavior of composite fuselage structures realized with embedded viscoelastic damping treatments*, The 3rd International Conference of the European Aerospace Societies (CEAS), Venice - Italy, October 2011
- [72] PATRAN, *Quick Reference Guide*